Towards circular cement

Evaluation of the reactivity of cementitious binder retrieved from recycled cement stone.

Anna Alberda van Ekenstein

Towards circular cement

Evaluation of the reactivity of cementitious binder retrieved from recycled cement stone.

In partial fulfilment of the requirements for the degree of

Master of Science
in Civil Engineering

at Delft University of Technology,
to be defended publicly on 24-04-2020

Colophon

Master thesis report. Towards circular cement: Evaluation of the reactivity of cementitious binder retrieved from recycled cement stone.
April, 2020

Author

Name	Anna Alberda van Ekenstein
Student number	4197135
University	Delft University of Technology
Faculty of	Civil Engineering and Geosciences
Department	Building Engineering
Specialisation	Structural Design

Graduation committee

Prof.dr.ir. E. Schlangen	TU Delft, Materials and Environment
Dr. H.M. Jonkers	TU Delft, Materials and Environment
Dr.ir. M. Ottelé	TU Delft, Materials and Environment
Dr.ir. H.R. Schipper	TU Delft, Building Engineering

Cover photo: [93]

Preface

This master thesis serves as the final product of the graduation research and was written as part of the master Building Engineering, specialization Structural Design, at Delft University of Technology, faculty of Civil Engineering and Geosciences.

This research focusses on the evaluation of cementitious binder retrieved from recycled cement stone. The need for environmental protection increases and landfill capacity continues to decrease. Traditionally, concrete from demolished structures is crushed in such a way that it devalues the concrete components. When new concrete structures need to be build, new concrete has to be used. From the concrete components, cement is the component with the largest influence on the environmental footprint. This spikes the interest in the possibility of reusing cement. Novel concrete crushing techniques, such as the Smart Crusher, aim to optimize the separation of the concrete components. The cement fraction obtained from the Smart Crusher and hydrated reference cement are evaluated during this research to determine if the secondary cementitious binder will still contain reactivity to obtain a fully functional binder that can replace primary cement in constructions and structural elements. Characterisation of the material used in this research is followed by analysing different thermal treatments for the upcycling of the secondary cementitious binders and assessment of the performance after upcycling by performing strength tests.

During my studies I gained interest in sustainability and innovations within the construction industry. I have always liked to take into account current challenges within the building industry and try to find possible solutions. The ongoing discussion about the circular economy and the need to become energy-neutral sparked my interest in determining a direction for my graduation research. Especially, the need for more research which could help to benefit the problem regarding greenhouse gas emission in the concrete industry. I became enthusiastic about the possibility to do experimental research, which eventually led to the research topic of this thesis.

Finally, I would like to thank my graduation committee who supported me during this whole process. Thank you Prof.dr.ir. E. Schlangen, Dr. H.M. Jonkers, Dr.ir. M. Ottelé and Dr.ir. H.R. Schipper for your insights, enthusiasm and help whenever I needed it. Additionally, I would like to thank Smart Crusher BV. and the Rutte Groep, with special thanks to Koos Schenk and René Rutte, for providing the materials for this research, your enthusiasm and insights. Of course, I would also like to thank the staff of the laboratory for their help during my experiments and familiarizing me with all the experimental methods I needed for this research. Finally, I would like to thank my family, friends and fellow students for their support and encouragements throughout this whole process.

A.T.M. Alberda van Ekenstein
Delft, April 2020

Abstract

The changing climate and the need for a new purpose for End-of-Life concrete increased the importance and interest of concrete recycling. To decrease the environmental footprint of concrete, in which cement has the highest contribution, it would be of great importance to be able to recycle cement, which would positively affect the environment. The separation efficiency plays an important role in the cement properties. The Smart Crusher is a novel concrete crushing- and separation technology developed to optimize the separation efficiency of the concrete. This study investigates the recycling potential of the cementitious fractions obtained from the Smart Crusher. The aim of this research is to evaluate the reactivity of the cementitious binder retrieved from recycled cement stone to obtain a fully functional binder that can replace primary cement in constructions and structural elements.

To gain more insight in the reactivity of cementitious binder retrieved from recycled cement stone, the Smart Crusher cement fractions, which in this study had an unknown origin, are compared with non-hydrated and hydrated reference cements CEM I 52.5 R and CEM III/B 42.5 N. Therefore, the different materials are characterized, using TGA, DSC, MS, XRF and XRD. Analysis of the chemical and mineralogical composition showed the presence of hydration products in the hydrated Smart Crusher, CEM I 52.5 R and CEM III/B 42.5 N samples. Additionally, quartz is found in the cementitious fractions of the Smart Crusher, which indicates the presence of aggregate particles such as sand in these samples. Furthermore, the absence of P_2O_5 in the cementitious Smart Crusher fractions proved that there is no or a not measurable amount of fly ash present in the cementitious Smart Crusher fractions.

Upcycling of the hydrated Smart Crusher, CEM I 52.5 R and CEM III/B 42.5 N materials is done by thermal treatment. To assess the upcycling, again the chemical and mineralogical composition is analysed. Red colouration (500 °C and 800 °C) and melting (1400 °C) of the cementitious Smart Crusher fractions again show the presence of aggregate particles in the material. During thermal treatments of the Smart Crusher, CEM I 52.5 R and CEM III/B 42.5 N materials, the decomposition of hydration products and calcite are monitored, using TGA, DSC and MS. The thermal treatment at 800 °C showed the formation of alite and belite phases in all the samples and was therefore seen as the treatment with the most potential in this research. The only material that shows the formation of alite and belite during other thermal treatments was CEM I. After the thermal treatments the composition and crystalline phases were determined, using XRD and XRF.

Insight in the mechanical performance of the different binders was obtained by flexural and compressive strength tests. Mortar prisms were made, containing CEM I and CEM III/B as reference cement and thermally treated CEM I, CEM III/B, 0.0 – 0.063 mm and 0.063 – 0.125 mm cementitious Smart Crusher fractions. The mortar mixtures with the thermally treated binders were observed to be rather dry as a result of an increasing water demand. Compared to new cement, the increase in water demand led to a low degree of compaction, resulting in return to strength properties that were practically unmeasurable. The reference cement showed a lower early strength for CEM III/B compared to CEM I and comparable strength after 28 days due to the higher gain of strength of CEM III/B. Especially the flexural and compressive mechanical tests showed that more research is necessary.

To conclude, this study showed that a certain reactivity can be expected in the secondary binders after upcycling, but that the unmeasurable strength properties of the upcycled materials showed the need for more research to make a better estimation of that reactivity.

Table of contents

List of Figures

List of Tables

List of Abbreviations

C-S-H	Calcium silicate hydrate
C_2S	Dicalcium silicate, belite
C_3A	Tricalcium aluminate
C_3S	Tricalcium silicate, alite
C_4AF	Tetracalcium aluminoferrite
CH	Calcium hydroxide, portlandite
CO_2	Carbon dioxide
DSC	Differential Scanning Calorimetry
DTG	Derivative thermogravimetry
EoL	End-of-Life
MS	Mass Spectrometry
OPC	Ordinary Portland Cement
TG	Thermogravimetry
TGA	Thermogravimetric Analysis
XRD	X-Ray Diffraction
XRF	X-Ray Fluorescence

1 INTRODUCTION

This first chapter contains the description of the research project. To have a clear understanding of research significance, insight will be given in the current problem. The research scope states the content that will be covered during the research. This is followed by the aim of the research as well as the main research question. In order to answer the main research question, multiple sub-questions are formulated. Additionally, the methodology will elaborate on the structure of the thesis. Finally, the content of the each chapter will be described in the outline.

1.1 Background

One of the major challenges of the 21st century is to use a much greater efficiency to handle raw materials. During the last century the demand for raw materials has increased rapidly and this will further increase due to the global population growth, the rapid growth of the middle class in emerging economies and the development of new technologies. The ever-increasing demand for raw materials will not only lead to the risk of natural resource depletion, but will also heighten the environmental, climate-related and other sustainability issues. Additionally, the use of raw materials contributes considerably to the CO_2 emission and the energy consumption. Therefore, to guarantee preservation of our current living standards the economy has to shift to an economy that meets the needs of the people without the depletion of natural resources and without having an unacceptable impact on the environment [28].

1.1.1 The need for cement-based materials

After water, cement-based materials, specifically concrete, are the second most consumed substance on Earth. The need for cement-based materials comes from the necessity to meet the increasing demand for infrastructure and buildings. At this point in time, concrete is the only material available in quantities necessary to meet this demand. Reason for this are the low costs, durability, strength, flexibility in its possibility to build complex and large structures, resilience to fire, floods and pests, its availability in most parts of the world and the abundance of its raw materials. Therefore, it is no surprise that cement is the largest manufactured product by mass on Earth. Over the last 65 years, the production of cement has increased rapidly. The growth of the demand of cement is considerably higher than that of other manufactured materials such as steel. As the living standards improve all over the world the demand of cement will increase even more, especially in emerging economies. The global demand of cement is expected to increase with 12 – 23% in the period between 2014 and 2050 [46; 88].

If no changes are made, the increase of the demand of cement will have major consequences, such as the depletion of natural resources and an increase in CO_2 emission. Of the global greenhouse gas emissions 77% of its emissions is caused by CO_2. The third largest CO_2 emitting industrial sector is the building material sector, which is dominated by the cement production. The cement production accounts for approximately 5% of the anthropogenic CO_2 emissions in Europe and up to 7% worldwide. These percentages show that the cement production represents a large part of the CO_2 emissions. Therefore, it is important to know the cause of the emissions in the cement industry as actions on cement level have the potential to contribute considerably to the reduction of CO_2 emissions [10; 14; 32; 100].

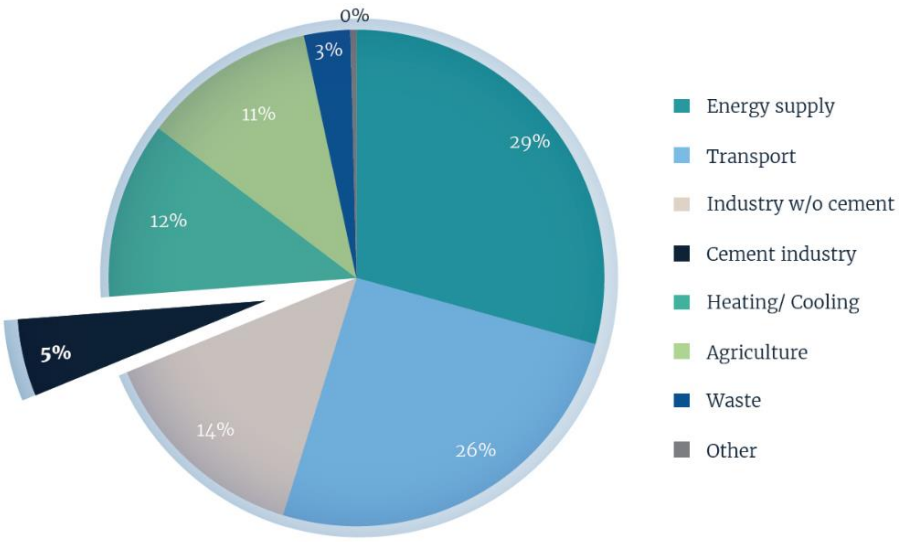

Figure 1: Division of the CO_2 emissions by sector for EU countries [32].

The CO_2 emissions of the cement industry can be divided in two distinct sources, namely "energy-use CO_2" and "process CO_2". The energy-use CO_2 is the result of the combustion of fuels that are used during sintering and calcination of the raw materials. It is related to the thermal energy efficiency and the type of fuel during the burning process. The production of CO_2 is not directly related to the fuel consumption, but is the result of chemically produced CO_2 such as the decarbonisation process of the raw materials in the kiln [10; 77]. Besides the emissions produced due to the combustion of the fuel and the chemical reactions in the kiln, only a small part of the emissions is allocated to the transportation of the raw materials and the generation of electricity. Significant reduction of the CO_2 emission can therefore be achieved if the cement can be obtained in such a way that the combustion of fuels and the raw materials, used in the cement production, do not result in the emission of CO_2 [14].

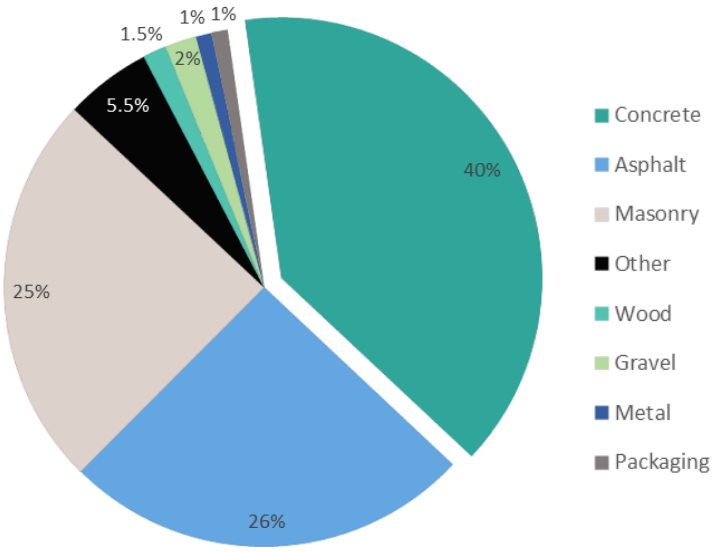

Figure 2: Division of the construction and demolition waste in the Netherlands [108].

The increasing need for cement-based materials due to a growing population and urbanization comes from an increasing demand for infrastructure and buildings. This, in turn, leads to the production of large amounts of construction waste [59]. The VROM (2001) estimated that concrete the material is with the largest contribution to the amount of construction waste was in the Netherlands in 2001.

With 40% nearly half of the construction waste consist of concrete [108]. Since 1997, it is no longer allowed to dispose the construction and demolition waste in landfill sites [83]. The European Parliament adopted different directives, which have to be implemented within two years. The Directive 2008/98/EC (2008) includes a 70% target for the recycling, re-using and other recovery options of construction and demolition waste. Additionally, the Directive (EU) 2018/850 (2018) requires a reduction in waste disposal by landfilling. Disposal in landfills should no longer be permitted for waste suitable for recycling or other recovery options. Only in exceptional cases is the use of landfills allowed [102; 103]. In the case of the Netherlands most of the End-of-Life (EoL) concrete is used as road fill. It is expected that the amount of EoL concrete used as road fill will decrease significantly in the future. Additionally, it is expected that the amount of EoL concrete will become equal to the amount of concrete used in the future. Therefore, a new purpose has to be found for the EoL concrete. This leads to the need of recycling EoL concrete in such a way that it can be used as new concrete [7].

1.1.2 Scientific gap

During the 20th century, rising interest in the need for environmental protection and a continuing decrease in landfill capacity led to an increasing importance of concrete recycling. Currently, most research on the recycling of concrete focusses on crushing of the waste concrete and using it as aggregates for new concrete. In general, this recycled aggregate has a lower quality than the primary aggregates and more cement is needed to obtain equivalent strength and workability properties. The reason for this is the presence of residual cement stone, which requires more water and this has to be compensated by using more cement in the concrete mixture [36; 44]. Cement has the largest influence on the environmental footprint of concrete. The increasing amount of cement will not have the aspired impact on the goals regarding the raw materials, CO_2 emission and need for a new purpose for the concrete waste. Therefore, to reduce the need for raw materials and lower the CO_2 emissions of the concrete industry insight in the recycling of cement is needed.

Shui et al. (2009) found that dehydrated cement can successfully be rehydrated after dehydrating the cement using thermal treatments, although the compressive strength was still lower compared to primary cement [91]. Kwon et al. (2015) reported that the recycled cementitious powder needed to be treated with very high dehydration temperatures, but the compressive strength was still lower than that of primary cement. The explanation was that the fine aggregates could not be effectively separated from the cementitious powder [54]. Wang et al. (2018) found satisfying results for the compressive strength of the rehydrated cement material by using two year old cement samples, but the workability properties were poor [109]. The deviation in the results of the current research was mostly associated with the efficiency of the separation of the concrete components. A low separation efficiency showed lower properties compared to primary cement, while a complete separation showed promising results.

Currently, new crushing and separation techniques are under development. These innovative techniques aim to optimize the separation of the concrete components. One of these techniques is the Smart Crusher, which was developed specifically for concrete recycling. The Smart Crusher takes into account the difference in strength and hardness of the cement and the other concrete components and only crushes the cement stone [87; 93]. Further examination of the benefits of crushing concrete, using the Smart Crusher, is needed. Especially, investigation of the influence of the Smart Crusher on the material properties to obtain cement, which can be re-used in concrete mixes, is required [33]. It can be concluded that research on the material properties of secondary cementitious material, retrieved from recycled cement stone, and its similarity with the primary cement properties is needed.

1.2 Research scope

This thesis researches the use of secondary cementitious binder retrieved from recycled cement stone to replace cement to potentially reduce the need for raw materials in the production process, lower the CO_2 emissions and close the cement material cycle. By closing the material cycle and making fully functional cementitious binder from recycled cement stone, which would theoretically be able to fully replace cement, there would be no need for the production of new Portland cement. In other words, the use of raw materials and the emission of CO_2 during the production process could be significantly reduced.

In this research, the focus lies on secondary cementitious binder obtained from the novel concrete crushing technique Smart Crusher and different reference cements. The determination of the reference cements is based not only on the most used type of cement worldwide, but mainly on the types of cement mostly used in the Dutch concrete industry. This resulted in the use of CEM I and CEM III/B cements. Additionally, fly ash and blast furnace slag are taken into account during characterization of the Smart Crusher material, which is also referred to as cementitious Smart Crusher fractions, to gain insight in the cement composition. Other types of cement are generally beyond the scope of this thesis, because these types of cement are not widely used and the chances are small that they are present in the material received from the Smart Crusher.

Both the cementitious Smart Crusher fractions and the chosen reference materials will be characterized and undergo upcycling treatments. The focus of the upcycling treatments lies on thermal treatment of the material by using several dehydration temperatures. Examination of the chemical and mineralogical composition will be used for the characterization of the material and to evaluate the effect of the thermal treatments. Assessment of the influence of the upcycling treatments on the different materials will give an indication of the most promising treatment. The evaluation of the material properties of the mentioned materials, with and without upcycling treatment, will lead to the establishment of similarities and deviations between the materials.

Additionally, the performance of the cementitious Smart Crusher fractions and the reference materials after upcycling treatment will be evaluated in this thesis. Based on the upcycling assessment the most promising upcycling treatments will be determined. The performance of the materials after being treated with the chosen upcycling treatment are evaluated by compressive strength tests, which give insight in the functional quality of the materials.

1.3 Aim of the research

Previous studies focused mostly on the recycling of aggregates, although cement is seen as the component within concrete which has the biggest contribution to the environmental footprint. On the recycling of cement few studies are available. Most of them focus on the rehydration of dehydrated cementitious binder and their properties. The cementitious binder used in these studies is obtained by using traditional crushers and sieving the material to obtain the fraction seen as the binder fraction. The use of traditional crushers results in an inefficient separation of the binder fraction from the other concrete components. This results to a cementitious binder with strength properties lower than the properties of primary cement. Developing novel concrete crushing and separation techniques, such as the Smart Crusher, aim to optimize the separation efficiency of the concrete components. With regards to this novel technology, question still remains if the obtained cementitious binder has properties comparable to those of primary cement. The aim of this master thesis is therefore to evaluate the reactivity of the cementitious binder retrieved from recycled cement stone. A comparison will be made

between cementitious binder obtained by the novel technique the Smart Crusher and cementitious binder retrieved by hydrating and crushing reference cement, avoiding contact with the other concrete components.

The main research question of this thesis therefore is:

Does cementitious binder retrieved from recycled cement stone still contains reactivity to obtain a fully functional binder that can replace primary cement in constructions and structural elements?

The following subsection addresses the different aspects of this main research question by formulating multiple sub-questions.

1.3.1 Sub-questions

Multiple sub-questions have been formulated to answer the main research question of this thesis. The sub-questions are:

1. *What are the characteristics of the secondary material compared to the primary material?*
    a. *Which methods can be used for the characterization of the materials?*
    b. *How can the characterization be linked to the reactivity of the materials?*

2. *What is the best approach to upcycle the secondary materials?*
    a. *How do the different upcycling treatments influence the materials?*
    b. *Can a distinction be made between the different types of materials?*

3. *What is the functional quality of the retrieved cementitious binders?*
    a. *How is the strength development influenced by the type of materials?*
    b. *Can the cementitious binder be upcycled to obtain satisfying functional quality?*

1.4 Methodology

This thesis can be divided into three parts, namely a literature review, experimental research with discussion and the conclusions.

Part I: Literature Review
For part I, relevant topics for the research will be explained. Insight in separation techniques and the different aspects of cement will be given by a literature study. Additionally, the current state-of-the-art of cement recycling will be discussed. Particular attention is given to the dehydration methods of the hydrated cementitious binder and the changes, which can occur in concrete and cement exposed to elevated temperatures.

Part II: Experimental Research
In part II, the cementitious fractions from the Smart Crusher and the reference materials will be studied experimentally. Characterization of the cementitious Smart Crusher fractions is performed to gain insight in the composition of the material, because the Smart Crusher material is a complete blackbox. The type of concrete used in the crushing process is unknown. Additionally, it is unknown if the material was mixed with materials containing other cement types during storage. This characterization is followed by characterising the effect of the upcycling treatments on the material properties. For the

initial characterization as well as the characterisation of the effect of the upcycling treatments the following experimental methodology is used:

- Thermogravimetry (TGA), differential scanning calorimetry (DSC) and mass spectrometry (MS) to measure the weight loss as a result of the dehydration of the hydration products. The observation of phase transitions belonging to concrete components other than cement implies that the cement was not completely separated of the other concrete components.
- X-ray fluorescence (XRF) to analyse the chemical composition and deviations in the chemical composition as a result of the upcycling treatments.
- X-ray diffraction (XRD) to analyse the crystalline phases and changes of the crystalline phases as a result of the upcycling treatments.

The characterisation and assessment of the upcycling treatments will result in the determination of the most promising upcycling treatment. Using this treatment the next part of the experimental research will be conducted. This part consists of testing the functional quality of the secondary cementitious binders with respect to its compressive and flexural strength. The cementitious materials will be treated, using the most promising upcycling treatment, before a compressive and flexural strength test is conducted on the samples. The results will give insight in the performance of the cementitious material in comparison with primary cement.

During the experimental research an approach based on the principle of the "Wheel of Science" by Wallace will be used. Scientific theories and research continuously shape each other. It works as a continuous loop in which knowledge based on scientific discovery leads to new theories. These theories lead to new testable questions, the hypotheses. Observations are used to test these hypotheses and empirical generalization results in findings, which might influence the theory and the cycle begins again [82].

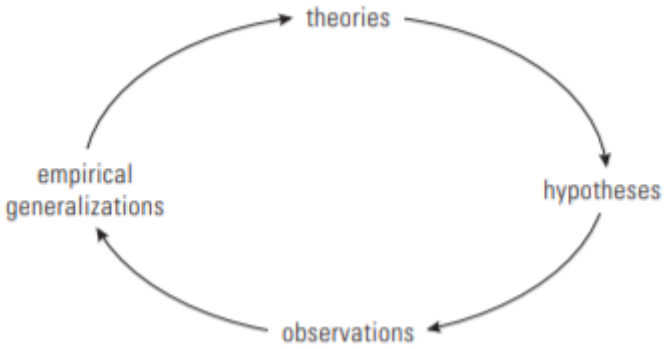

Figure 3: Wheel of Science by Wallace [75].

Part III: Conclusions

This is the final part of the research. The results of the previous part, the experimental research, are used to answer the research questions. A final conclusion is drawn, which leads to the answer of the main research question. When the research questions are answered, recommendations can be given with respect to future research and the industry.

1.5 Outline

The contents of every chapter will be explained, starting with chapter 1. This is the introduction of the research and is described in this chapter. The other chapters can be divided within the three parts mentioned previously.

Part I: Literature Review

Chapter 2 describes three separation techniques, namely the traditional crusher, Advanced Dry Recovery (ADR) and the Smart Crusher. The similarities and difference between the technologies will become clear in this chapter. Additionally, insight will be gained about the extend in which the technologies aim to recover cement with respect to the reuse for structural elements and constructions. The two types of cement with the highest usage share in the Dutch concrete industry will be discussed in chapter 3. Both Ordinary Portland Cement and Blast Furnace Cement will be discussed. First insight will be given in the composition of the material as well as the crystal structure. Subsequently, the hydration of the materials will be discussed and possible distinctions between the hydration products of the two materials will be mentioned. Additionally, the production process will be described. Finally, the identification of the diffraction patterns of the mineralogical phases of the components using x-ray powder diffraction is mentioned. Chapter 4 analyses different upcycling techniques. A state-of-the-art literature review focussed on the influence of elevated temperatures on the concrete and cement properties is performed to gain insight in possible heating regimes, which can be used during the experimental research.

Part II: Experimental Research

Chapter 5 presents an overview of the materials and experimental methods used in this research. Insight will be given in the origin and selection of the materials. Additionally, the different categories in which the materials can be divided will be discussed. Subsequently, the description of the experimental methods will include sample preparation, equipment type and experimental setup. To conclude this chapter, a tree diagram with an overview of the possible experimental methods and the pathway within this thesis is shown. The characterization of the cementitious fractions obtained from the Smart Crusher is discussed in chapter 6. The results of the characterization consist of particle size distribution, chemical reactions and composition, mineralogical transformations and crystalline phases. The results of the analysis of the cementitious Smart Crusher fractions will be discussed and compared with the reference materials. Assessment of the upcycling treatment is presented in chapter 7. Upcycling of the cementitious binder is performed by using different thermal treatments. Both the cementitious fractions of the Smart Crusher and the reference materials are thermally treated. By comparing the results of the various materials and the different thermal treatments the influence on the chemical composition and crystalline phases will be analysed. Changes in the chemical composition or crystalline phases can give an indication of the most promising upcycling treatment. Therefore, the results will also be compared to untreated primary cement. Chapter 8 presents the performance of the cementitious binder based on compressive and flexural strength tests. The cementitious fraction of the Smart Crusher and the reference materials will be treated, using the most promising thermal treatment, before undergoing compressive and flexural strength tests. A comparison of the different samples gives insight in the performance of the materials and their functional quality.

Part III: Conclusions

Chapter 9 will summarize the most important research conclusions. In this chapter the main research question will be answered. To arrive at a final conclusion the sub-question will first be answered. Finally, recommendations and further research will be discussed.

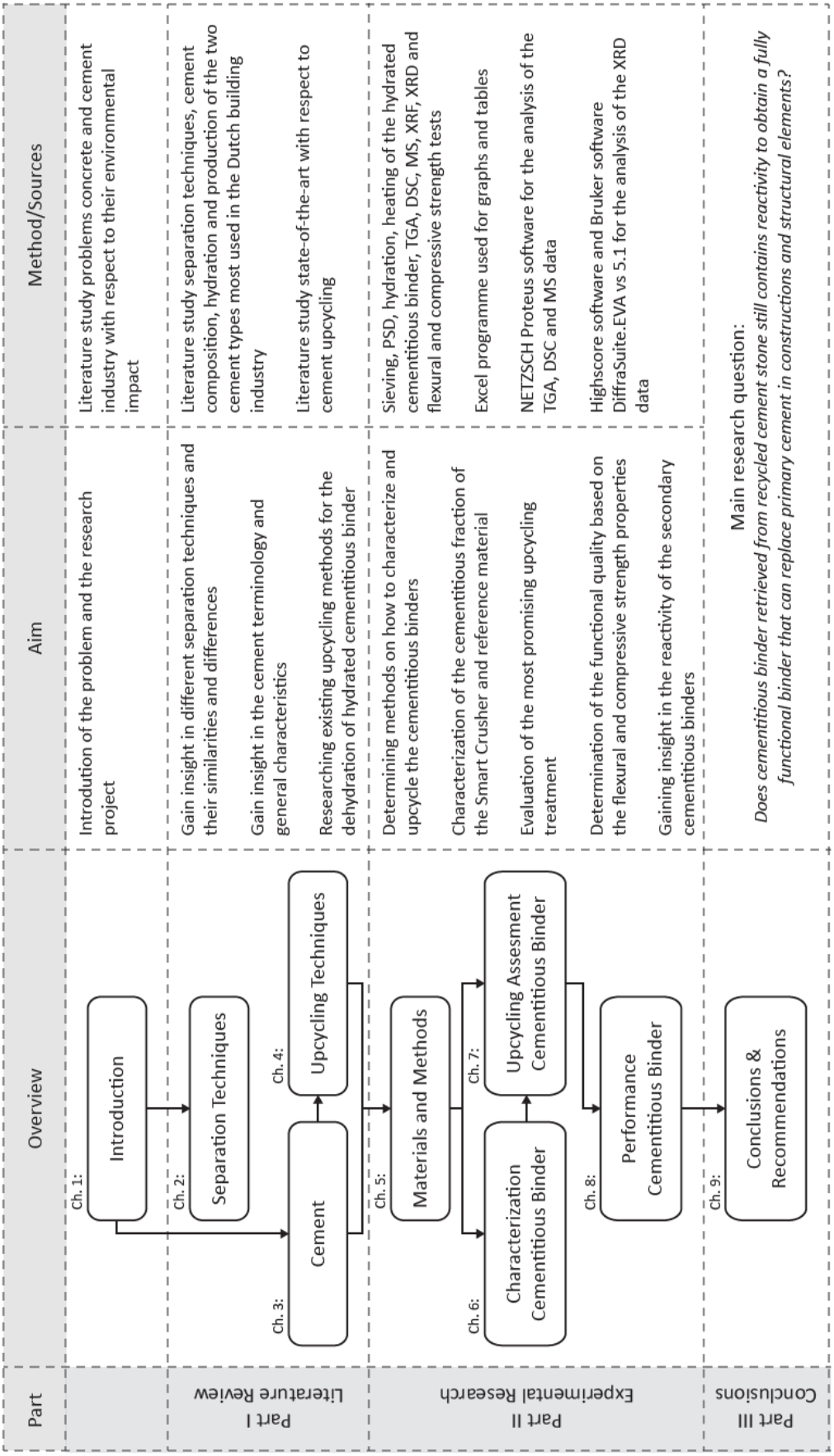

Figure 4: Schematic overview of the main setup of the entire project.

PART I
LITERATURE REVIEW

2 SEPARATION TECHNIQUES

When concrete structures reach the end of their lifespan, they get demolished. In most cases, traditional concrete crushers crush the concrete elements into smaller particle sizes. After separation into different particle size fractions only part of this concrete is reused as a support material. New technologies are being developed, which take into account the reuse of the concrete components in such a way that the material will become partially or fully circular. Interesting to see is in what extent the techniques take into account the recycling of the concrete material in their crushing process. This chapter will mention different separation techniques. Techniques that will be mentioned are the traditional concrete crushers, the Advanced Dry Recovery method and the Smart Crusher.

2.1 Traditional crusher

The crushing of concrete debris to obtain a granular product of a given particle size can be seen as the basic method of recycling. Often, contaminants such as wood, metals and plastics can be found within the concrete debris. The first generation recycling plants did not have the possibility to remove this contaminants. Therefore, the second generation processing plants were developed, which could remove the foreign matter before crushing by means of dry or wet classification. The concrete debris arriving at the processing plants is crushed, using traditional concrete crushers. In total the debris is crushed in two crusher. First in a primary crusher after which the fine material (< 40 mm) is eliminated and the plus 40 mm material is moved to a secondary crusher. Examples of traditional concrete crushers are the jaw crushers, cone crushers, hammer crushers and impact crushers [43]. A short description of the jaw and cone crusher will be given below.

Jaw crushers can be distinguished by two rigid plates called jaws. One of the plates is fixed and serves as a stationary breaking surface. The other plate is the movable jaw, which exerts the force to break the material. Due to compression the material is broken until the desired particle size was reached. The material stays in the crusher as long as these dimensions are not reached. Because the jaw crusher is suitable to crush large pieces of debris, it is often used as primary crusher. The cone crusher uses two cones, where a truncated cone is located around the eccentric axis within a casing that has the shape of a reversed truncated cone. Crushing occurs due to the constantly changing space between the inner and outer cone. Crushed material falls lower into the cone crusher until it has reached the desired particle size [16].

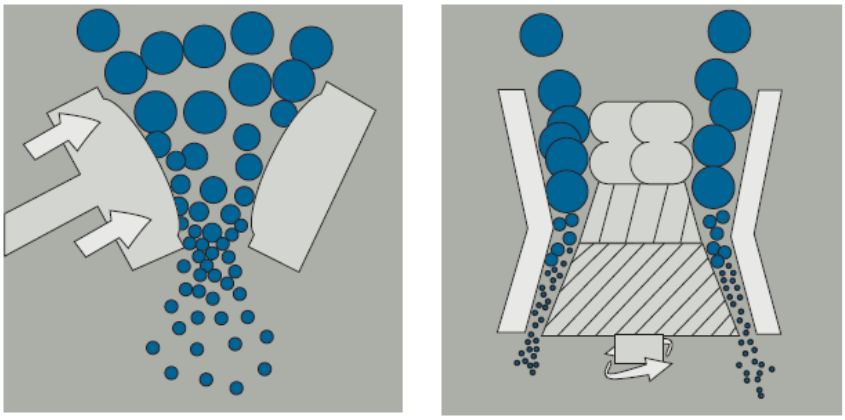

Figure 5: Jaw crusher (left) and cone crusher (right) [16].

Traditional crushers crush the concrete by applying stresses to the particles. These stresses between and in the concrete pieces lead to strains. The material fails when the these strains exceed the elastic limit of the material [113]. The traditional crusher randomly crush the material without taking into account and separating the original concrete components in its crushing process. The purpose of the crushing devices is generally to crush the material into the desired particle size. Where the breaking occurs, is of no importance [87].

2.2 Advanced Dry Recovery (ADR)

The Advanced Dry Recovery method is a separation method for materials in which the components are hard to separate. The method is used after the concrete debris has been crushed by the traditional concrete crushers [16]. Its primary goal is to reduce the amount of fines within the concrete waste. Kinetic energy is used within the ADR-unit to break the water bond associated with the fine particles. After breaking the water bond, the fine particles can be separated from the coarse material [27]. This separation is done based on the particle size and the density [16].

Advanced Dry Recovery performs in a moist state, without drying or wet screening the material. The fine fraction contains not only the cement paste, but also light contaminates such as wood, plastics and foams. Material with the fraction size of 0-16 mm is put into the ADR-unit and after the separation the 4-16 mm fraction contains the coarse material, which is free from any fine particles. The size at which the input material is separated can be adjusted [21]. This method is therefore not a crushing technique, but a method which to reuse the different components after the concrete has been crushed by traditional concrete crushers.

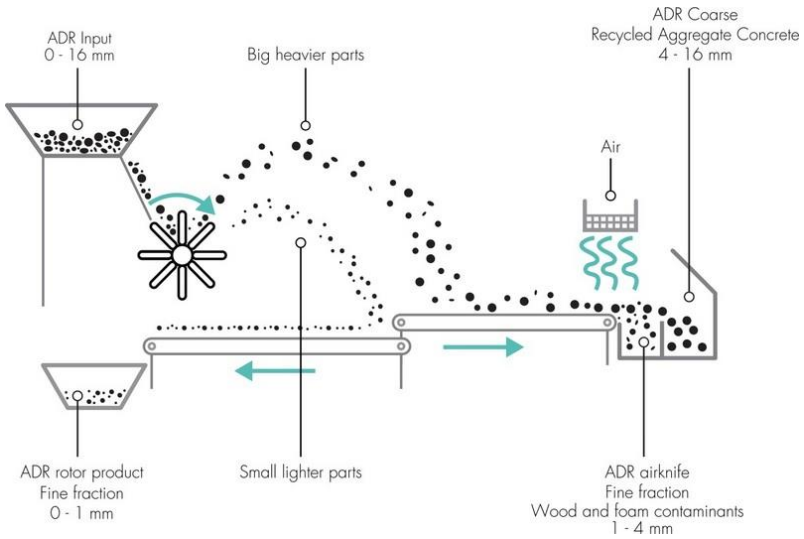

Figure 6: Advanced Dry Recovery principle [21].

2.3 Smart Crusher

The Smart Crusher was developed specially for concrete recycling. The invention was invented by Koos Schenk and patented in 2011. In the patent the invention, which will be called Smart Crusher in this thesis, is described as a separating device for crushing concrete. It aims to separate the components of concrete, such as cement stone, unhydrated cement, gravel and sand, in such a way that a high-value output is realized. The traditional crusher is generally used to reduce the particle sizes and will crush all the components of the concrete randomly. Crushing takes place through the gravel and sand,

because it was not deemed important where the breaking occurs. The Smart Crusher on the other hand, can be adjusted in such a way that crushing of certain components within the concrete is prevented [87]. The way the Smart Crusher works can be explained in five steps:

1. Concrete is fed into the machine in chunks. Using the advanced 'SlimBreken' method the concrete chunks are broken.
2. At the top of the machine the hydrated cement can be extracted and placed in a silo. The hydrated cement consists of the smallest particles and is currently still used as filler for the production of new concrete.
3. At the front of the machine the rest of the crushed concrete, which consists of gravel, sand and unhydrated cement, comes out.
4. Advanced screens can separate the gravel, sand and unhydrated cement. The unhydrated cement is the active material, also called freement.
5. When the materials are separated they are removed and stored in silos or bunkers [86].

Sand and gravel have a different strength and hardness then cement. The Smart Crusher takes this difference into account and only crushes the cement stone. The sand and gravel are left undamaged and are sifted out and they can be used directly as sand and gravel fractions [93]. The pressure exerted by the crushing members can be adjusted depending on the material entering the machine. For concrete the critical limit is about 100 N/mm^2 as to prevent breaking of the gravel. Forces exceeding the limit have an increased risk of breaking the gravel, which is not preferred. The fractions leaving the machine will be separated using different sorting techniques. During sorting of the different concrete components, the relatively large concrete pieces can be filtered and placed back in the separating device [87].

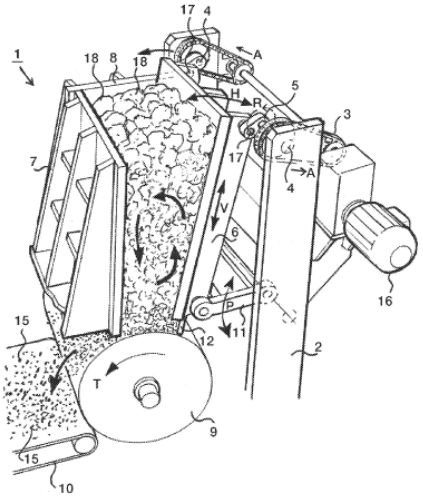

Figure 7: Separating device [87].

3 CEMENT

A large amount of the materials used, consists of cementitious materials. Within the concrete industry different types of cement are used, depending on the project and its requirements. Within the Dutch concrete industry Blast Furnace Cement (CEM III/B) and Ordinary Portland Cement (CEM I) are the cement types with the highest usage share [24]. This chapter will discuss the composition of these two types of cement, because the material used in the experimental research comes from crushed concrete of the Dutch construction industry. Besides the composition, this chapter will also elaborate on the hydration and production processes. Additionally, the identification of the components within the cement types will be discussed. Finally, the workability aspects of cementitious materials will be mentioned.

3.1 Ordinary Portland Cement

Ordinary Portland Cement (OPC) as we know it now, was patented in 1824 by Joseph Aspdin and can be defined as a cement made by burning a mixture of calcareous materials, such as limestone, and argillaceous materials, such as clay, at a clinkering temperature and grinding the obtained clinker. The clinker is usually mixed with gypsum to control the setting rate [70]. According to NEN-EN 197-1 Portland cement clinker is said to be a hydraulic material of which calcium silicates take up a minimum of two-thirds of the mass. The ratio $(CaO)/(SiO_2)$ has to be larger or equal to 2.0 and the amount of magnesium oxide should be smaller or equal to 5.0% of the mass [72]. Within Ordinary Portland Cement four major phases can be distinguished, namely alite (C_3S), belite (C_2S), aluminate phase (C_3A) and ferrite phase (C_4AF). The single letters are an abbreviation based on the following system:

C = CaO	S = SiO_2	A = Al_2O_3	F = Fe_2O_3
M = MgO	K = K_2O	$\bar{S}$ = SO_3	N = Na_2O
T = TiO_2	P = P_2O_5	H = H_2O	$\bar{C}$ = CO_2

Of the four major phases alite and belite are the most important, because of their contribution to the strength development of the cement. Alite influences the early strength, while belite has the most influence on the final strength. The aluminate phase is beneficial during the manufacturing of the cement, but apart from that it is an undesirable phase within the cement. The ferrite phase is the phase with the lowest impact on the behaviour, but it can accelerate the hydration of the alite and belite [70]. The four main phases within the cement will be discussed in detail.

3.1.1 Alite

Alite is a solid solution of a calcium silicate, also seen as impure forms of tricalcium silicate (Ca_3SiO_5). Substitutions of small amounts of Mg^{2+}, Al^{3+} and Fe^{3+} ions can occur, resulting in changes within the composition and crystal structure [20]. Tricalcium silicate, Ca_3SiO_5, can also be written as $3CaO \cdot SiO_2$ or in cement chemistry notation as C_3S. This last notation as well as the use of the term alite will be used to refer to the impure forms of tricalcium silicate in this thesis. As mentioned before, alite influences the early strength of the cement at ages up to 28 days and is seen as the most important component for the strength development due to its high reactivity. Portland cement clinker consists for approximately 50-70% of alite, which is therefore the main mineral phase [101].

All major phases within OPC exhibit a somewhat complex polymorphism depending on impurities or temperature. Polymorphism comes from the Greek language, meaning many shapes. Purohit & Venugopalan (2009) define polymorphism as "the ability of a substance to exist as two or more crystalline phases that have different arrangements or conformations of the molecules in the crystal lattice" [80]. Alite exhibits seven polymorphs, which means that the same molecules can arrange in seven different ways. The seven polymorphs can be divided into three crystal systems; the polymorphs T_1, T_2 and T_3 are triclinic, the polymorphs M_1, M_2 and M_3 are monoclinic and the polymorph R has the rhombohedral crystal system [29]. The sequence of the reversible polymorphic transformations of alite upon heating/cooling are as follows:

$$T_1 \overset{620\,^\circ C}{\longleftrightarrow} T_2 \overset{920\,^\circ C}{\longleftrightarrow} T_3 \overset{980\,^\circ C}{\longleftrightarrow} M_1 \overset{990\,^\circ C}{\longleftrightarrow} M_2 \overset{1060\,^\circ C}{\longleftrightarrow} M_3 \overset{1070\,^\circ C}{\longleftrightarrow} R$$

Figure 8: Polymorphic transformations of alite [101].

The approximation of the crystal structure of the different polymorphs within alite shows that they are built from Ca^{2+}, SO_4^{4-} and O^{2-} ions. Looking at the Ca^{2+} and O^{2-} ions, the positions are closely similar, but the SO_4^{4-} tetrahedra can have a disorder in the orientation. Structural differences between the polymorphs are caused by differences in the atomic position. These structural differences affect the coordination of the Ca^{2+} ions and oxygen atoms within the SO_4^{4-} tetrahedra. Due to the disorder in the orientation of the SO_4^{4-} tetrahedra, several calcium sites with different coordination between individual atoms can be found [101].

Most of the polymorphs are not stable at room temperature even when C_3S is quenched. Pure C_3S exists at room temperature only in its triclinic T_1 form, while the other six higher temperature forms can only be stabilized by using foreign ions [60]. At temperatures above 1070 °C, C_3S has the rhombohedral form. Upon cooling, this polymorphic form will no longer be stable and will transform into monoclinic and triclinic forms. The foreign ions, or impurities, will influence the form of the polymorphs that will be obtained and help stabilizing C_3S at room temperature [45].

Within alite different foreign ions, also called impurities or stabilizing ions, in the shape of minor oxides such as MgO, Al_2O_3, Fe_2O_3 and alkali oxides can be found. The content of the stabilizing ions can vary widely between the clinkers. Figure 9 shows an overview of the possible occurrence in wt.% of the foreign oxides in Portland cement clinker.

	Fe_2O_3	Al_2O_3	MgO	Na_2O	K_2O
Minimum	<0.1	0.6	0.1	<0.1	<0.1
Maximum	4.5	2.7	2.1	1.2	0.9
Typical	0.7	1.0	0.8	0.1	0.1

All data are in wt.%.

Figure 9: Occurrence of foreign oxides in OPC clinker [97].

The kind of substitution that will occur is determined by the ionic radii and preferred coordination [97]. For MgO this means a substitution of Mg^{2+} for Ca^{2+} , because of their comparable ionic radii. For Al_2O_3 the substitution was partly of 2 Al^{3+} for Ca^{2+} + Si^{4+} and partly of 4 Al^{3+} for 3 Si^{4+} and an empty octahedral site. For Fe_2O_3 2 Fe^{3+} could be substituted for Ca^{2+} + Si^{4+}. The amount of substitution of MgO was not influenced by the presence of Al^{3+} and Fe^{3+} and vice versa, while an increase in the amount of Al^{3+} meant a decrease for the substitution limit for Fe^{3+} and vice versa [101]. Not only the type of foreign ions influences the substitution, but also the amount of foreign ions that are substituted. Research has

shown that an increasing amount of foreign ions stabilize high temperature polymorphs. Generally, several different foreign ions are present and the complex interaction between these ions can have different effects on the structure and reactivity of alite. Different factors influencing the interaction can be mentioned, besides the other clinker minerals. Examples are viscosity, appearance, surface tension and amount of liquid formed. It was also found that multiple foreign ions seem to stabilize the high temperature polymorphs more easily than single foreign ions [60].

The contents of MgO and SO_3 play an important role in the stability of the M_1 and M_3 polymorphs. High SO_3 content will result in the formation of larger crystals which result in the M_1 polymorph, while high MgO content will result in smaller crystals which will result in the M_3 polymorph. However, when the alkali to SO_3 ratio is high the formation of the M_1 polymorph will decrease [101]. Staněk and Sulovský (2002) found that the increase of the MgO/ SO_3 ratio resulted in the stabilisation of the M_3 polymorph, while a decrease resulted in the stabilisation of the M_1 polymorph. This is in accordance with what Taylor (1997) stated. Additionally, Staněk and Sulovský (2002) found that when the M_3 polymorph transformed to the M_1 polymorph, the compressive strength increased with 10% after 2, 7 and 28 days. A decrease in strength was observed with an increase in MgO content when the SO_3 content is constant. The increase in MgO content resulted in the transformation of the M_1 polymorph into the M_3 polymorph [96].

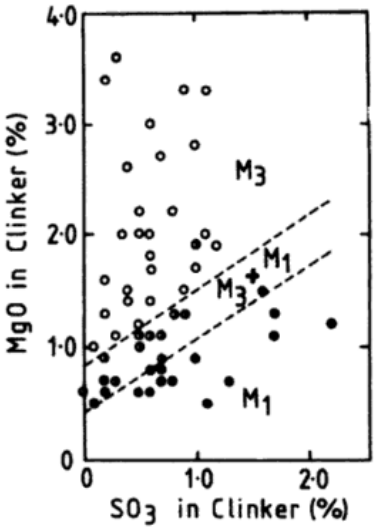

Figure 10: MgO and SO_3 influence on polymorphic transformation [101].

Besides foreign ions, other factors can also influence the polymorphic transformations of alite. The initial properties of the raw meal can have a high influence on the polymorph formations. These properties may include its chemical composition, grain size distribution, mineral composition, contents of minor oxides, especially MgO and SO_3, and the homogeneity at macro- and microlevel. Additionally, factors related to the burning and cooling process can also influence the polymorphic transformation of alite. This includes, the intensity and grade of burning as well as the cooling conditions of the clinker, where the rate of cooling can also play an important role in the transformation of one polymorph towards the other, the duration and temperature at calcination and the evaporation of volatile components such as alkali and SO_3 [96].

3.1.2 Belite

Belite is a solid solution of another calcium silicate, also seen as impure forms of dicalcium silicate (Ca_2SiO_4). Just like alite substitution of small amounts of foreign ions can occur, influencing the crystal structure and composition. Approximately 15-30% of the OPC consists of belite [20]. Dicalcium silicate, Ca_2SiO_4, can also be written as $2CaO \cdot SiO_2$ or in cement chemistry notation as C_2S. As was also mentioned with alite, this last notation as well as the use of the term belite will be used to refer to the impure forms of dicalcium silicate in this thesis. Due to its slow reaction with water, belite contributes little to the early strength, but considerably to the strength after longer times. Pure alite and pure belite will reach comparable strengths after one year under comparable conditions [101].

Dicalcium silicate can exist in multiple polymorphic forms, just like tricalcium silicate. Overall five polymorphs of belite can be identified, namely the α (hexagonal), α'_H (orthorhombic), α'_L (orthorhombic), β (monoclinic) and γ (orthorhombic) polymorphs. Upon heating and cooling belite

undergoes several polymorphic transformations. Each of these transformations is accompanied by a change in volume [25]. The sequence of the polymorphic transformation of belite is as follows:

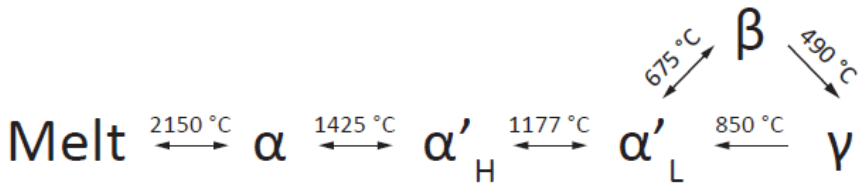

Figure 11: Polymorphic transformations of belite [69].

With increasing temperature, belite undergoes several phase transitions. At low temperatures the γ phase is the most stable. The sequence of phase transitions γ → α'_L → α'_H → α can be distinguished upon heating. The occurring polymorphic transformations are partly reversible, though at the lower temperatures the order deviates upon cooling due to the formation of the metastable β phase. Additionally, the γ phase will undergo a volume change upon cooling [81]. Because the reversible transformation of β-C_2S to γ-C_2S takes place below 500 °C, both phases normally coexist. The α, α'_H and α'_L phases do not exist in the clinker in most cases, because they will easily transform into β-C_2S upon cooling [114].

Upon cooling, the α phase will transform into the α'_H phase, which will in turn transform into the α'_L phase. The α'_L phase will not transform into the γ phase, but a metastable β phase is inserted between the α'_L phase and γ phase. The transformation from the α'_L phase to β phase occurs around 675 °C. Further cooling will result in a transformation from the β to γ phase at temperatures below 500 °C of approximately 490 °C. This transformation from β-C_2S to γ-C_2S involves a volume change of about 12% and an angular unit-cell change of 4.6° [25]. This also becomes clear when looking at the densities of the two phases, 3.28 g/cm^3 for β-C_2S and 2.97 g/cm^3 for γ-C_2S. The increase in volume results in stress, which is high enough to pulverize the clinker nodules [114]. This phenomenon is also known as dusting and can sometimes be recognized by the white powder in the clinker production [81].

Where the stabilized polymorphs of C_3S have similar hydration rates, this cannot be said of the C_2S polymorphs. Even though γ-C_2S is stable at room temperature, it is weakly hydraulic and therefore not beneficial for the long term strength development. This means that the other polymorphs, which are metastable and have a greater hydraulic reactivity, should be stabilized at room temperature [11].

The incorporation of foreign ions is one of the possibilities to stabilize the polymorphs of C_2S. Al^{3+} and Fe^{3+} are the most commonly found foreign ions, but S^{6+}, Mg^{2+} and K^+ are also observed sometimes. Additionally, it was found that P_2O_5 and B_2O_3 are both very successful stabilizers, especially boron [111]. Many researchers have investigated the effects of foreign ions on the stability of the different polymorphs, but due to differences in experimental conditions the results could vary. Chan et al. (1992) found that K_2O and Al_2O_3 dopants resulted in a metastable retention of β-C_2S at room temperature. Besides this, it was also mentioned that the stabilization of β-C_2S against the transformation to γ-C_2S also depends on the cooling kinetics, microstructure, previous undergone transformations and amorphous phases [25]. Wesselsky and Jensen (2009) found that B_2O_3 is a good stabilizer for β-C_2S and that α'-C_2S can be stabilized by B_2O_3 in combination with Na_2O [111]. Benarchid et al. (2005) looked into the stabilizing effects of iron (Fe_2O_3) and phosphorous (P_2O_5) additions and concluded that these additions resulted in the formation of β-C_2S, α'-C_2S and α-C_2S at room temperature. Additionally, it was mentioned that an increasing P_2O_5 concentration could stabilize the belite forms following the sequence β → α' → α [13].

Ghosh (1983) identifies two types of stabilization, namely crystal chemical stabilization and physical stabilization. The first one involves the foreign ions, also mentioned as stabilizing ions. The latter one involves external influences, such as the cooling rate [37]. When belite is quenched after heating to 1550 °C, β-C_2S is mostly formed due to the fast transformation of α → $α'_H$ resulting in small $α'_L$ crystals. But when belite is quenched after being slowly cooled to 1400 °C, mostly γ-C_2S is formed [38].

Looking at the structure of the belite polymorphs it was found that all the polymorphs consist of free SiO_4 tetrahedra linked by calcium ions, but the difference in the polymorphs can be found in changes in the reciprocal arrangement of the tetrahedra and calcium coordination [38]. The $α'_H$ and $α'_L$ phases are said to be similar in structure and it is believed that these phases are fairly complex superstructures of the α' structure. Additionally, it was mentioned that the displacive transformation between the $α'_H$ and $α'_L$ phases is seen as very weak [9]. First the transformation from the α' to β phase will be discussed. In α'-C_2S the coordination of the Ca-ions is eightfold, while β-C_2S has a different coordination number for both Ca-ions. One of the Ca-ions has a coordination number of eight, while the other has a coordination number between six and nine. During the transformation the SiO_4 tetrahedra will undergo a rotation together with breaking a few Ca-O bonds. The γ phase is in most cases described as somewhat different from the α' and β phases, but a slight similarity can still be found. For the SiO_4 tetrahedra and one of the Ca-ions the relative positions are identical, while the other Ca-ion is shifted, but still related to the same SiO_4 tetrahedra. A rotation of the SiO_4 tetrahedra together with a change in coordination of Ca results in the transformation from the γ to the α' phase and the β phase to the γ phase. The γ phase has a lower density, which can be explained by the coordination of the structure, namely a sixfold coordination of the Ca. During cooling the α' phase transforms into the β phase due to their similarity. This similarity shows insight in the reason why the transformation to the γ phase does not occur [94].

As mentioned before the γ phase is weakly hydraulic, whereas the β phase has a good reactivity. Their difference in reactivity can be explained due to the difference in their crystal structure, especially the differences in their calcium coordination. The reactivity is linked to the splitting of the Ca-O bonds. It is said that the total strength of the bonds around an ion has to be equal to its formal charge. Looking at oxygen this would mean two units. Because one of the units of bond strength belongs to a Si-O bond, the other unit has to be divided among the n Ca-ions to which the oxygen is coordinated. For the γ phase n equals 3, while the β phase has a n equal to 3 or 4. Additionally, the Ca-O bonds in the β phase are weaker. This means that the hydrogen ion has a higher probability of splitting a Ca-O bond in the β phase [94].

3.1.3 Aluminate phase

The aluminate phase can occur as a series of solid solutions within Portland cement and is mostly referred to as tricalcium aluminate ($Ca_3Al_2O_6$). Foreign ions, especially Si^{4+}, Fe^{3+}, Na^+ and K^+, can modify the composition and sometimes also the structure of the aluminate phase. Around 5-10% of the OPC consists of aluminate phases. Tricalcium aluminate, $Ca_3Al_2O_6$, can also be written as $3CaO \cdot Al_2O_3$ or in cement chemistry notation as C_3A. This last notation will be used to refer to the impure forms of tricalcium aluminate in this thesis. As mentioned before the aluminate phase is beneficial during the manufacturing of the cement, but apart from that it is an undesirable phase within the cement. Because the aluminate phase reacts rapidly with water a set-controlling agent, usually gypsum, is added to make sure the undesirable rapid setting of the material does not occur [101].

Approximate Na_2O (%)	Compositional range (x)	Designation	Crystal system	Space group
0–1.0	0–0.04	C_I	Cubic	Pa3
1.0–2.4	0.04–0.10	C_{II}	Cubic	$P2_13$
2.4–3.7	0.10–0.16	$C_{II}+O$	–	–
3.7–4.6	0.16–0.20	O	Orthorhombic	Pbca
4.6–5.7	0.20–0.25	M	Monoclinic	$P2_1/a$

Figure 12: C_3A modifications [39].

C_3A in its pure form does not exhibit polymorphism. The pure form is cubic and the structure consists of Ca^{2+} ions and rings of six AlO_4 tetrahedra [39]. In impure form tricalcium aluminate is one of the main components in Ordinary Portland cement. The holes within the sixfold rings, composed of two distorted AlO_4 tetrahedra, contain either the Ca atoms or are left vacant. In total eight vacant holes can be distinguished within the C_3A structure [67]. Within the impure form of the C_3A structure the Ca^{2+} ions can be substituted by Na^+ ions with incorporation of another Na^+ ion in a vacant hole. The degree of substitution influences the structure. Up to a substation of 1% Na_2O the structure does not undergo any changes, but with higher substitution percentages a series of variations occur in the structure. The structure as described before has a maximum of 1% Na_2O present and the crystal structure can be described as the cubic C_I structure. A minor variant of this structure is the cubic C_{II} structure, with a maximum of 2.4% Na_2O present and a lower symmetry. The additional Na^+ ions in both structures are placed in the centre of the Al_6O_8 rings, which can be found in the subcells of the C_3A structure. The orthorhombic O structure shows similarities with the previous mentioned crystal structures, but is completely different in the arrangement of the rings within the unit cell. The monoclinic M structure is a slightly deformed variant of the O structure. Within the production of cement clinkers mostly the cubic or orthorhombic structures can be found. The monoclinic structure is normally not found [101]. The reason that the monoclinic modification does not occur, is because it changes to orthorhombic at a transition temperature. Varma et al. (1981) believes that besides the primary role Na_2O plays in the appearance of different modifications, also compounds like K_2O enter the lattice, but that elements like Mg, Na, Si, etc. are needed to encourage the modification. Additionally, they believe that there is an excess of K^+ needed in soluble sulphates [106].

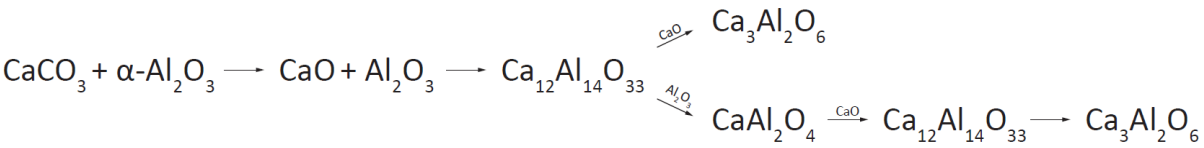

Figure 13: Reaction scheme of the formation of C_3A [66].

Mohamed and Sharp (2002) give an indication of the mechanism of formation of C_3A. When the temperature reaches about 900 °C, calcite will decompose into lime. This lime (CaO) will react with alumina (Al_2O_3) upon further heating, resulting in the formation of $Ca_{12}A_{14}O_{33}$ which can be seen as the principal reaction intermediate. After this, there are two possibilities for the proceeding reaction, namely a reaction with CaO, resulting directly in C_3A, or a reaction with Al_2O_3, resulting in an intermediate phase CA, which will then reacts until C_3A is formed [66].

Besides Na^+ ions stabilizing different polymorphs, other ions, such as Si^{4+} and Fe^{3+}, or a combination of these ions with Na^+ can also have a stabilizing effect on certain polymorphs. Si^{4+} can substitute Al^{3+} when it reaches a certain quantity, which results in enlarging the range of stability of the orthorhombic polymorph. Additionally, Fe^{3+} can also have a stabilizing effect on the orthorhombic phase within C_3A. Besides the presence of foreign ions, which need to be present in a certain amount to have a stabilizing effect, the bulk composition, temperature conditions and cooling rate also have an effect on the polymorphs. The boundaries between polymorphs may differ somewhat based on the cooling rate [55].

3.1.4 Ferrite phase

The ferrite phase can occur as a series of solid solutions and is mostly referred to as tetracalcium aluminoferrite (Ca_2AlFeO_5). The composition changes under the influence of ionic substitutions and variations in the Al/Fe ratio. The Portland cement clinkers consist of approximately 5-15% ferrite phases. Tetracalcium aluminoferrite, Ca_2AlFeO_5, can also be written as C_4AF in cement chemistry notation [101]. Taking a closer look at the composition of the ferrite phase, it can be seen as a limited solid solution between C_2F and C_6A_2F with $C_4A_xF_{(1-x)}$, where $0<x<0.7$. This means that C_4AF is only one of the possible compositions in the series [11]. In this thesis the C_4AF notation will be used to refer to the ferrite phase.

Unlike the other major components within Portland cement, C_4AF has no known polymorphs, but as mentioned before the composition can differ slightly [95]. The crystal structure is made out corner-sharing octahedra alternating with layers of tetrahedra chains, combined with Ca^{2+} ions. Within the structure each Ca^{2+} ion has 7 oxygen neighbours and a distribution of iron and aluminium atoms can be distinguished between the octahedral and tetrahedral sites. The temperature influences the amount of aluminium entering the tetrahedral sites [101].

Ghosh (1983) mentions that the ferrite contains a large amount of foreign ions as impurity. Impurities which can be found within the lattice of this phase are Mg^{2+}, Si^{4+}, Ti^{4+}, Mn^{3+} and Cr^{3+} [37]. The Fe^{3+} ions can be fully replaced by Mn^{3+} and the Al^{3+} ions can be replaced by Mn^{3+} up to 60%. Mg^{2+} and Si^{4+} incorporation within the ferrite phase can have an increasing effect on the cell parameters. The Ti^{4+} substitution occurs in a relatively small amount and causes stacking changes with the ferrite phase. As mentioned before additional factors may also influence the structure of the ferrite phase, such as the cooling and heating conditions of the clinker [101].

3.1.5 Hydration

The term hydration can be defined as “a reaction of an anhydrous compound with water, yielding a new compound, a hydrate” [45]. Within cement chemistry this means that cement or one of its components, in non-hydrated form, will react with water. This reaction with water results in changes in the system. Depending on the amount of water available for the reaction the cement can be partly or completely hydrated. The amount of water or the water/cement (w/c) ratio does not only influence the progress of the hydration, but also the properties of the hydrated cement and its workability. Besides the used water/cement ratio, there are multiple factors influencing the hydration progress and its kinetics, especially the fineness of the cement, the curing temperature, the composition of the cement and the presence of foreign ions, chemical admixtures or additives [45].

The hydraulic reactivity of the components within Portland cement are dependent on the crystal structure, polymorphic forms, defects or disorder in the crystals, stabilizing ions and solid solutions. The four main components, which were discussed previously, differ in their hydraulic reactivity. All the components are hydraulic, but C_3A was found to be the component with the highest hydraulic reactivity. In order of highest to lowest hydraulic reactivity the aluminate phase is followed by alite, then the ferrite phase and finally belite [37]. Insight will be given into the different hydration reactions occurring within Portland cement.

During the hydration of the two calcium silicates, alite and belite, calcium silicate hydrates are the products formed. Written in cement chemistry notation, the following approximate hydration reactions are found:

$$C_3S + 6H \rightarrow C_3S_2H_3 + 3CH$$
$$2C_2S + 4H \rightarrow C_3S_2H_3 + CH$$

The hydration products are mostly referred to as C-S-H and calcium hydroxide (CH), also mentioned as portlandite. C-S-H is a rough approximation and the dashes imply that a particular composition is not implied. Not only is C-S-H very poorly crystalline, but also more than one variety is formed during the hydration process. C-S-H is the most important contributor to the early compressive strength development of Portland cement and is also seen as the main binder for the hardened Portland cement paste. Belite hydrates slower than alite, but the formed hydration products are similar. The amount of calcium hydroxide is less than during the hydration of alite. This can be advantageous for the strength development, because the bigger the portion of C-S-H to calcium hydroxide the better the compressive strength will become [37].

During the hydration of the aluminate phase the following hydration reaction is found, written in cement chemistry notation:

$$2C_3A + 21H \rightarrow C_2AH_8 + C_4AH_{13} \rightarrow C_3AH_6$$

In first instance, the hydration of C_3A forms hexagonal plate hydrates, which eventually convert to a more stable cubic form. When the temperature is high enough the stable cubic form can also directly be formed during hydration. The hydration of the ferrite phase is similar to that of the aluminate phase in a lime medium, which is present in Portland cement, both with and without the presence of gypsum. C_3A has a fast reaction with water and develops a large amount of heat. The rapid reaction with water, the progressive reaction of C_3S and the contribution of the other phases result in an increase in temperature and irreversible stiffening. This is followed by an undesirable rapid setting, referred to as “flash set”. To prevent this and to control the setting reaction, gypsum is added to the clinker. The addition of gypsum results in the formation of ettringite, which is a very insoluble and alkaline calcium sulphate solution. The ettringite forms a barrier against the rapid hydration, by forming a layer on the surface of the C_3A. This way the reaction rate depends on the diffusion rate of the water through the ettringite layer and flash set is avoided [37]. The hydration reaction of the aluminate phase in the presence of gypsum, resulting in the formation of ettringite, can be written as follows in cement chemistry notation [65]:

$$C_3A + 3C\bar{S}H_2 + 26H \rightarrow C_6A\bar{S}_3H_{32}$$

As mentioned before, C_4AF forms similar hydration products as C_3A, but the reactions are slower and less heat is formed. The presence of gypsum retards the hydration of C_4AF even more. Changes in the composition of C_4AF will influence the hydration rate only. For example, a larger iron content results in a slower hydration reaction. Additionally, gypsum will increase the hydration rate of the calcium silicates [65].

The hydration reactions within the Portland cement are exothermic. This means that all the hydration reactions are accompanied by the liberation of heat. The heat evolution is mostly determined by C_3S and C_3A, which can be explained by their fast hydration rate, especially during the early hydration times. From the main components C_2S has the slowest reaction rate and therefore also the smallest amount of heat evolution. Looking at a typical heat evolution curve the contributions of C_3S and C_3A can generally be distinguished [65]. This curve can be divided into the five stages, which occur during the hydration of Portland cement. These five stages correspond mainly to the hydration of alite [61]. The following stages occur:

Compounds	Reaction Rate	Amount of Heat Liberated	Contribution to Cement: Strength	Contribution to Cement: Heat Liberation
C_3S	Moderate	Moderate	High	High
C_2S	Slow	Low	Low initially, high later	Low
$C_3A + C\bar{S}H_2$	Fast	Very high	Low	Very high
$C_4AF + C\bar{S}H_2$	Moderate	Moderate	Low	Moderate

Figure 14: Characteristics of the hydration of the cement compounds [65].

I. Initial dissolution
II. Induction period
III. Acceleration period
IV. Deceleration period
V. Diffusion stage

The first stage shows an exothermic peak due to the dissolution of anhydrous phases and the wetting of the cement surface. Additionally, ettringite precipitation occurs. After this, the reaction suddenly slows down and the induction period starts. The induction period can be seen as a latent period, which marks the end of a period of chemical activity and the onset of the acceleration period. During the acceleration period the dissolution of C_3S increases. This can be recognized by the main peak. Additionally, a large precipitation of CH and C-S-H occurs. After this the reaction slows down, which is the starting point of the deceleration period. In this period another peak can be distinguished, which represents the high dissolution of C_3A and the larger precipitation of ettringite. When the deceleration period is finished a period of low activity starts, which is known as the diffusion stage [61].

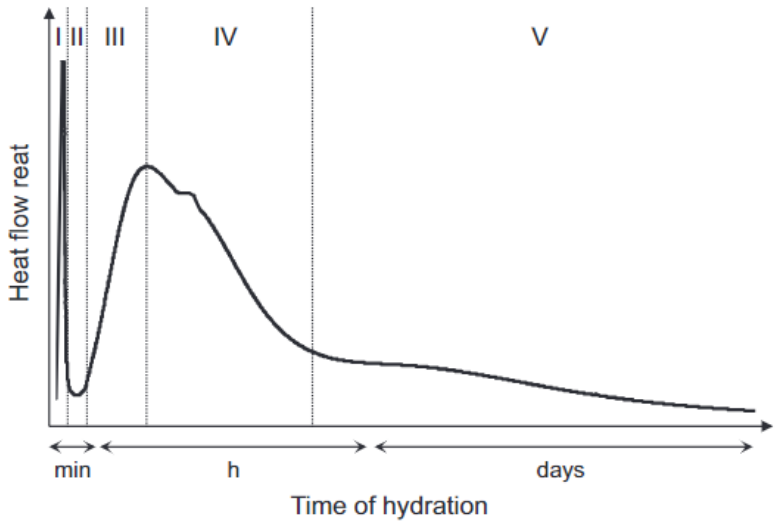

Figure 15: Heat release and different stages during the hydration of Portland cement [61].

3.1.6 Production

By grinding of Portland cement clinker with gypsum and/or anhydrite, Portland cement is made. Hewlett (2004) mentions in Lea's Chemistry of Cement and Concrete different standards defining cement and shows requirements for the cement composition. The first one mentioned is the European Standard ENV 197-1, which mentions that the sum of the reactive calcium oxide and the reactive silicon dioxide has to be at least 50% by weight. This is compared with the ASTM (American Society for Testing and Materials) Standard C 150-95, which mentions an optional maxima of 35% for tricalcium silicate, 7% for tricalcium aluminate and a minimum of 40% for dicalcium silicate. Differences in the requirements for the cement composition can be found in these standards. For example, ENV 197-1 dictates a limit for the amount of magnesia of 5.0%, while ASTM C 150-95 dictates this limit to 6.0% [45]. Therefore, it is important to take into account which standards are applicable.

To obtain the desired composition and fineness, raw materials are selected, crushed, ground and proportioned. As mentioned before, Portland cement is mostly made of calcareous (limestone or chalk) and argillaceous material (clay or shale). Other silica-, alumina-, and iron-oxide bearing materials can be added to obtain the required composition [70]. The chemical composition can also be influenced by additional elements entering the system. These can come from the fuel or the raw meal and need to be watched to make sure it will not affect the production of the clinker negatively. Not only the chemical composition of the raw materials is of importance, but also the physical form. The raw materials differentiate in hardness and fineness. It was mentioned that to obtain an suitable alite size for sufficient strength-giving properties, the quartz and acid-insoluble materials present have to be smaller than 45 µm. Additionally, the calcite component has to be smaller than 125 µm [45].

Calcium silicates belong to the main components of Portland cement. Therefore, calcium and silica play an important part in the production of the cement. Limestone and chalk, but also marl and sea-shells are calcium carbonate materials and can be used as sources of calcium. Within these materials impurities are usually present, which can influence the composition. Examples of impurities are clay or dolomite. Additional silica can be obtained from clay or shales, but also from quartz. Although quartz is not preferred, because it does not react with lime easily. To form the calcium silicates, aluminum, iron, magnesium ions, and alkalies are added, because of their mineralizing effect. This means that the calcium silicates can be formed at lower temperatures. The addition of these components can be done using clay, which contains alumina (Al_2O_3), iron oxide (Fe_2O_3) and alkalies, or through addition of bauxite and iron ore. As a result, also aluminates and aluminoferrites of calcium are present within the Portland cement. The main raw materials undergo the following chemical reaction in the cement kiln [63]:

$$\begin{aligned}
&\text{Limestone} && \rightarrow \ \mathrm{CaO} + \mathrm{CO_2} \\
&\text{Clay} && \rightarrow \ \mathrm{SiO_2} + \mathrm{Al_2O_3} + \mathrm{Fe_2O_3} \\
&\text{Limestone} + \text{Clay} && \rightarrow \begin{cases} 3\mathrm{CaO} \cdot \mathrm{SiO_2} & \mathrm{C_3S} \\ 2\mathrm{CaO} \cdot \mathrm{SiO_2} & \mathrm{C_2S} \\ 3\mathrm{CaO} \cdot \mathrm{Al_2O_3} & \mathrm{C_3A} \\ 4\mathrm{CaO} \cdot \mathrm{Al_2O_3} \cdot \mathrm{Fe_2O_3} & \mathrm{C_4AF} \end{cases}
\end{aligned}$$

Certain constituents can have an adverse effect on the production and performance of the product. Even in small amounts the effects can be influenced negatively. Alkalis, including sodium and potassium, is one of the most important constituents to take into account. When the alkalis reacts with certain aggregate types in the presence of moisture, known as alkali-silica reaction, a gel is formed. This gel has expansive properties, which can result in cracking of concrete or mortar. Additionally, the

amount of sulfate in combination with alkalis has to be taken into account, because sulfate has the ability to maintain the alkalis as their sulfates. When the amount of sulfate is not sufficient, Na_2O entering C_3A increases the reactivity, possibly resulting in setting problems. Another possibility is that K_2O enters C_2S and again increases the reactivity and inhibits its conversion to C_3S. The viscosity of the flux can also be influenced by the alkalis content, decreasing the viscosity when the alkalis are present as their sulfates. This results in an increasing formation of C_3S and increases its crystal size, restricting its hydraulic reactivity. The maximum amount of chlorides present also need to be taken into account and limited, because it can result in serious corrosion of the reinforcement in concrete. Besides alkalis, sulfur and chlorides, fluorine is also of interest. The addition of certain amounts of fluorine can reduce the viscosity of the flux, enlarges the setting time and hardening at lower temperatures, and lower the strength. Aside from the mentioned minor constituents, which are the most important to be aware of, other minor constituents, such as manganese oxide, titanium oxide, zinc oxide, etc. should also be taken into account [45].

The manufacturing process of cement can be split into different components, such as the preparation of the raw material and fuel supply, pyroprocessing, storage, packing, and loading. Within cement manufacturing, pyroprocessing of raw materials can be seen as the core function. A rotary kiln is used during this process, which consists of a long tube that is inclined and rotates slowly. The crushed raw material mix entering the kiln, will increase in heat as it moves from the upper end to the lower end of the kiln. During the heating of the raw material mix, chemical reactions occur resulting in the formation of the clinker minerals. These reactions are dependent on which kiln technology is used. Different dry kiln technologies can be used, but the oldest technology used, are the wet kilns, which are also the largest kilns in use today. Furthermore, the wet kilns consist of all five major pyroprocessing functions, namely the drying, preheat, calcining, sintering or burning and cooling zone [105].

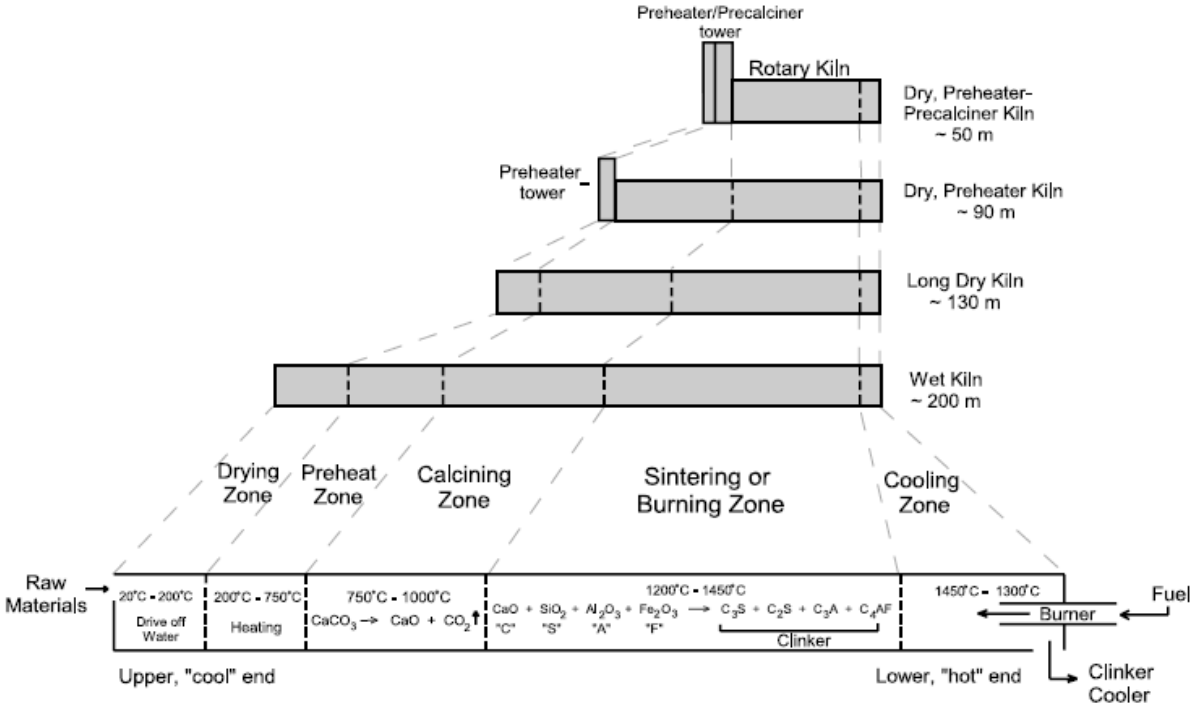

Figure 16: Different rotary kilns and their functional zones [105].

Van Oss and Padovani (2002) mention though that the scheme of figure 16 is too rigid in its splitting of the different zones, because a large part of the calcination can occur in the preheating zone [105]. Peray (1986) looked into the rotary kiln, not only theoretical, but also the kiln operation. He mentions slightly different reaction zones, but the overall occurring reactions are comparable. Five reactions zones are mentioned within the kiln system. The upper-transition zone and the sintering zone are defined by kiln operators as one unit, namely the burning zone. In the drying and preheating zone the temperature is raised until the evaporation temperature of water is reached. This results in the evaporation of the free water after which the temperature is raised until the chemically bound water will be liberated. Subsequently, the feed is raised to the calcining temperature. In the calcining zone calcination occurs, which can be described by the following two reactions [78]:

Reaction zones	Temperature range of material [°C]
Drying and preheating zone	15-805
Calcining zone	805-1200
Upper-transition zone	1200-1400
Sintering zone	1400-1510
Cooling zone	1510-1290

Figure 17: Reaction zones in the rotary cement kilns [78].

$$CaCO_3 \text{ (Limestone)} \rightarrow CaO + CO_2$$
$$MgCO_3 \text{ (Magnesium carbonate)} \rightarrow MgO + CO_2$$

Important is that the kiln feed has to be calcinated completely before entering the burning zone, otherwise it will be difficult to burn. In the calcining zone the amount of limestone is reduced, while free lime is formed. Within the upper-transition zone interim-phase formations can occur, but there is also an area within the kiln in which calcination and interim-phase formations can overlap each other. Interim compounds are formed after calcination due to a reaction with silica, iron or alumina. The final stages of the clinker formation, which results in the formation of the major compounds of cement, occur in the sintering zone. Within this zone the mix reaches its maximum temperature, after which the clinker moves towards the cooling zone or lower-transition zone. The cooling of the clinker is an important part of the production process. Cooling can be done either slow or rapid and has a big influence on the quality of the material. Looking at quality and grindability, a rapid cooling is preferred. In the first quenching compartment the clinker undergoes rapid cooling [78]. When the cooling is slow, C_3A can crystalline and alite can redissolve into the liquid phase, resulting in the formation of secondary belite [45].

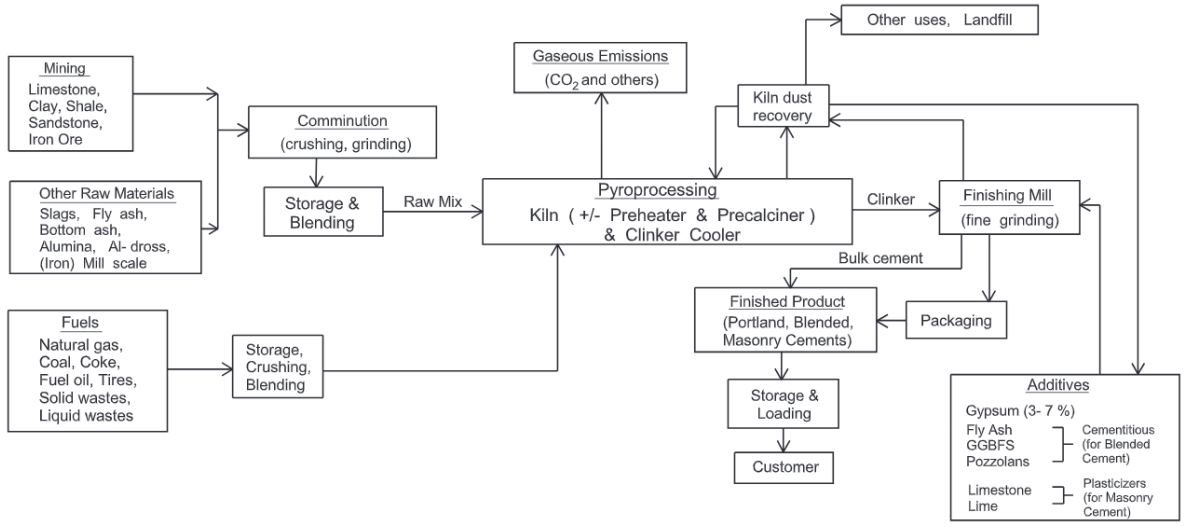

Figure 18: Simplified overview of the clinker and cement manufacturing [105].

3.2 Blast Furnace Cement

Blast furnace slag is formed during the manufacturing of pig iron, when slagging agents are added to the iron ore for the removal of impurities. A non-metallic liquid, also called molten slag, floating on top of the molten iron forms during the reduction of iron ore to iron and is separated from the metallic liquid after which it is cooled. Ground granulated blast furnace slag is the slag produced after quenching the molten slag with a fast enough cooling rate using water. It is a latent hydraulic material, which means that the material has pozzolanic and cementitious properties [57]. According to NEN-EN 197-1 granulated blast furnace slag has hydraulic properties when it is properly activated and contains at least two-thirds of glassy slag. The sum of calcium oxide (CaO), magnesium oxide (MgO) and silicon dioxide (SiO_2) has to be at least two-thirds by weight. Additionally, the ratio (CaO + MgO)/(SiO_2) has to be larger than 1.0 [72]. Blast furnace cement is one of the most frequent used cement types within the Dutch concrete industry and therefore more insight in the material will be of significant help for the experimental research.

3.2.1 Composition and structure

The major components within blast furnace slag are: MgO, Al_sO_3, SiO_2 and CaO. The process that is used to make the steel and the type of steel has a large influence on the chemical composition of the slag [35]. The most common ranges of the constituents are:

SiO_2	CaO	Al_2O_3	MgO	Fe_2O_3	S	Cr_2O_3	Na_2O+K_2O	MnO_2	P_2O_5	TiO_2
27–40%	30–50%	5–33%	1–21%	<1%	<3%	0.003–0.007%	1–3%	< 2%	0.02–0.09%	<3%

Figure 19: Chemical composition range of blast furnace slag [35].

The ranges of the constituents can vary widely depending on the ores and furnace operation. Additionally, the chemical composition can vary for each country, but it was found that slags of different countries have similar SiO_2 and CaO contents. A noticeable difference could be found in the MgO, Al_sO_3 and TiO_2 contents [90]. The chemical composition determines the structure of a glassy slag. This structure uses a two-dimensional framework of SiO_4 tetrahedra. The internal structure of slag glasses can be discussed, using a proposed network theory, called vitreous structure theory, which assigns the components of a glass to three different groups, namely network formers, network modifiers and intermediates. Four oxygen atoms are surrounding the network formers, which have the highest possible ionic valency and small ionic radii. Within blast furnace slag possible network formers are Si and P. A kind of disruptive three-dimensional network through tetrahedra is formed by the network forms in combination with the oxygen atoms. A higher amount of network formers will result in a higher degree of condensation of the glass. Examples of network modifiers are Na, K and Ca. In contrast to the network formers, network modifiers have large ionic radii. They disorder and depolymerize the network. The third group contains the intermediates, such as Al and Mg, which can be both network formers as network modifiers. When the amount of network formers increases, the glass will become less reactive [90].

Within glassy slags the Si-O-Si bonds can be broken and neutralized by network modifiers. Bridging oxygen atoms isolate or polymerize the silica tetrahedra. Within the cavities of the network the octahedrally coordinated Ca^{2+} or Mg^{2+}, which can be either octahedral or both octahedral and tetrahedral, neutralize the negative charge of the condensed group. When magnesium is octahedral it will act as a network modifier and when it is tetrahedral it will act as a network former [45].

Granulated slag has a low hydraulic activity, but when it is combined with some suitable activators the hydraulic activity is found to be remarkable. Possible activators are Portland cement, lime, alkalis, calcium or magnesium. Except for its lower lime content, the slag is similar in composition to Portland cement. Therefore, mixing the slag with limestone will bring the composition to the required value in a mixture for Portland cement [45]. The slag is either blended or interground with Portland cement clinker. Attention has to be paid to the difference in grindability of the slag and Portland cement, because slag is usually harder to grind. When grinding both materials together, the slag could be grinded too coarsely, while the Portland cement clinker could be grinded too finely. Therefore, separate grinding of the materials may be preferred. Another point of interest is that the slag can lower the early compressive strength, while the eventual compressive strength can increase slightly. This is influenced by the amount of slag used to replace the Portland cement. The reactivity of the slag plays a primary role in its suitability for use in cement. Besides the reactivity the grindability, water content and content of undesirable components also need to be taken into account. The most important factors influencing the reactivity are the fineness, bulk composition and glass content [101]. Wang et al. (2005) mentions that the reactivity increased when the fineness increased. For the compressive strength up to 7 days the 20-0 µm fraction was the crucial fraction, while the fractions of larger fineness did not affect the compressive strength. Looking at the compressive strength after 28 days, the 40-20 µm fraction also participated. Larger fractions have an almost inert behaviour. Therefore, the slag needs to be grounded to a particle size of 40 µm or smaller to obtain an effect on the strength after 28 days [110]. Additionally, the ASTM C 989-04 mentions an maximum amount of 20% obtained when wet screened on a 45 µm sieve [4].

3.2.2 Hydration

Looking at the hydration of slag cement, many studies indicate that the hydration products are similar to those of Portland cement. A difference can be found in the amount of CH found. Hydration of slag cement results in a lower amount of CH compared to Portland cement [101]. Generally, within blast furnace cement it is assumed that calcium hydroxide and gypsum act as activators. From these two, gypsum does not have the most activating effect, but is important for the formation of the ettringite related phase. The activator calcium hydroxide provides hydroxyl ions, which attack the glassy slag [38]. Therefore, the hydration of the slag influenced by the calcium hydroxide is of interest. The hydration products formed by the Portland cement cover the slag surface. After this, the slag surface is attacked by Ca^{2+} ions from the saturated solution, resulting in the formation of the inner hydrate. This layer appears to be dense and crystallized. The skeleton hydrate layer is formed due to the dissolution of Ca^{2+} and Al^{3+} ions form the slag. Ca^{2+} ions are supplied to the skeleton layer, which then transforms into the inner hydrate. From the skeleton hydrated layer to the outer hydrate the Ca/Si ratio increases, while the Al decreases. Additionally, a higher concentration of Mg^{2+} ions is found in the skeleton hydrate than in the inner hydrate or anhydrous slag. For research purposes a gold coated surface was added before the hydration. This surface showed the position of the original slag solution after hydration [45].

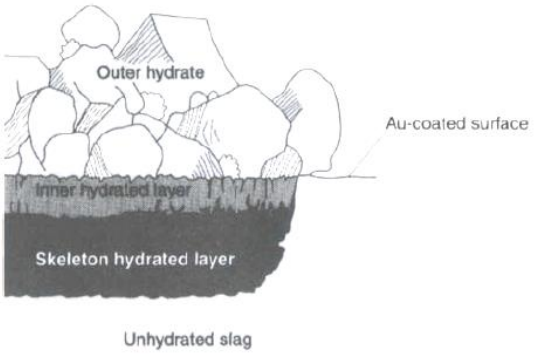

Figure 20: Slag hydrates distribution in cement paste [45].

In the early stages, of about one day, of the hydration reaction NaOH and KOH are found to be the major components, instead of CH. Due to the presence of CH the supply of OH^- ions continues. Continuing the hydration reaction the reaction of blast furnace slag with CH takes place [40]. During the reaction, little net movement of magnesium or oxygen in or out the latter occurs, but mostly fractions of silicon, aluminium and calcium move out. The amount of calcium needed to change the ratios of C-S-H increases, which results in less formation of CH and a partly decrease in the Ca/Si ratio of the C-S-H [101].

3.2.3 Production

Different requirements have to be taken into account with regard to blast furnace cement depending on the country, just as with Portland cement. According the British Standard BS 146:1958 and the standard in the USA ASTM C 595-68 a mixture of Portland cement and granulated slag can contain a slag content of up to 65 percent, while in Germany two types are specified in DIN 1164 of which one has a maximum slag content of 85 percent [45]. The European Standard EN 197-1 mentions three types of blast furnace cement, namely CEM III/A, CEM III/B and CEM III/C. The difference between the three types can mainly be found in the blast furnace slag content. The standard mentions a maximum slag content of 95 percent [72].

At temperatures of about 1230-1550 °C in a blast furnace, iron ore is reduced by coke, producing blast furnace slag and molten iron. The main product of a blast furnace is the molten iron, which was formed from the ore. The other components formed in a blast furnace form a liquid slag. Due to its smaller density, the liquid slag forms a layer on top of the molten iron. The liquid slag is separated from the molten iron and cooled with air or water [92]. The cooling rates and the chemical composition influence the density, particle size and porosity. In total three types of slag can be produced, depending on the cooling method. The three slag types are air cooled slag, expanded slag and granulated slag. Air cooled slag is formed when the molten slag is either slowly cooled in an open pit or rapidly cooled in air (quenching). Expanded slag is formed when the molten slag is cooled under controlled rapid cooling in water or in water combined with compressed air or steam. Granulated slag is formed when the molten slag is quenched into glass, using high-pressure water jets. This prevents the crystallization of minerals, resulting in a granular, glassy composition. This last type of slag is particularly used in the cement production, because of its hydraulic cementitious characteristics [49].

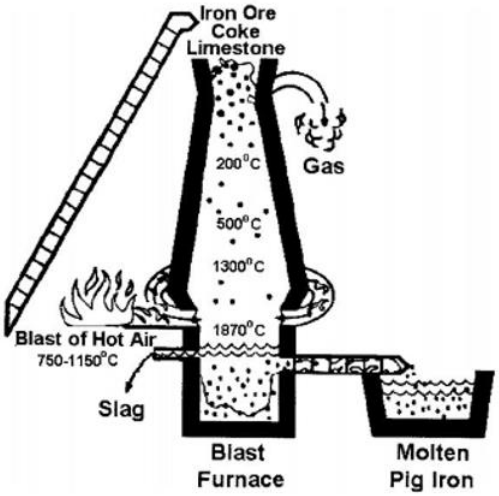

Figure 21: Blast furnace [90].

3.3 Identification

Ordinary Portland Cement consists of multiple components, which can exist in different polymorphic phases. To understand and gain more insight in the components and the performance of cement, it is important to identify the different mineralogical phases of all the components within the cement. The method that will be used for the identification of the components within the cementitious material is X-ray powder diffraction. This method is very suitable for qualitative and quantitative phase analyses of clinker and cement. By comparing the experimentally determined and the theoretically calculated

diffraction patterns, the components within the cementitious material can be identified. The identification of the individual components is still a very complex procedure, not only because each component has several polymorphic phases that must be identified, but also because all the main phases of cement have large overlapping diffraction peaks in the range of 2θ is 30° to 35°. Within this overlapping zone the identification of the individual components will be very difficult [47].

Because the alite polymorphs have similar diffraction patterns, they are difficult to identify. Therefore, the identification is done by using 'fingerprint' regions [22]. Of the seven polymorphic forms of alite the initial focus for the identification lays on the following polymorphs: monoclinic (M1 and M3), triclinic (T1) and rhombohedral (R). The peak for the M3 phase is a doublet at 2θ = 51.7°, for the T1 phase a triplet between 51°-52° and for the R phase a singlet at 51.16°. The monoclinic M1 phase, which is not shown in a figure, has a peak which has the form of a singlet at 2θ = 51.7° [47]. Additionally, differences can be found in the peaks in the range 2θ = 31° to 33°, but because this lies within the overlap zone, where these peaks will overlap with peaks of other phases, these peaks are less useful [53]. Some polymorphs can be identified, using peaks within the overlap zone, but this is very difficult even when 'fingerprint' regions are used for the identification [22]. For example, the M3 phase has a major peak at 2θ = 29.35° which can be used for identification, because this peak is free from overlap of other phases [47].

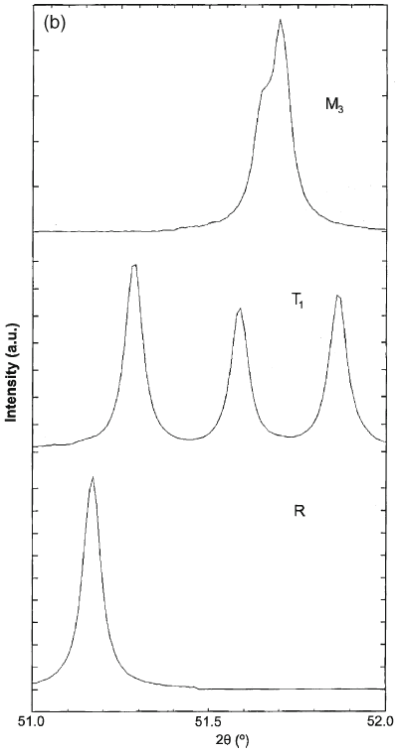

Figure 22: Alite peaks around 51°- 52° 2θ [47].

The identification of the polymorphs of the belite might be difficult due to the existence of multiple modifications. Additionally, the presence of other phases makes the identification even more complex, because within the diffraction pattern the large diffraction peaks overlap. Therefore, weaker peaks will be needed to identify the polymorphs. This identification by weaker peaks can be done when the belite content is over 12%. For the polymorphs α'_H-C_2S or α'_L-C_2S identification is difficult, because the peaks cannot be recognized by a single pattern [22]. The identification for the belite polymorph β-C_2S can be done, using the peak at 31.1° and the weaker peak at 35.29°. All the other large peaks overlap with the monoclinic M3 phase of alite. Even though the two identification peaks lay within the overlap zone, they can be used for the analysis of the cement, because these peaks are free from overlap. The γ-C_2S phase can be identified, using the peaks at 2θ = 29.63° and 47.53° [47].

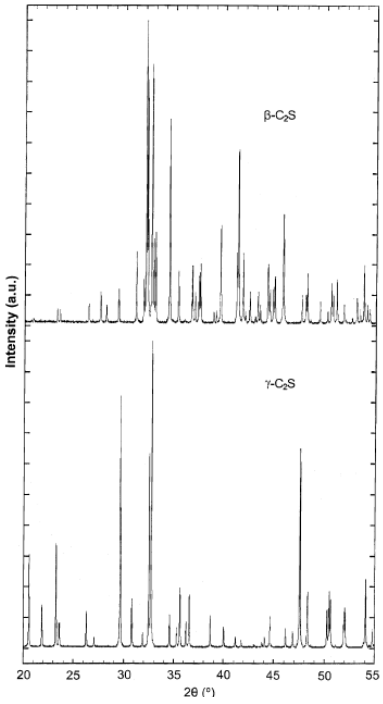

Figure 23: Belite polymorphs [47].

In most cases cubic or orthorhombic forms of the aluminium phase are found within production clinker, whereas the monoclinic form was not detected. The identification of the cubic phase of the aluminate phase is done by using a strong peak at 33.17°. Instead of the strong peak at 33.17° for the cubic, the orthorhombic form can be identified by a doublet at 32.95° and 33.23°. Although the 33.23° peak will be difficult to use, because of overlap with other phases. Therefore, identification will focus on the 32.95° peak. An additional peak which may be useful for the identification of the cubic form may be 28.61°, even though it is weak it is free from overlap [47].

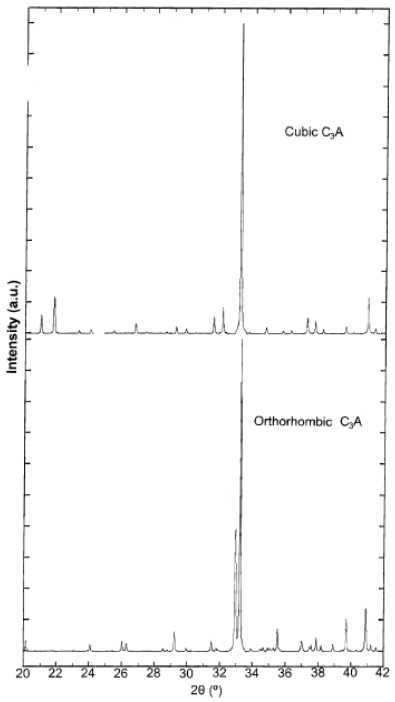

Figure 24: Aluminate polymorphs [47].

For the ferrite phase the focus lays on the identification of the brownmillerite phase. Important peaks for identification are visible at 12.1°, 24.4° and 33.7°, where the peak at 33.7° will be less useable, because of the overlap with other phases. Therefore, identification of the ferrite phase focuses on the first two mentioned peaks [47]. It has to be mentioned that the diffraction patterns of the ferrite phase are influenced by the cooling rate. In case of zoning and the phase being poorly crystalline, broadening of the peaks may occur. This results in a large difficulty in identifying the ferrite phase [101].

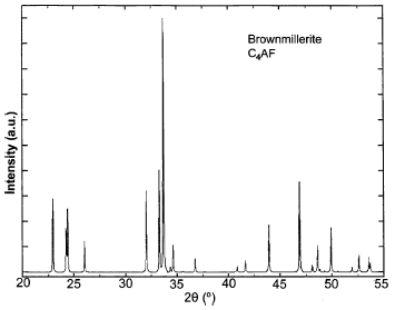

Figure 25: Aluminoferrite polymorph [47].

For the smaller phases within the cementitious material figure 26 shows identification peaks which can be used. One of those phases which might be interesting to look into is gypsum. Especially for the dehydrated cement insight in the availability of gypsum might be interesting, because gypsum influences the setting rate of the material. The identification of the gypsum phase can be done, using the peaks at 11.71° and 20.80° [47].

Because the obtained material could not only contain Ordinary Portland Cement, but also Blast Furnace Cement, the diffraction pattern of blast furnace slag will also be explained. When looking at slags, like blast furnace slag, the diffraction pattern will show an asymmetric, diffuse band peaking at 31° 2θ. The asymmetric, diffuse band extends from about 20° to 37° and a weaker band can be found at about 48° 2θ [101].

Phase	Polymorphs	P.D.F. card no.	Distinct features of diffractograms
Alite (C_3S)	Monoclinic M_3	42–551	Strong peak with a shoulder at 51·7°
	Triclinic T_1	31–301	Triplet between 51–52° (51·3°, 51·58° and 51·85°)
	Rhombohedral, R	16–406	Strong singlet at 51·16°
	For M_3 phase, major peaks at 29·35° and 51·7° are essentially free from overlap and may be used for identification and quantitative analysis		
Belite (C_2S)	β-C_2S	33–302	Strong peaks at 32·05°, 32·61° 34·40° and 41·28°
	Peak at 31·10° and 35·30° are weak, but essentially free from overlap and can be used for quantitative analysis		
	γ-C_2S	31–297	Strong peaks at 32·72°, 29·63° and 47·53°
Tricalcium aluminate (C_3A)	Cubic	38–1429	Strong peak at 33·17° may be used for identification
	Peak at 28·61 is weak, but free from overlap and may be used for quantitative analysis		
	Orthorhombic	32–150	Two peaks at 32·95° and 33·23° are observed in place of single peak at 33·17° as observed in cubic case
	Major peaks 33·23° is in the region of overlap and difficult to use for quantitative purpose		
Calcium aluminoferrite ($Ca_2(Fe_xAl_{1-x})_2O_5$)	C_4AF-Ca_2FeAlO_5 (Brownmillerite)	30–226	Key diffraction peaks at 12·1°, 24·4° and 33·7°
	For quantitative analysis suitable peaks at 12·1°, 24·4° can be used		
Calcium sulphate dihydrate (Gypsum)	$CaSO_4 \cdot 2H_2O$	33–311	Key diffraction peaks which can be used for identification and quantitative analysis are 11·71°, 20·80°
Calcium sulphate hemihydrate ($CaSO_4 \cdot 0{\cdot}5H_2O$)	$CaSO_4 \cdot 0{\cdot}5H_2O$	41–224	Key diffraction peak at 14·73° can be used for identification and quantitative analysis
Tripotassium sodium disulphate	$K_3Na(SO_4)_2$	20–926	Distinct doublet observed at 30·45° and 31·47°

Figure 26: Identification of the phases and their polymorphs within cementitious materials [47].

4 UPCYCLING TECHNIQUES

Within the cementitious material a distinction can be made between a non-hydrated and hydrated fraction. These fractions need to be processed in different ways and will influence the properties of the cementitious material. To reuse the hydrated fraction it has to first be dehydrated. The height of the dehydration temperature has an influence on the eventual properties. Besides heating, cooling may also influence the cementitious material, resulting in deviating properties for different cooling rates. The non-hydrated fraction may deviate in quality, which may also result in different properties of the cementitious material. This chapter will discuss possible upcycling techniques, which may influence the final properties of the cementitious material. Insight will be given in possible heating regimes. Cooling regimes do not belong to the scope of this thesis.

4.1 Heating regimes

Multiple studies have been done on the influences of elevated temperatures on the microstructure of cement paste. The decomposition reactions occurring within the cement paste upon heating with different temperatures can give insight in what temperatures may be of interest for the dehydration of the cementitious material. When hardened cement paste is heated, water evaporates from the material. First, the free water will evaporate, followed by the capillary water and physically bound water. Finally, the chemically bound water, which is bound with cement hydrates, will evaporate. Ettringite will start decomposing before the temperature reaches 100 °C [41]. Initially, it was mentioned that the dehydration of C-S-H starts between 200 °C and 400 °C, but a closer look shows that the C-S-H slowly starts dehydrating at the beginning of the heating of the material and increases with increasing temperature. The second phase of the decomposition of the C-S-H takes place at temperatures higher than 600 °C, which results in morphological changes of the C-S-H gel [34]. At temperatures between 450 °C and 550 °C, hydroxylation of portlandite takes place. This decomposition of the portlandite results the release of the hydroxyl group (OH) by forming a water molecule and at the same time an increase in CaO content can be observed. Up to approximately 900 °C the decarbonation of calcium carbonate takes place [41]. Most of the occurring decompositions result in a weight loss due to the loss of water or carbon dioxide. Besides these decompositions, also a phase transformation, which does not lead to weight loss, occurs. This change in structure is the transformation of crystalline silica from the α to the β form [34].

Temperature range	Changes
20–200°C	slow capillary water loss and reduction in cohesive forces as water expands; 80–150°C ettringite dehydration; C-S-H gel dehydration; 150–170°C gypsum decomposition ($CaSO_4 \cdot 2H_2O$); physically bound water loss;
300–400°C	approx. 350°C break up of some siliceous aggregates (flint); 374°C critical temperature of water;
400–500°C	460–540°C portlandite decomposition $Ca(OH)_2 \rightarrow CaO + H_2O$;
500–600°C	573°C quartz phase change $\beta - \alpha$ in aggregates and sands;
600–800°C	second phase of the C-S-H decomposition, formation of β-C_2S;
800–1000°C	840°C dolomite decomposition; 930–960°C calcite decomposition $CaCO_3 \rightarrow CaO+CO_2$, carbon dioxide release; ceramic binding initiation which replaces hydraulic bonds;
1000–1200°C	1050°C basalt melting;
1300°C	total decomposition of concrete, melting.

Figure 27: Changes in concrete components, cement paste and aggregates during heating [41].

Besides research of the influence of elevated temperatures on the microstructure of the cement paste, various studies also investigated the rehydration ability of cement paste subjected to elevated temperatures. Because the microstructure of the cement paste undergoes different reactions at different temperatures, the height of dehydration temperatures may also have an influence on the rehydration ability of the cement paste. Additionally, it can be said that because the dehydration

process and the degree of dehydration of the hydration products are influenced by the temperature that it is likely that the rehydration ability of the cement paste will also deviate when different dehydration temperatures are used.

Shui et al. (2009) mentions that the initial hydration products can be recovered when the dehydrated phases of the cement paste react with water. During the decomposition of portlandite (CH) and calcium carbonate ($C\bar{C}$) CaO is formed. When the CaO reacts with water, the occurring rehydration reactions will result in the formation of CH again. Additionally, during the rehydration processes ettringite and C-S-H gel are also recovered [91].

Shui et al. (2009) used a controlled heating regime with all temperatures in the range of 300 °C to 900 °C. The furnace was heated from room temperature at a rate of 10 °C/min and when the desired temperature T_c was reached the hydrated cement samples were heated in the oven for 2.5 hours after which they were cooled down in the oven to room temperature. After the cooling process was finished the specimens were tested on their compressive strength development. The compressive strength of the specimens increased with increasing dehydration temperatures, with a maximum at 800 °C. The resulting compressive strength at 800 °C was still lower than the strength of primary cement. For temperatures higher than 800 °C a decrease in compressive strength was found. Additionally, with an increase in dehydration temperature the microstructure of the rehydrated cement paste became more close-grained. This led, among other things, to the conclusion that the cementitious capability of the dehydrated cement paste depends on the dehydration temperature [91].

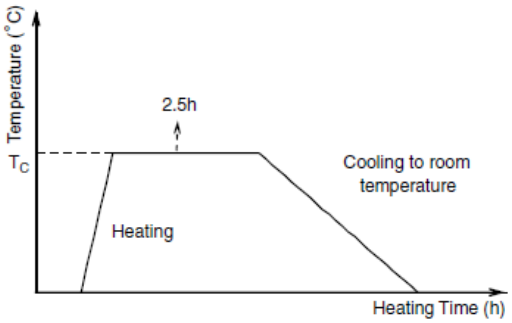

Figure 28: Heating process Shui et al. (2009) [91].

Kwon et al. (2015) based their dehydration temperatures on the processes connected to the four major phases within cement. The temperatures used were 1200 °C, at which C_2S was formed, 1300 °C, at which C_3S was formed, 1350-1400 °C, at which C_3A and C_4AF are liquified, and 1450 °C, at which Ordinary Portland Cement is manufactured. The furnace was heated until the desired temperature was reached and the samples were heated at that temperature using a firing time of 90 minutes. The compressive strength and the workability were tested using samples with a mixture of fine aggregate added in the range of 0-65 wt.%. The results of the compressive strength tests showed that the compressive strength of the samples using the dehydrated cement paste was lower than that of the primary cement, but the sample with 0 wt.% fine aggregate gave the better results. Therefore, it was concluded that more research into the effective separation of the components has to be done to obtain high-quality recycled cement [54].

Wang et al. (2018) used a slightly different approach. The prepared samples were placed in a furnace and heated at a heating rate of 7 °C/min. When the target temperature was reached, the samples were heated for 8 hours, before being cooled down naturally to room temperature. The target temperatures were based on the results of the thermogravimetry and differential thermogravimetry (TG/DTG), which showed the weight loss due to decomposition or phase changes at the end of each stage. This led to the following temperatures:

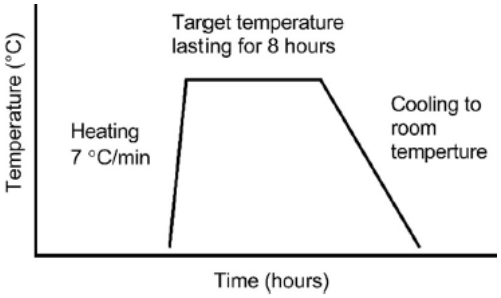

Figure 29: Heating process Wang et al. (2018) [109].

120 °C, which showed the loss of physically bound water in C-S-H and the decomposition of ettringite, 450 °C, showing the loss of chemically bound water in C-S-H and the decomposition of portlandite, 750 °C, showing the additional loss of chemically bound water in C-S-H and the decomposition of calcium carbonate, and 1150 °C, which was the maximum burning temperature. The samples heated to a dehydration temperature of 450 °C gave the best results, concerning the compressive strength, and resulted in a compressive strength comparable to primary cement. However, the workability was inadequate, which could be improved by the addition of ground granulated blast furnace slag [109].

Alonso and Fernandez (2004) used samples of Ordinary Portland cement mixed with distilled water, which were sealed and cured at room temperature. After a curing period of 70 days the samples were subjected to different heating regimes. Four target temperatures were chosen, namely 100 °C, 200 °C, 450 °C and 750 °C. Each of the samples was placed in a furnace and heated at a heating rate of 1 °C/min. When the target temperature was reached, the samples were cured for 2 hours, before cooling down slowly to room temperature. For the 100 °C sample the heating regime was slightly different. This sample was placed in the furnace when it was already heated to 100 °C and was kept in the furnace until a constant weight loss was reached. After this, the sample was cooled down slowly inside the furnace to room temperature [3].

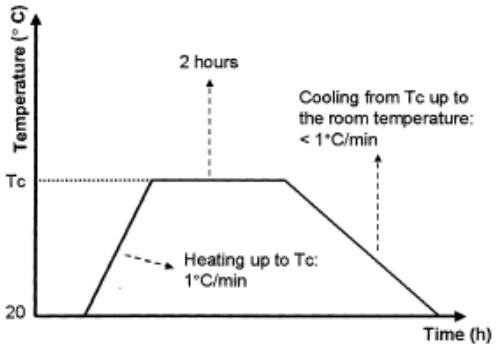

Figure 30: Heating process Alonso and Fernandez (2004) [3].

PART II
EXPERIMENTAL RESEARCH

5 MATERIALS AND METHODS

The research focusses on cementitious binder obtained from the novel concrete crushing technique the Smart Crusher. The initially obtained material consists of fines in the size range of 0 - 4 mm. By sieving this material the material fraction of interest for the research could be retrieved. This chapter will discuss the different sample types used in this research and their origin. Additionally, the methods to upcycle the cementitious material will be mentioned as well as the methods to characterize the material before and after the upcycling treatment. Furthermore, attention will be given to the process that will be followed during the experimental research.

5.1 Sample types and origin

Different types of cementitious material were used throughout this study namely, secondary cementitious binder, blast furnace cement (CEM III/B 42.5 N) and two strength classes of Portland cement (CEM I 52.5 R and CEM I 42.5 N). Both blast furnace cement and the two strength classes of Portland cement were chosen as a reference material to evaluate the characteristics of the secondary cementitious binder.

The material (0 – 4 mm) from which the secondary cementitious binder was separated, was provided by Smart Crusher BV. The material consisted of crushed concrete, using a novel concrete crushing technique, and needed to be sieved to obtain the fractions containing the cement fractions. The following hypothesis was used to determine which fractions could be seen as the cement fractions: material passing the 0.125 mm sieve, resulting in a particle size below 0.125 mm, will contain the cement fraction. The 0.063 mm sieve was added to take into account possible sand particles passing the 0.125 mm sieve. Therefore, the 0.00 - 0.063 mm fraction contains only cement, whereas the 0.063 – 0.0125 mm fraction may contain some sand particles. Different types of upcycling treatment were performed on the cement fractions to gain insight in the recycling potential of the secondary cementitious binder. Within the sieved fractions no distinction was made between the hydrated and non-hydrated fraction.

Initially, three reference materials were selected based on the types of cement mostly used in the Dutch concrete industry as well as in the concrete industry worldwide. Generally, Portland cement is the most common cement type in use around the world. Besides Portland cement blast furnace cement is also of interest for this study , because this is the most used type of cement in the Dutch concrete industry. Consequently, the following reference materials were selected: CEM III/B 42.5 N, CEM I 42.5 N and CEM I 52.5 R. The reference materials were provided by the Stevinlab of the TU Delft and produced by ENCI. The composition of the cement types as provided by ENCI can be found in table 1. The cement types CEM I 42.5 N and CEM I 52.5 R have comparable compositions. If the test results confirm the equal composition, CEM I 52.5 R will be chosen as reference material and two reference materials remain in this study.

Cement type	**Main constituents [%]**		**Minor additional constituents [%]**
	Clinker	Blast furnace slag	
CEM I	95 - 100	-	0 - 5
CEM III/B	20 - 34	66 - 80	0 - 5

Table 1: Cement types and their composition in percentage by mass divided in main and minor additional constituents [30].

The materials used during this study can be distinguished in three different categories, namely:

- Blackbox: this category will contain the two cement fractions, 0.0 – 0.063 mm and 0.063 – 0.125 mm. Both fractions are regarded as hydrated (the possible presence of unhydrated cement particles is not taken into account in this study), will not undergo any treatment in this category and are seen as a Blackbox, because its origin is unknown.
- Reference material: this category will contain the mentioned reference materials CEM III/B 42.5 N, CEM I 42.5 N and CEM I 52.5 R. This category will be divided into reference material without any treatment and reference material undergoing hydration. The hydrated reference material undergoes the same treatment as the heated material.
- Heated material: this category will contain the materials which undergo a temperature treatment or upcycling treatment. Part of the Blackbox material as well as the hydrated reference material will undergo this treatment. Three different thermal treatments are used, namely heating to 500 °C, 800 °C and 1400 °C.

5.2 Methods

Different experimental methods were used to investigate the recycling potential of secondary cementitious binder. The fractions will be characterized by using several experimental techniques. Additionally, the fractions will be dehydrated, using different thermal treatments. Characterization of the dehydrated fractions and comparing the results with the reference material can give a first indication of the applicability of secondary cementitious binder. The thermal treatment, which shows the biggest potential, can then be further analysed on its functionality.

5.2.1 Sieving

Before the material will be sieved into different fractions, the material needs to be dried properly. To make sure the smaller particles are not only present in the bottom part of the bucket in which the material has been stored, the material has to be mixed first. This is done by placing all the material on a canvas and dividing it in four parts. These parts are mixed together. After the first mixing, a part of the material is restored in the bucket. The remaining material is divided again in four parts. This mixing was repeated several times to assure a good distribution of the particles. When the mixing was finished, 500 grams of the material was weighed and placed in an oven for 45 minutes at a temperature of 100 °C. After 45 minutes the material was removed from the oven and cooled for 15 minutes to room temperature. After cooling the material was weighed to determine the amount of evaporated water, where after it was placed in the HAVER EML 200 Pure sieving machine. This machine contains multiple sieves with different sizes and is used to obtain different fractions of the material. In total seven different sieve sizes were used, namely 4 mm, 2 mm, 1 mm, 0.5 mm, 0.25 mm, 0.125 mm and 0.063 mm, resulting in eight different material fractions. The machine sieves the material for 30 minutes. Hereafter, the different sieves contain the different fractions. To make sure that no smaller particles are present on the different sieves, extra sieving by hand was performed.

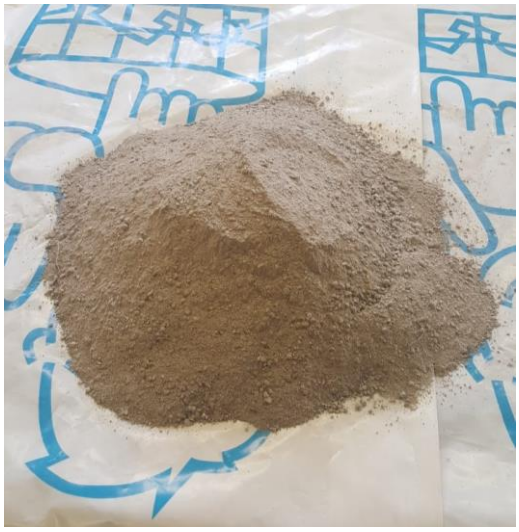

Figure 31: Smart Crusher material of the 0 - 4 mm fraction before sieving.

5.2.2 Particle Size Distribution

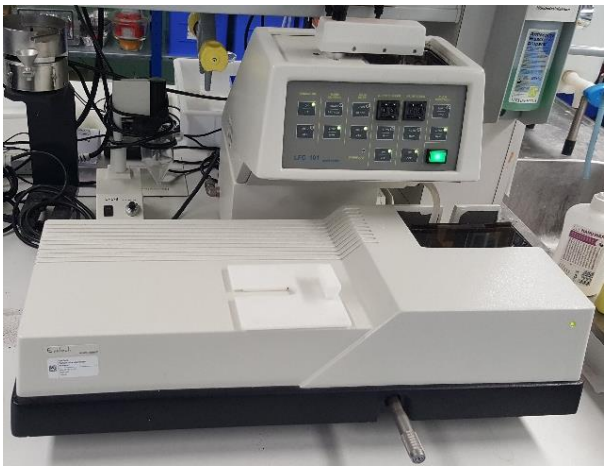

Figure 32: EyeTech Laser diffraction machine.

In this research both the particle size distribution of the material provided by Smart Crusher BV as well as the fractions, which are assumed to contain cementitious material were studied, using different methods. The first method is the sieving method, which was described in the previous paragraph. By weighing the material on the different sieves a particle size distribution of the material could be estimated. The fractions assumed to contain the cementitious material are the 0.0 – 0.063 mm and the 0.063 – 0.0125 mm fraction. The particle size distribution of these fractions will be compared with the particle size distribution of the reference materials. Particle size distribution measurements are performed with an Eve Tech Laser diffraction machine. Before starting the measurements, the machine underwent a cleaning process using ethanol in the following way: cleaning the machine, analysing the particle size distribution of the samples, followed by cleaning of the machine again before inserting the next sample. In each cleaning step as well as during the particle size distribution measurements 800 ml of ethanol was used. Ethanol was chosen instead of water, because the samples consist of cementitious material which will undergo hydration when water is used. For the measurement 0.5 grams of the samples are weighed and added to the ethanol. If needed extra sample is added until the program showed a sufficient concentration for the test. From every sample three measurements were done to determine the repeatability and reproducibility.

5.2.3 Hydration Reference Material

As part of this research the reference materials will be hydrated, using a water/cement ratio of 0.5. The reference materials are weighed and water is added in the before mentioned ratio. After adding the water and cement, the mixture is stirred until the mixture is homogeneous, where after the mixture is placed in a closed storage jar to prevent evaporation, and is placed into an oven. The jar was kept in the oven for two weeks at a temperature of 40 °C. By placing the hydrating cement in the oven at 40 °C, the hydration of the reference materials is accelerated. After two weeks, the hydrated material was removed from the oven and grinded into powder using the Retsch RM200 Mortar Mill. The Retsch RM200 can only grind grains with a maximum grain size of 8 mm. Therefore the material is grind and the size is reduced by manual breaking. The Retsch RM200 reduces the size of the material to a powder. Part of this powder will then undergo thermal treatment, using a certain heating regime, before further characterization. The results of the characterization of these hydrated reference materials is compared with the results of the characterization of the material provided by Smart Crusher BV.

CEM III/B 42.5 N

CEM I 52.5 R

Figure 33: Reference material CEM III/B and CEM I after hydration.

5.2.4 Heating Regime

Upcycling of the obtained cement fractions is performed by heating to different temperatures to gain insight in the behaviour of the materials. The selected thermal treatment temperatures were based on the literature study and are 500 °C, 800 °C and 1400 °C [41; 54; 91]. These temperatures also lie in or close to the temperature range in which important phase changes occur. A comparison between the influence of the temperatures on the material characteristics gives an indication of the best thermal treatment for upcycling of the cementitious material. The cement fraction was placed in porcelain or Alsint (Al_2O_3 material) bowls and placed in the furnace. For the 500 °C and 800 °C treatment the Carbolite chamber furnace with a maximum possible temperature of 1100 °C was used, while for the 1400 °C treatment the Carbolite chamber furnace for higher temperatures was used. A heating rate of 10 °C/min was used to heat the samples, starting from room temperature. When the target temperatures were reached the samples were kept in the furnace for 2.5 hours, where after the samples were cooled in the oven to room temperature. When the cooling process was finished the material was sealed and stored in plastic bags until further testing.

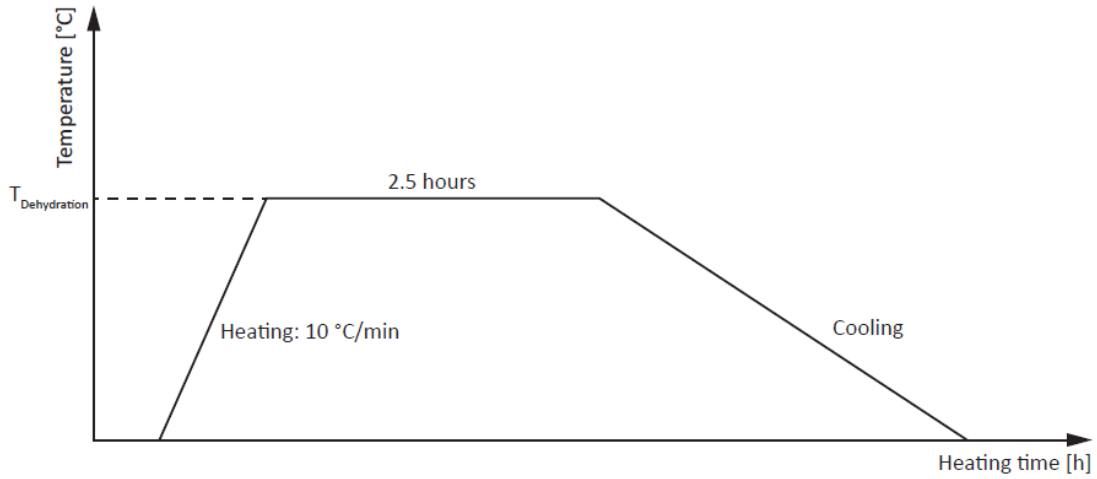

Figure 34: Heating process in which the material is heated with a heating rate of 10 °C/min and is kept at the target temperature for 2.5 hours before cooling.

5.2.5 Thermalgravimetric Analysis, Differential Scanning Calorimetry and Mass Spectrometry

The following analyses were conducted to gain insight in the mass loss of the different samples during the heating process. Additionally, the analysis would help to provide information about certain physical and chemical phenomena. The presence of certain compounds within the samples can be determined by analysing the temperatures at which certain mass losses occur. Thermalgravimetric (TGA) and differential scanning calorimetry (DSC) experiments are performed simultaneously using a NETSCH STA 449 F3 Jupiter machine with a temperature interval of 40 - 1000 °C under an argon atmosphere. The heating rate is 10 K/min. Alumina crucibles are used as sample pan. At least three samples were tested and compared to investigate the repeatability and reproducibility. To perform mass spectrometry (MS) experiments the NETSCH STA 449 F3 Jupiter was coupled to the QMS 403C Aëolos and TGA, DSC and MS were performed simultaneously under the same conditions as mentioned before.

The literature study showed that cement consists mainly out of four phases, which can be distinguished in tricalcium silicate (C_3S), dicalcium silicate (C_2S), tricalcium aluminate (C_3A) and tetracalcium aluminoferrite (C_4AF). Additionally, it was found that during the hydration process different hydration products can be formed of which calcium silicate hydrate (C-S-H) and portlandite (CH) are the main

products. During the increase in temperature the hydrated cement starts to dehydrate and decompose. An overview of the different phases, which can occur when the cement undergoes decomposition reactions with an increase in temperature, is shown below:

- 30 – 120 °C: evaporation of the free water and part of the bound water [2].
- 120 – 250 °C: Loss of water from decomposition of C-S-H and loss of most of the bound water [3].
- 400 – 550 °C: Portlandite decomposition [41].
- 700 – 900 °C: Calcium carbonate decomposition [2].

Figure 35: NETZSCH STA 449 F3 Jupiter for simultaneous TGA and DSC with QMS 403C Aëolos for MS.

5.2.6 X-Ray Fluorescence

X-Ray fluorescence (XRF), a non-destructive analytical technique, was used to analyse the chemical composition of the sieved fractions and the reference materials by using a Panalytical Epsilon 3XL spectrometer. The samples are irradiated by high energy x-rays, produced by a x-ray source. The emission of characteristic x-rays caused by the high energy bombardment, gives insight in the chemical elements present in the samples, which can be used to determine the chemical composition of the sample. The following sample categories can be distinguished:

- Without treatment: this category contains the samples, which did not undergo any specific treatment. The Blackbox material, the partly hydrated sieved fractions 0.0 – 0.063 mm and 0.063 – 0.125 mm, as well as the unhydrated reference materials, CEM I 42.5 N, CEM I 52.5 R and CEM III/B 42.5 N, are part of this category. The sieved fraction are (partially) hydrated and will later undergo thermal treatment, whereas part of the reference materials will first be hydrated before undergoing thermal treatment.
- With hydration treatment: this category contains the samples, which were hydrated in the laboratory. The reference materials CEM I 52.5 R and CEM III/B 42.5 N underwent an accelerated hydration and will later undergo thermal treatment.

- With thermal treatment: this category contains the samples, which were treated with different dehydration temperatures. In total three dehydration temperatures, namely 500 °C, 800 °C and 1400 °C, were used. The materials, which were thermally treated, are the sieved fractions 0.0 – 0.063 mm and 0.063 – 0.125 mm and reference materials CEM I 52.5 R and CEM III/B 42.5 N.

5.2.7 X-Ray Diffraction

X-Ray diffraction (XRD), a non-destructive analytical technique, was used to identify the crystalline phases within the powder samples using a Philips PW 1830 X-Ray diffractometer applying CuKα (1.54 Å) radiation and tube settings were 40 kV and 40 mA. Additionally, a Bruker D8 Advance diffractometer Bragg-Brentano and Lynxeye position sensitive detector, applying CuKα radiation, divergence slit V12, a scatter screen height of 5 mm and tube settings were 45 kV and 40 mA was used for part of the samples. The samples were scanned in the 2θ range of 5-70° with a step size of 0.030° 2θ and a rate of 3.0 seconds per step. In the case that the particle size of the materials would not be small enough to form a compact sample, the materials had to be ground into a fine powder. This was done using a mortar and pestle. The powder samples have to be compressed into an aluminium holder, using a glass sheet. The mortar and pestle as well as the aluminium holder and glass sheet were cleaned to ensure the samples would not be contaminated by residual material from previous tests.

Figure 36: Sample preparation for XRD analysis. Grinding the material into a fine powder before compressing the powder in an aluminium holder, which can be placed in the diffractometer.

The crystals within the samples all have a certain atomic structure, which will diffract the x-ray beams in specific directions. The XRD measurement results in a diffractogram, which shows the phases present in the samples, the phase concentrations, amorphous content and crystallite size/strain. The identification of the crystalline phases within the samples can be done by comparing the X-Ray diffraction pattern of the samples with a database containing a large amount of reference patterns.

Figure 37: Philips PW 1830 X-Ray diffractometer.

5.2.8 Compressive and Flexural Strength

To investigate the functional quality of the secondary cementitious binder, compressive and flexural strengths were tested. The determination of the compressive and flexural strength of cement mortar was performed according to NEN-EN-196-1 [73]. The cement mortar composition consists of one part cement, three parts CEN Standard sand and half a part of water. For a batch of three test specimens each of the specimens consist of 450 g of cement, 1350 g of sand and 225 g of water. The materials for the cement mortar were mixed using a HOBART mixer. Sand was added to the cement at low speed and the mixture was mixed for one minute. After this the water was added and the mixture was again mixed at low speed for one minute. Subsequently, the mixer was stopped and the bottom and wall parts of the bowl were scraped to make sure the materials will be fully mixed. Then, the mixture is placed back inside the mixer and mixed at a higher speed for one minute. The fresh mixture was placed inside a mould (40 mm x 40 mm x 160 mm), which was first covered with a thin layer of oil as a demoulding agent. When the moulds were filled, the prisms were covered with a thin plastic sheet. Demoulding of the samples was done 24 hours after casting and then cured without sealing in a fog room.

Compressive and flexural strength were tested at an age of 1 and 28 days with a hydraulic compression machine. Due to the limited amount of material available, the choice was made to test after 28 days for the samples with little amount material for both time intervals. A three-point flexural bending test was done on the 40 mm x 40 mm x 160 mm prisms following NEN-EN-196-1 [73]. The three-point flexural bending test resulted in two halves, which were then used for the compressive strength test. The flexural and compressive strength was calculated as an average of the samples. In total six different materials were tested, namely CEM I 52.5 R and CEM III/B 42.5 N as the references, CEM I hydrate, CEM III/B hydrate, 0.0 – 0.063 mm cementitious Smart Crusher fraction and the 0.063 – 0.125 mm cementitious Smart Crusher fraction.

The flexural strength can be calculated using the following formula [73]:

$$R_f = \frac{1.5 \times F_f \times L}{b^3} \tag{5.1}$$

Where:
R_f = Flexural strength [MPa]
F_f = Failure load [N]
L = Distance between the supports [mm]
b = Side of the square section of the prism [mm]

The compressive strength can be calculated using the following formula [73]:

$$R_c = \frac{F_c}{A} \tag{5.2}$$

Where:
R_c = Compressive strength [MPa]
F_c = Failure load [N]
A = Area of the auxiliary plates (1600 mm^2) [mm^2]

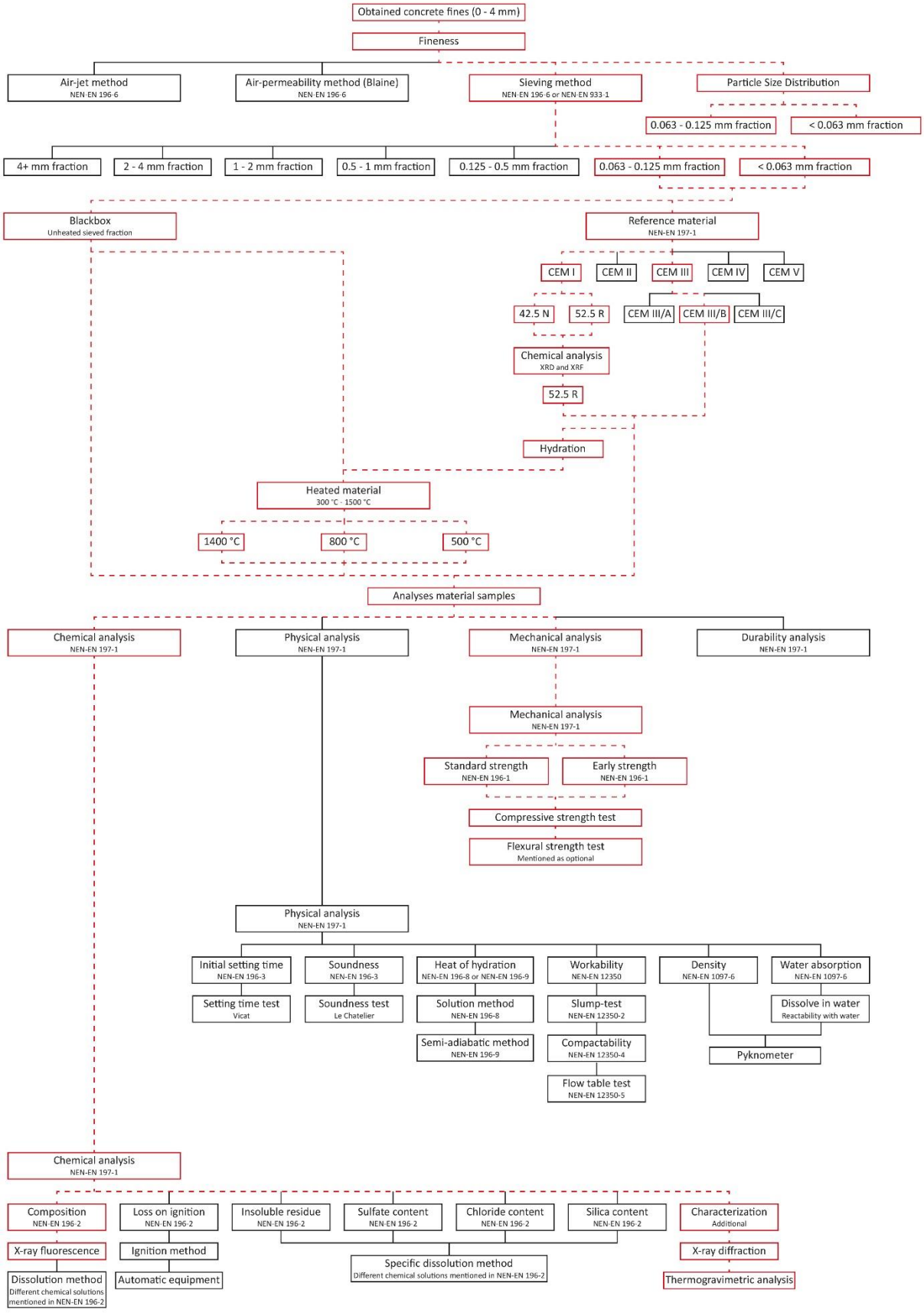

Figure 38: Tree diagram of the possible experimental methods during this research. The red dotted lines show the path followed in this thesis.

6 CHARACTERIZATION CEMENTITIOUS BINDER

The secondary cementitious binder, obtained from the novel concrete crushing technique the Smart Crusher and the hydration of the reference materials, will be characterized to gain insight in its composition and reactivity potential. A distinction was made between two size fractions containing the cementitious material, namely the 0.0 – 0.063 mm and 0.063 – 0.125 mm fraction, and the cementitious reference materials, CEM I 42.5 N, CEM I 52.5 R and CEM III/B 42.5 N. This chapter will discuss the results of the different characterization analyses. The results of the characterization analyses will be compared to the reference materials. The functional quality of the cementitious material without upcycling treatment can be indicated and compared to the required functional quality of cement.

6.1 Particle Size Distribution

A sieving test was used to determine the particle size distribution of the material (0 – 4 mm) provided by Smart Crusher BV. The curve, which could be drawn from the results of the sieving test, where compared to the design areas for particle fractions 0/8 of the Betonpocket [51], because the sieved material was mentioned to be in the size range 0 – 4 mm. In general, it is recommended to adjust a concrete mixture to the design areas. The design areas can give an indication about the water required in the concrete mixture. Design area II contains a larger amount of fine material and has a finer grain structure than design area I. This means that a particle distribution that can be placed in design area II has a larger water demand, which in turn means that more cement paste is needed to fill the cavities between the particles [15]. The fractions, which were assumed to be part of the cement fraction, were further analysed with a particle size analyser and compared to the reference materials. Literature was used to gain insight in the results. This resulted in three hypotheses:

1. The sieved material will result in a particle size distribution, which will be comparable to the design areas for particle fractions 0/8 of the Betonpocket.
2. The particle size distribution of the 0.0 – 0.063 mm fraction will fall between the particle size distribution of CEM III/B and CEM I.
3. The particle size distribution of the 0.063 – 0.125 mm fraction contains the largest particles, which will result in a curve placed furthest to the right side of the graph.

During sieving different sieves were used, which resulted in obtaining the following fractions: 0.0 – 0.063 mm, 0.063 – 0.125 mm, 0.125 – 0.250 mm, 0.250 – 0.500 mm, 0.500 – 1.0 mm, 1.0 – 2.0 mm, 2.0 – 4.0 mm and > 4.0 mm. The percentage of material for every fraction including their standard deviations can be found in Appendix A. The NEN-EN 206-1 mentions multiple values regarding the cementitious content of concrete structures in different situations [74]. Based on these values the assumption was made that the cementitious content within concrete will in most cases fall between 10 and 25 percent. Looking at figures A. 1 and A. 2 in Appendix A an indication can be given about the amount of cementitious material within the total sieved material. As mentioned previously, it was assumed that the material passing the 0.125 mm sieve, which gave a particle size below 0.125 mm, will contain the cement fraction. Figures A. 1 and A. 2 show that 17.11% of the sieved material is part of the cement fraction. Taking into account the deviation of the amount of material, which is assumed to be part of the cement fraction, varies between 13.08 and 19.43 percent. This range is in accordance with the assumption based on NEN-EN 206-1, where a range of 10 to 25 percent was assumed [74].

Additionally, it can be seen that the standard deviation of the sieved factions is larger for the fractions consisting of the larger particles, especially the fractions 2.0 – 4.0 mm and > 4.0 mm have a relatively larger variation in the percentage remaining in the sieve.

The cement fractions of the sieved material were also compared to the design areas for particle fractions 0/8. In figure 39 the red line shows the distribution of the sieved material. The black lines serve as boundaries for the two design areas, where the lower area is called area I and the upper area is called area II. The material passing through the smaller sieve falls within design area II, while the material passing through the lager sieve sizes falls above the upper limit if design area II. The Betonpocket mentions that there are no requirements for the particle distribution, but it is recommended to adjust the design of the mixture according to the design areas, because the particle distribution has a large influence on the water requirement and processing properties of the concrete mixture [51]. The material obtained from the Smart Crusher was not used directly, but kept in a storage area for a longer amount of time before being sieved. Therefore, these results may be different than the results, which would have been obtained, when the material was directly taken from the Smart Crusher. During the storage the smaller particles may have moved downwards, while the large particles stayed on top. Material directly taken from the Smart Crusher may therefore result in a particle size distribution, which falls completely within the design areas.

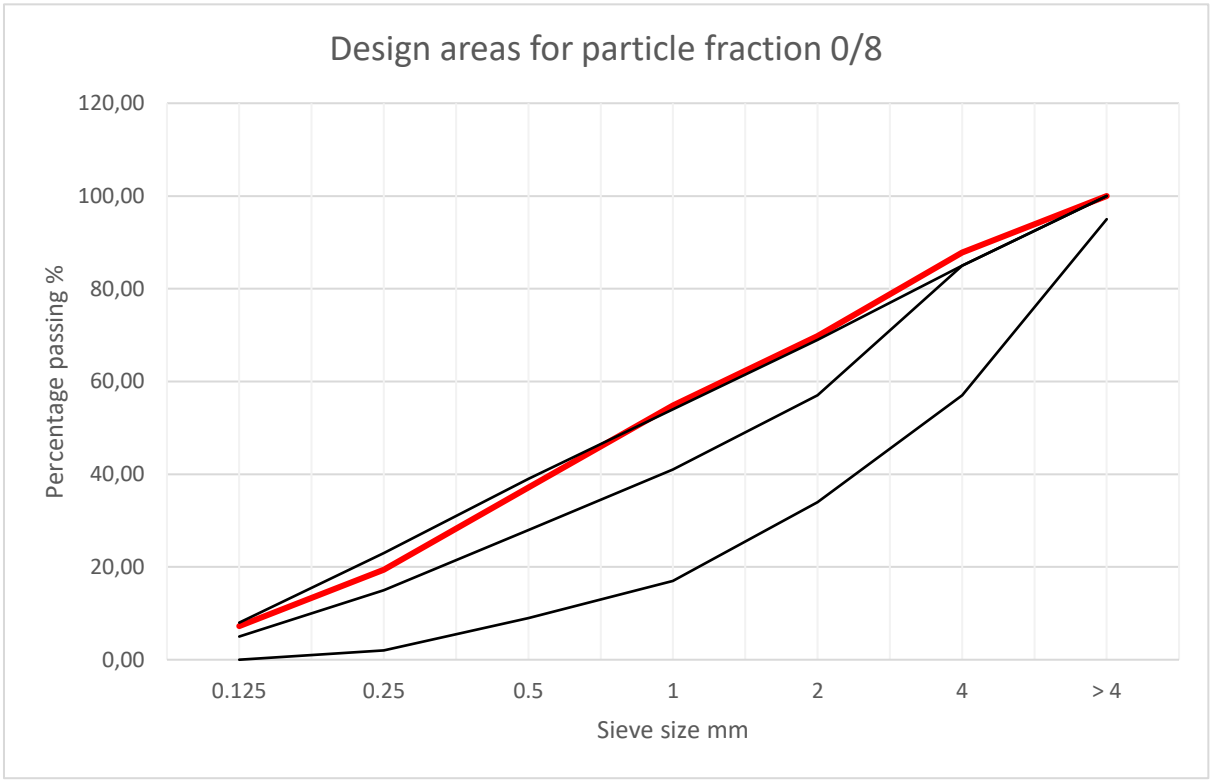

Figure 39: Design areas of the particle fraction 0/8. Black lines serve as the boundaries between the areas (the lower area is area I and the upper area is area II). The red line shows the distribution of the sieved Smart Crusher material. The smaller fractions fall in area II and the larger fractions fall above the upper limit of area II.

Looking at the distribution of the 0 – 4 mm material, special attention was paid to the cementitious Smart Crusher fractions. The reference material CEM III/B 42.5 N consists out of the smallest particles. Blast furnace slag particles generally are smaller than 45 µm, because coarser particles have more difficulty in hydrating [23]. Figure 40 shows the particle size distribution of the two cementitious Smart Crusher fractions and the three reference materials as traditional S-curves for cumulative volume. The samples show similarities in their particle size distributions. As can be seen in the figure, CEM III/B 42.5

N is the material with the smallest distribution, while the 0.063 – 0.125 mm fraction has the largest distribution. The particle size distribution of the 0.0 – 0.063 mm fraction lies in between the distribution of CEM III/B 42.5 N and the distributions of both the CEM I materials.

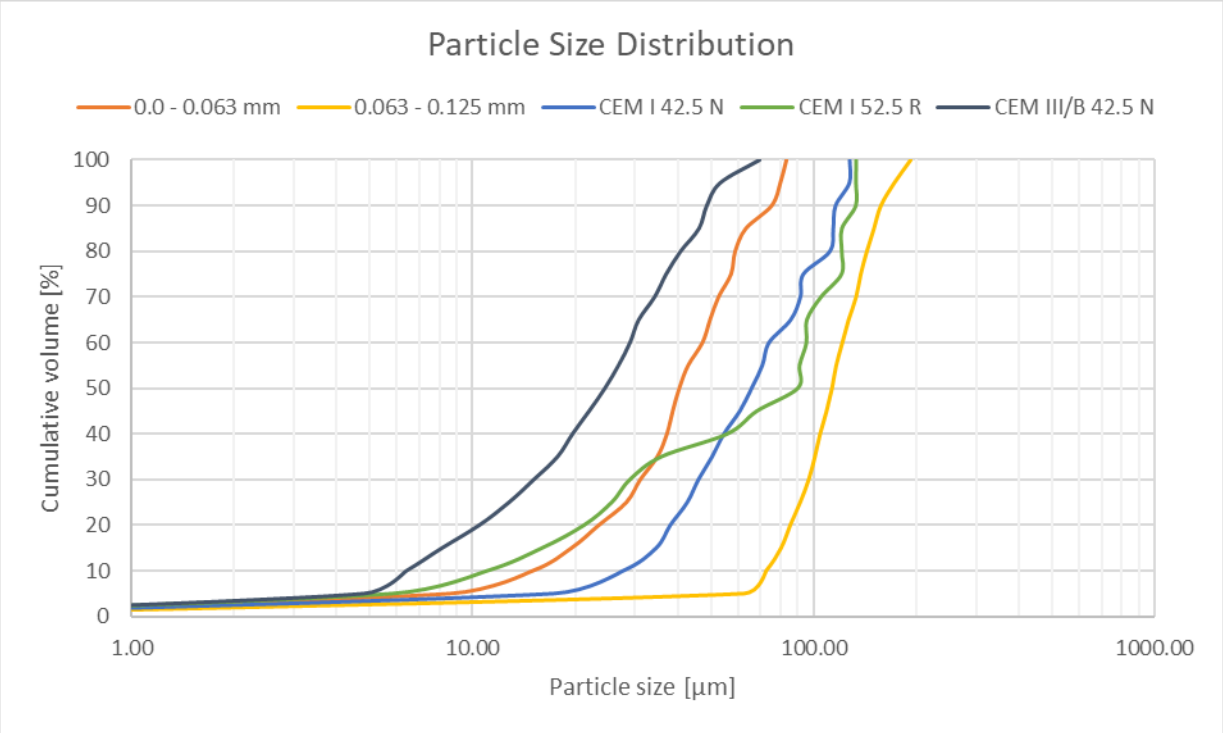

Figure 40: Particle size distribution of the cementitious Smart Crusher fractions and the reference materials. The 0.0 – 0.063 mm fraction lies between CEM III/B 42.5 N and CEM I and the 0.063 – 0.125 mm fraction has the biggest particles.

Table 2 shows the characteristics dimensions of the cementitious Smart Crusher fractions and the reference samples. The midpoint and range of the particle size of the curves in figure 40 are represented by the intercepts of the curves at 10%, 50% and 90%. The corresponding values are called D(10), D(50) and D(90) respectively, meaning that the corresponding diameters of 10%, 50% and 90% of the volume fractions consists of particles smaller than the corresponding diameters. The values for D(10), D(50) and D(90) confirm that CEM III/B 42.5 N has the smallest particle size distribution, followed by the 0.0 – 0.063 mm fraction and finally, the 0.063 – 0.125 mm fraction, which has the largest particle size distribution. The differences in the D(50) and D(90) values of the samples have the expected distribution in which CEM III/B 42.5 N is the smallest, followed by the 0.0 – 0.063 mm fraction, CEM I 42.5 N, CEM I 52.5 R and the largest being the 0.063 – 0.125 mm fraction. This trend can also be found for the D(10) values, although a slight deviation can be seen. The 0.0 – 0.063 mm fraction had a D(10) of 15.01 µm, whereas CEM I 52.5 R had a value of 11.07 µm and CEM I 42,5 N 27.69 µm. In this case CEM I 52.5 R had a smaller value for D(10) than CEM I 42.5 N and the 0.0 – 0.063 mm fraction in despite of having larger values for the other D-values. A large spread in particle distribution can be seen for both the CEM I 42.5 N and CEM I 52.5 R samples. The distribution of spreading of the particles for both CEM I 42.5 N and CEM I 52.5 R can be seen as comparable.

Materials	D_{min} [µm]	D_{max} [µm]	D(10) [µm]	D(50) [µm]	D(90) [µm]
0.0 – 0.063	0.15	83.19	15.01	40.36	75.32
0.063 – 0.125	0.15	192.46	72.56	113.21	157.35
CEM I 42.5 N	0.14	127.77	27.69	65.90	116.09
CEM I 52.5 R	0.15	133.46	11.07	90.04	133.17
CEM III/B 42.5 N	0.15	69.50	6.41	24.48	48.66

Table 2: Particle Size Distribution parameters D_{min}, D_{max}, D(10), D(50) and D(90) measured for the cementitious Smart Crusher fractions and the reference samples. The 0.0 – 0.063 mm fraction particles lie between CEM III/B 42.5 N and CEM I and the 0.063 – 0.125 mm fraction has the biggest particles.

6.2 Thermalgravimetric Analysis, Differential Scanning Calorimetry and Mass Spectrometry

The cementitious materials were analysed with thermogravimetry (TGA), differential scanning calorimetry (DSC) and mass spectrometry (MS) to determine the temperatures where chemical reactions and mineralogical transformations are taking place and what kind of gasses are emitted during these transformations. Based on the used materials within this research and the literature study certain results could be expected [2; 3; 41]. The expected outcomes are summarized in the following main hypotheses:

1. Transitions in the graphs occur in three temperature ranges, namely 30 – 250 °C, 400 – 550 °C and 700 – 900 °C.
2. In the 0.0 – 0.063 mm fraction, the relative amount of cement is larger than in the 0.063 – 0.125 mm fraction. Therefore, the mass change due to the loss of water will be larger in the 0.0 – 0.063 mm fraction.
3. The hydrated reference materials have the highest relative amount of cement and will therefore have a bigger mass change due to the loss of water compared with the 0.0 – 0.063 mm and 0.063 – 0.0125 mm fraction.

Table 3 shows characteristic values of the TG, DTG and DSC curves of the two factions obtained from the Smart Crusher, which are also referred to as cementitious Smart Crusher fractions in this study, in the three main temperature ranges. The TG, DTG and DSC curves with their characteristic values can be found in Appendix B, C and D respectively. The first mass loss for all the samples occurs between room temperature and 250 °C as a result of the evaporation of free water and the dehydration of hydration products, such as ettringite (hydrous calcium aluminium sulphate) and C-S-H. The next drop in the mass occurs in the temperature range of 400 – 550 °C, which corresponds with the decomposition of the hydration product portlandite (CH). The presence of portlandite in the samples indicates that hydration occurred. In the temperature range of 700 – 900 °C another sudden change in the mass can be distinguished. This mass loss corresponds with the decomposition of calcium carbonate. Besides the more abrupt weight loss of the samples, the samples also lose weight continuously due to the dehydration of calcium silicate hydrates, calcium aluminate hydrates and other minor hydrates [62].

		Samples cementitious material fractions					
Temperature range		1	2	3	4	5	6
30 - 250 °C	Weight loss in TG [%]	4.39	5.56	4.47	6.82	4.61	5.09
	Peak in DTG [°C]	133.0	132.4	126.8	133.0	131.9	133.0
	Area in DSC [J/g]	95.70	84.61	104.80	135.90	97.98	90.68
400 - 550 °C	Weight loss in TG [%]	0.27	0.18	0.25	0.21	0.40	0.18
	Peak in DTG [°C]	467.9	467.3	466.5	468.6	469.8	469.1
	Area in DSC [J/g]	6.28	0.97	7.08	1.70	5.51	1.29
700 - 900 °C	Weight loss in TG [%]	5.13	6.77	4.71	6.75	5.02	6.52
	Peak in DTG [°C]	819.9	826.4	804.0	827.0	815.1	830.3
	Area in DSC [J/g]	66.07	43.54	77.20	95.55	67.84	84.14
Total mass loss	Weight loss in TG [%]	13.12	16.99	12.48	18.65	13.60	16.64

Table 3: Characteristic values of TG, DTG and DSC curves of the cementitious Smart Crusher fractions. Where 1, 3, 5 are fraction 0.063 - 0.125 mm and 2, 4, 6 are fraction 0.0 - 0.063 mm. Three temperature ranges in which abrupt mass loss occurs, can be distinguished for both fractions. The 0.0 - 0.063 mm fraction has a larger total mass loss than the 0.063 - 0.125 mm fraction.

The three temperature ranges in which the abrupt mass losses occur, are accompanied with endothermic peaks in the DSC curves. Besides the endothermic peaks, which can be linked to mass

loss in the TG curves, another endothermic peak can be distinguished. This peak occurs around 570 °C in the DSC curves, but no abrupt mass loss occurs in the TG curves around this temperature. These transitions can be attributed to phase changes or transitions. According to the literature a quartz phase transition, which indicates the presence of aggregates such as sand particles, occurs at 573 °C [41]. The endothermic peak occurring around 570 °C is therefore suspected to be the phase transition of α-quartz into β-quartz (α-SiO_2 to β-SiO_2). The occurrence of this endothermic peak indicates the presence of components not belonging to the components usually present in cement, because the decomposition reactions of cement with increase in temperature occur within the three mentioned temperature ranges.

Table 4 shows characteristic values of the TG, DTG and DSC curves of the two hydrated reference materials CEM I 52.5 R and CEM III/B 42.5 N in two main temperature ranges. The TG, DTG and DSC curves with their characteristic values can be found in Appendix B, C and D respectively. The first transition in the TG curves occurs between room temperature and 250 °C as a result of the evaporation of free water and the dehydration of hydration products. The second transition is seen in the temperature range of 400 – 550 °C, which corresponds with the decomposition of the hydration product portlandite (CH). Both of these temperature ranges can also be found for the samples of the cementitious Smart Crusher fractions. In the temperature range of 700 – 900 °C no weight loss can be distinguished, in contradiction with the samples of the cementitious Smart Crusher fractions. This can be explained because the hydrated reference samples are prepared after hydration and after removing from the oven, grinding took place in the open air. During this preparation and grinding no significant amount of calcium hydroxide reacts with CO_2 from the air to form calcium carbonate, because this reaction is very slow. The decomposition of calcium carbonate takes place in the 700 – 900 °C range. Because no calcium carbonate is present no weight loss is seen in this temperature region. In table 4 the results of the TG, DTG and DSC are summarized.

		Samples hydrated reference material	
Temperature range		CEM I hydrate	CEM III/B hydrate
30 - 250 °C	Weight loss in TG [%]	8.13	11.85
	Peak in DTG [°C]	148.6	144.5
	Area in DSC [J/g]	150.6	188.7
400 - 550 °C	Weight loss in TG [%]	4.79	0.75
	Peak in DTG [°C]	502.4	482.5
	Area in DSC [J/g]	118.3	10.38
Total mass loss	Weight loss in TG [%]	20.07	22.17

Table 4: : Characteristic values of TG, DTG and DSC curves of the hydrated reference samples CEM I 52.5 R and CEM III/B 42.5 N. Abrupt mass loss occurs in two temperature ranges and no decomposition of calcium carbonate (mass loss in a third temperature range) was observed.

Comparing the values of table 3 and 4, it can be seen that the values of the hydrated reference samples are higher than those of the cementitious Smart Crusher fractions. Differences can be explained, using the values of the weight loss in the TG. In the first temperature interval, where temperatures range from room temperature to 250 °C, the cementitious Smart Crusher fractions lose 4.0 – 7.0% of their weight, while the CEM I hydrate loses 8.13% of its weight and the CEM III/B hydrate loses 11.85% of its weight. Pane and Hansen (2005) found that water would turn into gas completely at 140 °C and expected that this would also be the case for free (physically bound) water in the surface and pores of the cement samples [76]. This, together with the hydration age of the samples, could result in the higher weight loss of the hydrated reference samples. Additionally, the weight loss can also be influenced by the amount of hydraulic reactive material. A higher weight loss indicates a larger amount of hydraulic material, which suggests a higher relative amount of cement. The second temperature

interval, which ranges from 400 °C to 550 °C, results in a weight loss for the cementitious Smart Crusher fractions of 0.18 – 0.40%, for the CEM I hydrate of 4.79% and the CEM III/B hydrate of 0.75%. The value of the CEM III/B hydrate can be seen as comparable to the cementitious Smart Crusher fractions, whereas the value of the CEM I hydrate is significantly larger. The weight loss in this temperature range occurs due to the dehydration of portlandite, as was mentioned before. In the hydration process of slag cement two hydration steps can be distinguished. In the first step the cement reacts with water and hydrations products are formed, including portlandite, which is one of the activators for slag. In the second step the portlandite reacts with the slag, which is also called the slag hydration delay [50]. This last step results in a lower amount of portlandite in slag cements compared to Portland cement. A lower amount of portlandite can also explain the significant difference in mass loss between the CEM I hydrate and the CEM III/B hydrate and the cementitious Smart Crusher fractions. Equal to the first temperature interval, the weight loss can also be influenced by the amount of hydraulic reactive material, a higher weight loss indicating a larger amount of hydraulic material, which suggests a higher relative amount of cement. In the last temperature interval of 700 to 900 °C the hydrated reference materials show no weight loss, whereas the cementitious material do change in mass. The reason for this is the preparation of the hydrated reference samples, because the carbonation process is a slow process, as explained before.

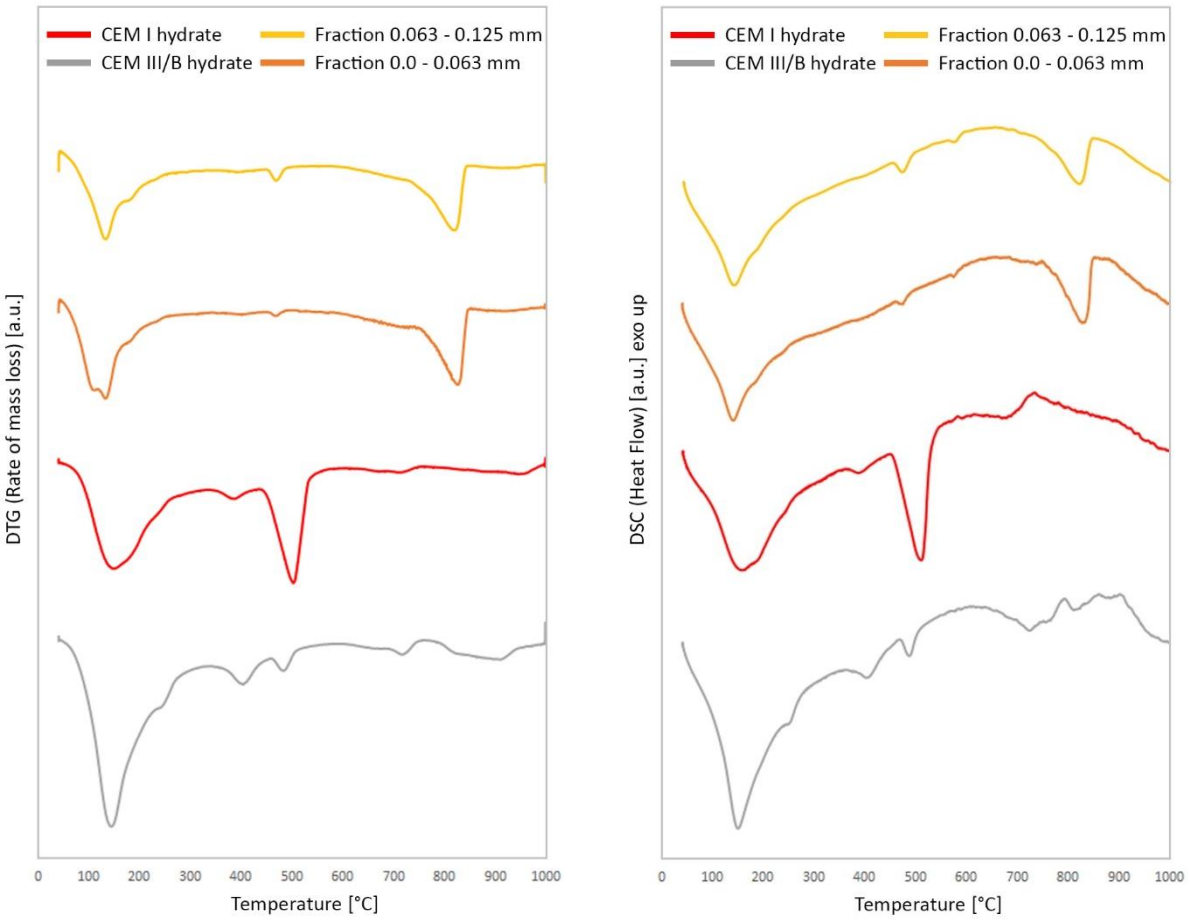

Figure 41: Comparison DTG (left) and DSC (right) curves. Abrupt mass loss occurs in three temperature ranges for the cementitious Smart Crusher fractions and in the first two temperature ranges for the reference samples. The DSC curves of the cementitious Smart Crusher fractions show an endothermic peak around 570 °C due to a phase transition of α-quartz to β-quartz.

Figure 41 shows a comparison between the DTG and DSC curves of the two cementitious Smart Crusher fractions and the hydrated reference samples. Both the DTG and DSC show that the peaks in the graphs of the first two temperature intervals occur at approximately the same temperatures. Additionally, it can clearly be seen that the two cementitious Smart Crusher fractions undergo decomposition of the

calcium carbonate, while this peak is not present in the graphs of the hydrated reference samples. Another interesting difference is found in the DSC graphs. An endothermic peak can be distinguished around 570 °C in the graphs of the two cementitious samples, which was suspected to be caused by the phase transition of α-quartz to β-quartz. This endothermic peak does not occur in the graphs of the hydrated reference samples. This confirms the presence of aggregates such as sand particles in the two cementitious Smart Crusher fractions.

In Appendix E the results of the mass spectrometry can be found. The results of the cementitious Smart Crusher fractions are in agreement with the described temperature ranges. For the hydrated reference samples the emission of water is also in agreement with the described changes in the temperature ranges, but besides water, also CO_2 and SO_2 were measured. The amounts are neglectable small and therefore are not found in the graphs of the TG. DTG and DSC. The reason for the small amount of CO_2 was already discussed previously. The SO_2 might be linked to the decomposition temperature of $CaSO_4$. In the presence of Fe_2O_3 this temperature is in agreement with the results of the mass spectrometry [64]. Another possibility for the release of SO_2 might be linked to the occurrence of the following reaction:

$$C_6A\bar{S}_3H_{32} \rightarrow C_3A + SO_2$$

Insight in the portlandite, calcite and bound water contents are usually used to investigate the hydration reaction of cement and supplementary cementitious materials and the carbonation progression. Weight changes in the TG curves at certain temperature ranges are used to identify the components [107]. To estimate the contents the following characteristic regions can be distinguished within the TG curves:

- Abrupt weight loss between 400 – 550 °C, which is related to the decomposition of portlandite.
- Abrupt weight loss between 700 – 900 °C, which is related to the decomposition of calcium carbonate.
- Continuous weight loss between 105 – 1000 °C, referred to the non-evaporable water content, due to dehydration of calcium silicate hydrates, calcium aluminate hydrates and other minor hydrates [62].

The determination of the non-evaporable water contents seems to be complex, because an accurate distinction between chemically bound water and evaporable water cannot be made and accurate knowledge of the composition of the hydration products and the relationship between the quantities of substances involved in the reaction is not known. Still, non-evaporable water is seen as a useful indicator of the hydration progress [62]. In this thesis, as a simplification, the non-evaporable water content will be seen as the weight loss between 105 – 1000 °C minus the weight loss due to the decomposition of portlandite and calcium carbonate. Table 5 shows the portlandite, calcium carbonate and non-evaporable water content.

Content [%]	**Samples**							
	1	2	3	4	5	6	CEM I hydrate	CEM III/B hydrate
Portlandite (CH)	0.27	0.18	0.25	0.21	0.40	0.18	4.79	0.75
Calcium Carbonate	5.13	6.77	4.71	6.75	5.02	6.52	-	-
Non-evaporable water	7.68	9.84	7.21	10.35	7.95	9.91	15.28	21.42

Table 5: Portlandite, calcium carbonate and non-evaporable water content of the cementitious Smart Crusher fractions and the hydrated reference samples. Hydrated reference samples have a larger CH and non-evaporable water content than the cementitious Smart Crusher fractions.

The non-evaporable water content will be used as an indication for the relative amount of cement in the samples. Assumed is that the samples with a larger relative amount of cement will have a larger weight loss due to the release of water. The non-evaporable water content for the 0.0 – 0.063 mm

fractions ranges from 9.84% to 10.35%, whereas the non-evaporable water content for the 0.063 – 0.125 mm fractions ranges from 7.21% to 7.95%. This means that the weight change due to the loss of water will be larger in the 0.0 – 0.063 mm fraction. This could mean that this fraction has more hydraulic reactive material and therefore the relative amount of cement is larger for this fraction. Using the same approach when comparing the cementitious Smart Crusher fractions to the hydrated reference samples, it becomes clear that the hydrated reference samples have a significantly larger non-evaporable water content. Therefore, the hydraulic reactive material is seen to be larger for the hydrated reference samples, which also implies a larger relative amount of cement. It has to be mentioned though, that the calculated value is a simplification used to make a comparison between the different samples. As was found by Pane and Hansen (2005) water would turn into gas completely at 140 °C. The non-evaporable water content is usually taken between 105 – 1000 °C, the values could be influenced by possible free (physically bound) water on the surface and in the pores of the cement samples [76].

6.3 Chemical composition

To gain insight in the chemical composition of the different samples, x-ray fluorescence (XRF) was used. The cementitious Smart Crusher fractions (0.0 – 0.063 mm and 0.063 – 0.125 mm) are compared with the three reference cements, hydrated and unhydrated, as well as fly ash and blast furnace slag, because the exact cement type of the Smart Crusher samples is unknown. Due to this the cementitious Smart Crusher fractions could be composed of either one of the reference cements or a combination of the reference cements with fly ash and/or blast furnace slag. The materials that are analysed and the literature study resulted in the following main hypotheses:

1. The chemical composition of the cementitious Smart Crusher fractions (0.0 – 0.063 mm and 0.063 – 0.125 mm) are comparable with the reference materials.
2. In the 0.0 – 0.063 mm fraction, the relative amount of cement is larger than in the 0.063 – 0.125 mm fraction. Therefore, the chemical composition of the 0.0 – 0.063 mm fraction will be more comparable with the reference material.

In table 6 the chemical composition of the two cementitious Smart Crusher fractions and hydrated references samples are listed. All oxides exceeding 0.01% of the mass of the sample were included in the table.

Chemical analysis [%]	0.0 – 0.063 mm	0.063 – 0.125 mm	CEM I hydrate	CEM III/B hydrate	Fly Ash	Blast Furnace Slag
CaO	36.65	33.74	71.54	57.80	6.32	44.80
SiO_2	47.63	51.46	16.25	23.28	54.48	30.25
Al_2O_3	6.94	6.72	3.84	7.00	23.77	12.62
MgO	1.67	1.66	1.63	5.08	1.10	8.24
SO_3	1.32	1.30	2.02	3.06	0.86	1.33
Fe_2O_3	3.91	3.31	3.18	1.67	9.20	0.56
TiO_2	0.46	0.40	0.36	0.96	1.23	1.13
K_2O	0.95	0.97	0.58	0.52	1.88	0.51
MnO	0.13	0.12	0.06	0.24	0.05	0.31
SrO	0.10	0.08	0.18	0.12	0.21	0.07
Cl	0.03	0.05	0.05	0.06	0.00	0.00
ZnO	0.04	0.04	0.07	0.03	0.03	0.00
Cr_2O_3	0.02	0.01	0.01	0.00	0.03	0.00
P_2O_5	0.00	0.00	0.13	0.00	0.47	0.00
Other	0.15	0.14	0.10	0.18	0.37	0.18

Table 6: Chemical composition of the cementitious Smart Crusher fractions and hydrated reference materials. The cementitious Smart Crusher fractions show a higher SiO_2 content and lower CaO content than the hydrated reference samples.

The composition of the cementitious Smart Crusher fractions appears to be comparable except for the CaO and SiO_2. Table 6 shows only a small difference between the different oxides. The biggest differences can be found for the CaO and SiO_2 contents of the samples. The 0.0 – 0.063 mm fraction contains 36.65% CaO and 47.63% SiO_2, whereas the 0.063 – 0.125 mm fraction contains 33.74% CaO and 51.46% SiO_2. The large SiO_2 contents are a conformation of the DSC results, which showed a phase transition of α-quartz to β-quartz. Appendix F figure F.2 shows examples of compositions as mentioned in NEN-EN 196-2 [73]. The values for CaO range from 61.2 – 68.8% and the values for SiO_2 range from 18.0 – 24.0%. Comparing these values with the results of the CEM I hydrate in table 6 it can be seen that the CaO content of the CEM I hydrate is higher, while the SiO_2 is lower than the values mentioned in NEN-EN 196-2 [73]. This can be explained by the particle size effect, which results in a disadvantage in the case of powder samples. The particle size effect causes a slight deviation of up to approximately 5% in the results, leading to a higher percentage CaO and a lower percentage SiO_2. This effect is seen for all powder samples. Taking into account the particle size effect, the CEM I hydrate results are comparable to the values mentioned in the appendix. The results for the CEM III/B hydrate are also comparable to the literature values [35] as well as the values shown in Appendix F figure F.3.

From table 6 it can be seen immediately that the CEM I hydrate is rich in CaO (71.54% CaO), while in the CEM III/B hydrate this is considerably lower (57.80% CaO). The cementitious Smart Crusher fractions are even lower than both the hydrated reference samples (36.65% CaO for the 0.0 – 0.063 mm fraction and 33.74% for the 0.063 – 0.125 mm fraction). On the other hand, the CEM I and the CEM III/B hydrate have a relatively low SiO_2 content (16.25% and 23.28% SiO_2 respectively), while the 0.0 – 0.063 mm and the 0.063 – 0.125 mm fraction have a considerably higher SiO_2 content (47.63% and 51.46% SiO_2 respectively). The XRF results together with the results of the DSC indicates the presence of components not belonging to the components usually present in cement in the cementitious Smart Crusher fractions. The composition of the cementitious Smart Crusher fractions and the hydrated reference samples cannot be seen as comparable due to the large deviations between the compositions, especially the CaO and SiO_2 contents. Appendix F figure F.1 shows the complete results of the XRF analysis. Not only for the main constituents there is a deviation, also for the minor constituents a deviation can be seen. A clear difference can be seen in the P_2O_5 content. In the cementitious Smart Crusher fractions, the CEM III/B hydrate and the blast furnace slag P_2O_5 is not present, while a small amount can be found in the CEM I hydrate and fly ash (see Appendix F figure F.1). The absence of P_2O_5 can be an indication that there is no or a not measurable amount of fly ash present in the cementitious Smart Crusher fractions.

NEN-EN 197-1 mentions different requirements for the cement constituents of Portland cement, blast furnace slag and fly ash. For Portland cements the CaO/SiO_2 ratio has to be larger or equal 2.0 and the MgO content may not exceed 5.0% by weight. In the case of blast furnace slag the $(CaO + MgO)/SiO_2$ ratio has to exceed 1.0 and $CaO + MgO + SiO_2$ has to be at least two-thirds by weight. Although fly ash is not used in practice as much as Portland cement and blast furnace slag, for this analysis fly ash is incorporated to see if the cementitious Smart Crusher fractions might contain some fly ash. For fly ash the requirements mention a reactive CaO content smaller than 10% and a SiO_2 content larger or equal to 25% by weight [72]. Table 7 summarizes the different values, which will be compared with the previous mentioned requirements. Both the CEM I and CEM III/B hydrate meet their respective requirements, while the cementitious Smart Crusher fractions only meet the requirements partly.

Requirements	0.0 – 0.063 mm	0.063 – 0.125 mm	CEM I hydrate	CEM III/B hydrate	Fly Ash
$CaO/SiO_2 \geq 2.0$	0.77	0.66	4.40	-	-
MgO < 5.0 wt%	1.67	1.66	1.63	-	-
$CaO + MgO + SiO_2 \geq 66.67$	85.95	86.86	-	86.16	-
$(CaO + MgO)/SiO_2 \geq 1.0$	0.80	0.69	-	2.70	-
CaO ≤ 10 wt%	36.65	33.74	-	-	6.32
$SiO_2 \geq 25$ wt%	47.63	51.46	-	-	44.80

Table 7: Requirements for the constituents. The hydrated reference samples meet the requirements and the cementitious Smart Crusher fractions only meet the requirements for MgO < 5.0 wt%, $CaO + MgO + SiO_2 \geq 66.67$ and $SiO_2 \geq 25$ wt%.

6.4 Crystalline Phases

For a qualitative mineralogical analysis of the crystalline phases in the samples, x-ray diffraction (XRD) was performed. For the characterization of the cementitious Smart Crusher fractions (0.0 – 0.063 mm and 0.063 – 0.125 mm), their diffraction patterns are compared with the three reference cements, hydrated and unhydrated, as well as fly ash and blast furnace slag. Additionally, the diffraction patterns could be used to gain insight in the availability of hydraulic minerals, hydration products and the presence of minerals usually not found in cementitious materials. Possible results that could be obtained during the tests were determined based on the materials and the literature study. The expected results are summarized below:

1. In the 0.0 – 0.063 mm fraction, the relative amount of cement is larger than in the 0.063 – 0.125 mm fraction. For this reason the peaks of cement components are more distinct in the diffraction pattern of the 0.0 – 0.063 mm fraction.
2. In the hydrated reference samples mainly hydration products are found, while in the unhydrated reference samples hydraulic minerals are present.
3. In the diffraction pattern of the cementitious Smart Crusher fractions the crystalline phases are linked to fine concrete aggregates, whereas these crystalline fractions are not present in the diffraction patterns of the reference samples.

Appendix G figure G.1 shows the diffractograms of the unhydrated reference samples CEM III/B 42.5 N, CEM I 52.5 R and CEM I 42.5 N. Looking at the diffractograms of CEM I 42.5 N and CEM I 52.5 R, both materials have comparable characteristics. In practice, mostly CEM I 52.5R is used and therefore the hydrated reference materials were chosen to be CEM I 52.5R and CEM III/B 42.5 N.

The diffraction pattern of the cementitious materials (0.0 – 0.063 mm and 0.063 – 0.125 mm) are shown in figure 42. As can be seen, the diffraction patterns of the cementitious materials are almost identical. However, a difference can be observed in the peak intensities. The 0.0 – 0.063 mm fraction has a slightly higher peak intensity for the cement hydration products. Both fractions mainly contain quartz (SiO_2) and calcite ($CaCO_3$), but cement hydration products such as ettringite and portlandite were also detected. The presence of quartz is in agreement with the results of the XRF analysis and indicates the presences of aggregates such as sand particles in the samples.

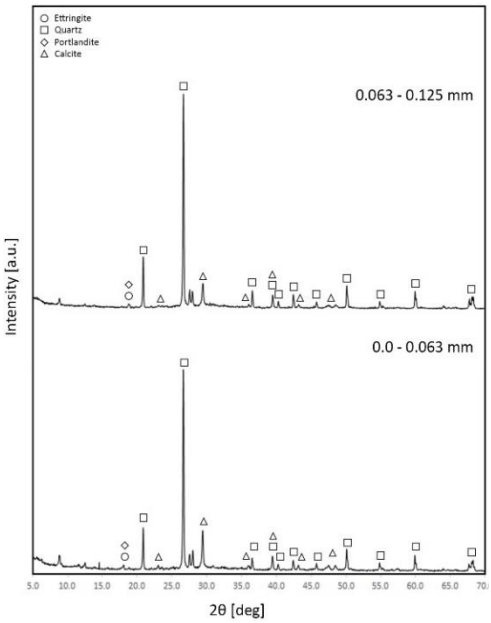

Figure 42: Diffraction pattern of the two cementitious Smart Crusher size fractions showing only minor differences in the composition. Quartz, portlandite, ettringite and calcite minerals are distinguished.

Figure 43 shows the diffraction pattern of the reference materials, CEM I 52.5 R and CEM III/B 42.5 N. Both samples contain mostly hydration products. For the CEM I hydrate the peaks with the larger intensities correspond to portlandite. Most of these portlandite peaks can also be distinguished in the CEM III/B hydrate, but have a lower peak intensity. This is an indication that the amount of portlandite in the CEM III/B hydrate is lower than in the CEM I hydrate. Less portlandite is the result of the reaction of portlandite with the slag in CEM III/B as portlandite is an activator for slag [50]. This is in agreement with the results of the TGA results. From the MS results in Appendix E followed that for both the hydrated reference samples the CO_2 emission was small, but the CO_2 emission for the CEM III/B hydrate was slightly higher. Additionally, it was found in literature that cement with an increasing amount of slag shows increasing carbonation rates [89]. This could also explain the presence of the calcite peaks in the diffraction pattern and a slightly larger CO_2 emission as observed in the MS results of the CEM III/B hydrate.

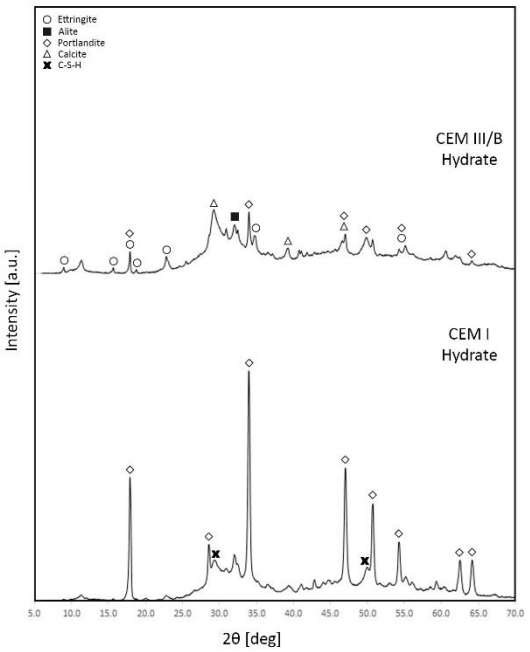

Figure 43: Diffraction pattern of the hydrated reference materials showing distinct peaks of ettringite, portlandite, C-S-H, alite and calcite minerals. Portlandite has a higher peak intensity in the CEM I hydrate than in the CEM III/B hydrate.

To compare the diffraction pattern of the hydrated reference samples and the cementitious Smart Crusher fractions, figure 44 was used. In this figure the quartz peaks with a high peak intensity were neglected for comparing the peaks corresponding to the crystal phases of cement. A clear difference between the cementitious Smart Crusher fractions and the hydrated reference materials is the presence of quartz peaks in the cementitious Smart Crusher fractions. These peaks are not present in the reference samples, which again indicates that the cementitious Smart Crusher fractions contain particles normally not present in cementitious binders, but belonging to aggregates such as sand particles. Additionally, a difference in the calcite peaks between the cementitious Smart Crusher fractions and the hydrated reference materials can be seen. The hydrated reference materials have no or a few small calcite peaks, whereas in the diffraction patterns of the cementitious Smart Crusher fractions numerous calcite peaks can be distinguished. This difference is in agreement with the TGA, DSC and MS results and can be linked to the slow carbonation process. The difference in age of the materials as well as the preparation of the hydrated reference samples has as result that no significant amount of calcium hydroxide reacts with CO_2 from the air to form calcium carbonate. The diffraction patterns of the hydrated reference materials show more cement hydration products than the cementitious Smart Crusher fractions. This indicates that the amount of cementitious material in the hydrated reference samples is larger than in the cementitious Smart Crusher fractions, which is confirmed by the XRF results.

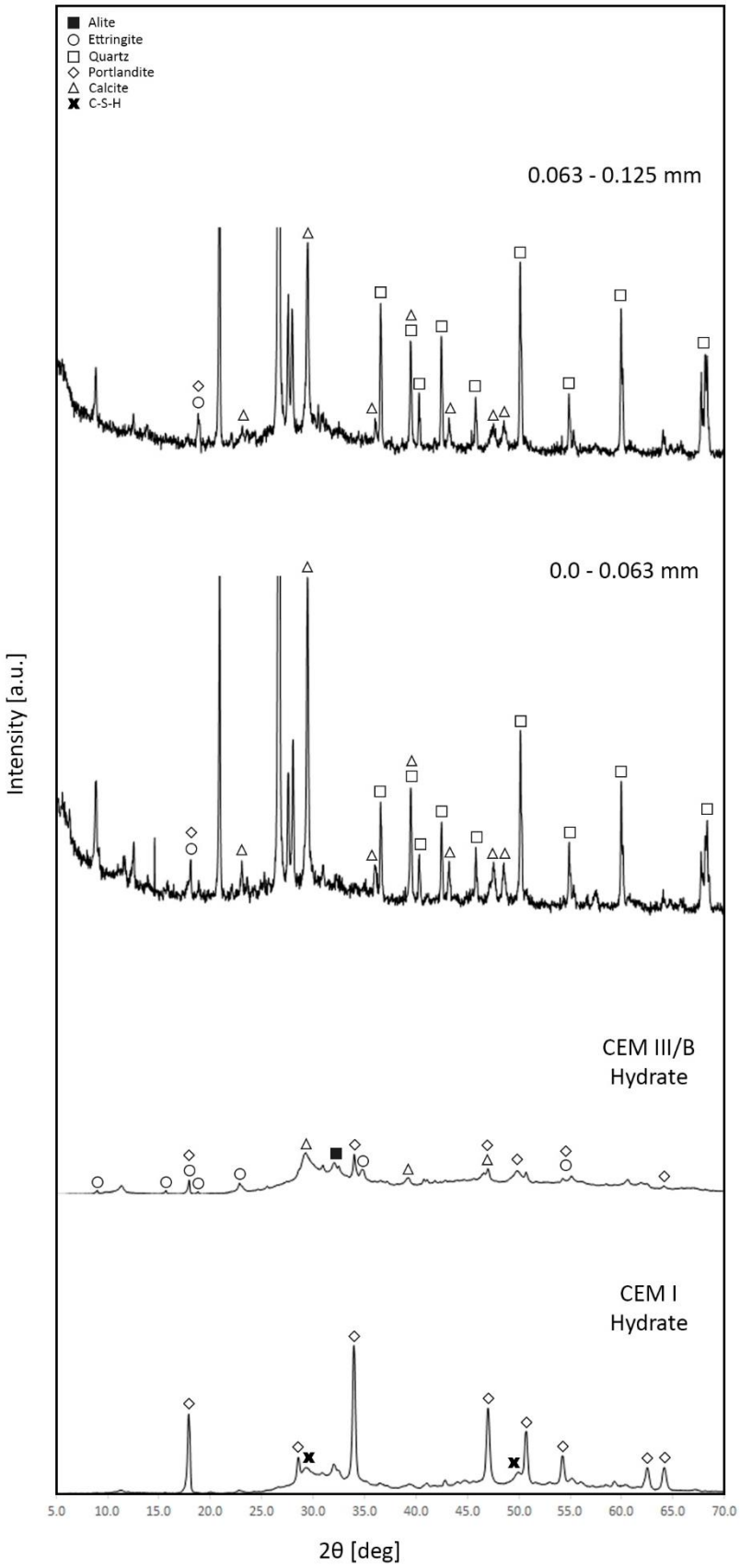

Figure 44: Diffraction pattern of the hydrated reference samples and the cementitious Smart Crusher fractions. The cementitious Smart Crusher fractions show mainly distinct quartz and calcite peaks and the hydrated reference samples show mainly peaks associated with the cement hydration products.

7 UPCYCLING ASSESMENT CEMENTITIOUS BINDER

For the upcycling of the secondary cementitious binder different thermal treatments were used. To take into account the possible influence of fine concrete aggregates in the cementitious Smart Crusher fractions, the reference samples were hydrated and also thermally treated. A comparison between the cementitious Smart Crusher fractions and the hydrated reference material will not only give insight in the functional quality of the materials, but can also give insight in the possibility of recycling cement. Additionally, the different thermal treatments will be analysed to gain insight in which thermal treatment would have the highest upcycling potential.

7.1 Thermal treatment

Powder samples of the two cementitious fractions of the Smart Crusher material and the two hydrated reference materials were exposed to different thermal treatments. The powder samples were exposed to temperatures of 500 °C, 800 °C and 1400 °C. A first distinction of the influence of the thermal treatment on the different powder samples could be observed after taking the samples from the oven. Figure 45 shows the powder samples in the following order: hydrated sample, 500 °C, 800 °C, 1400 °C and for the reference materials the non-hydrated powders. After the thermal treatments a change in the colour of the samples can be observed. The colour change of interest is the occurrence of a reddish colour in the two cementitious Smart Crusher fractions at 500 °C and 800 °C. Literature shows that concrete turns red in a temperature range of 300 °C to 600 °C and a greyish hue will start to develop between 600 °C and 900 °C resulting in a slight decrease of the red colour. The change of colour is caused by the presence of silicate aggregates, such as quartz, in the concrete. The iron within these aggregates dehydrates or oxidizes at elevated temperatures, which causes the red colouration [42; 56]. The two reference samples did not show a red colouration, whereas the cementitious Smart Crusher fractions showed a clear change in colour. The observation of the red colouration in the cementitious Smart Crusher fractions therefore shows that aggregates such as sand particles are present within the powder. This was confirmed by the DSC, XRF and XRD results.

CEM I 52.5 R

0.0 – 0.063 mm

CEM III/B 42.5 N

0.063 – 0.125 mm

Figure 45: Colour changes in the cementitious powders after thermal treatment showing the red colouration of the cementitious Smart Crusher fractions after thermal treatments at 500 °C and 800 °C.

Thermal treatments at 500 °C and 800 °C did not noticeably influence the state of the material. The powder samples remained a powder after their thermal treatment in contrast to the 1400 °C treatment. Figure 46 shows the state of the cementitious Smart Crusher fractions and the reference materials after a thermal treatment at 1400 °C. Both material types changed in a solid mass after the thermal treatment, but a difference between the solid masses can be observed. The reference materials seemed to be sintered into a more compact solid mass without liquification, whereas the cementitious Smart Crusher fractions seemed to be liquified before hardening during the cooling down process. Additionally, the compact reference material could be easily removed from the Alsint bowls, while the cementitious material could only be removed from the Alsint bowls by breaking the bowls. The difference in the state of the material indicates a reduction of the temperature at which liquification occurs for the cementitious Smart Crusher fractions. For quartz the transition temperature is lowered to 1315 °C in the presence of Al_2O_3. Additionally, the presence of CaO, B_2O_3, P_2O_5 or Na_2CO_3 in combination with quartz accelerated the formation of the glassy phase. Generally, cement minerals have a melting point, which lies above the 1400 °C. As explained before, calcite decomposes between 700 °C and 900 °C and results in the formation of CaO. Silica and iron oxide from the aggregates in combination with CaO may decrease its melting point below 1400 °C and the material can transform from a solid to a melt. Additionally, a substantial amount of silicon or magnesium reduces the melting point of the calcium aluminoferrite to 1350 °C [48; 79]. From the DSC, XRF and XRD results it became clear that the cementitious Smart Crusher fractions contain a substantial amount of quartz. The presence of quartz in combination with the cement components resulted in a decrease of the melting point of the material. This explain the difference between the state of the two material types.

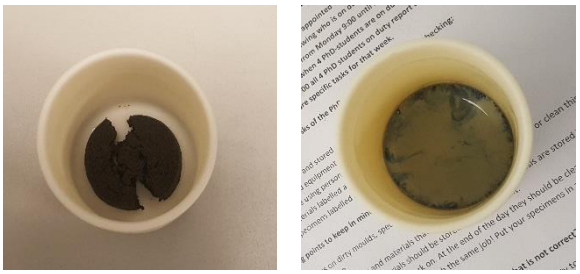

Figure 46: Material structure after the 1400 °C treatment. The reference materials (left) show a compact sintered solid mass and the cementitious Smart Crusher fractions (right) show a hardened melt.

7.2 Chemical composition

The two cementitious fractions of the Smart Crusher material and the hydrated reference material underwent different temperature treatments. Three dehydration temperatures were used, namely 500 °C, 800 °C and 1400 °C. Bogue's equations [99] will be used to estimate the percentage of cement minerals present in the samples. This equation is used for the unhydrated reference samples as well as the samples heated to 1400 °C, because these are assumed to be fully dehydrated. With this approach the amount of important cement minerals can be compared. The expected results of the XRF analysis were translated into the following main hypotheses:

1. The dehydration temperatures have no significant influence on the chemical composition of the analysed samples.
2. The 0.0 – 0.063 mm fractions have a larger relative amount of cement than the 0.063 – 0.125 mm fractions. Therefore the influence of the dehydration temperatures on the 0.0 – 0.063 mm fractions are more comparable to the influence of the dehydration temperatures on reference materials.

In Appendix F figure F.1 the results of the XRF analysis can be found. The chemical compositions of the samples are listed for different treatments, namely unhydrated, hydrated and the different dehydration temperatures. Figure 47 compares the influence of the different treatments on the oxide contents. The oxides with the largest contents were used in the comparison. No significant differences

occur in the chemical composition due to the different treatments for the CEM I 52.5 R and CEM III/B 42.5 N samples. Looking at for example the CaO and SiO_2 contents the values of the CEM I 52.5 R samples range from 70.47% – 71.54% for CaO and 16.25% – 17.07% for SiO_2 and the values of the CEM III/B 42.5 N samples range from 55.01% - 57.80% for CaO and 23.28% – 24.82% for SiO_2. For the 0.0 – 0.063 mm and 0.063 – 0.125 mm fractions the chemical composition is also comparable for the different treatments, only for the CaO and SiO_2 contents a change is observed at the 1400 °C dehydration temperature. For the hydrated, 500 °C and 800 °C samples, the contents of CaO range from 35.94% – 36.65% and 33.74% – 35.72% respectively and the SiO_2 contents range from 47.63% – 48.85% and 48.82% – 51.46% respectively. For the 1400 °C samples the amount of CaO decreases (31.44% and 25.71% respectively), while the amount of SiO_2 increases (54.42% and 62.52% respectively) for both fractions. Furthermore, all the samples treated with a dehydration temperature of 1400 °C showed significant changes in the amount of SO_3. The changes in SO_3 content could be the result of thermal decomposition of $CaSO_4$. When the temperature increases in the interval 800 – 1200 °C more SO_2 will be released [71]. For all the treatments the SO_3 content was comparable, but for the 1400 °C samples a decrease was observed in the SO_3 content.

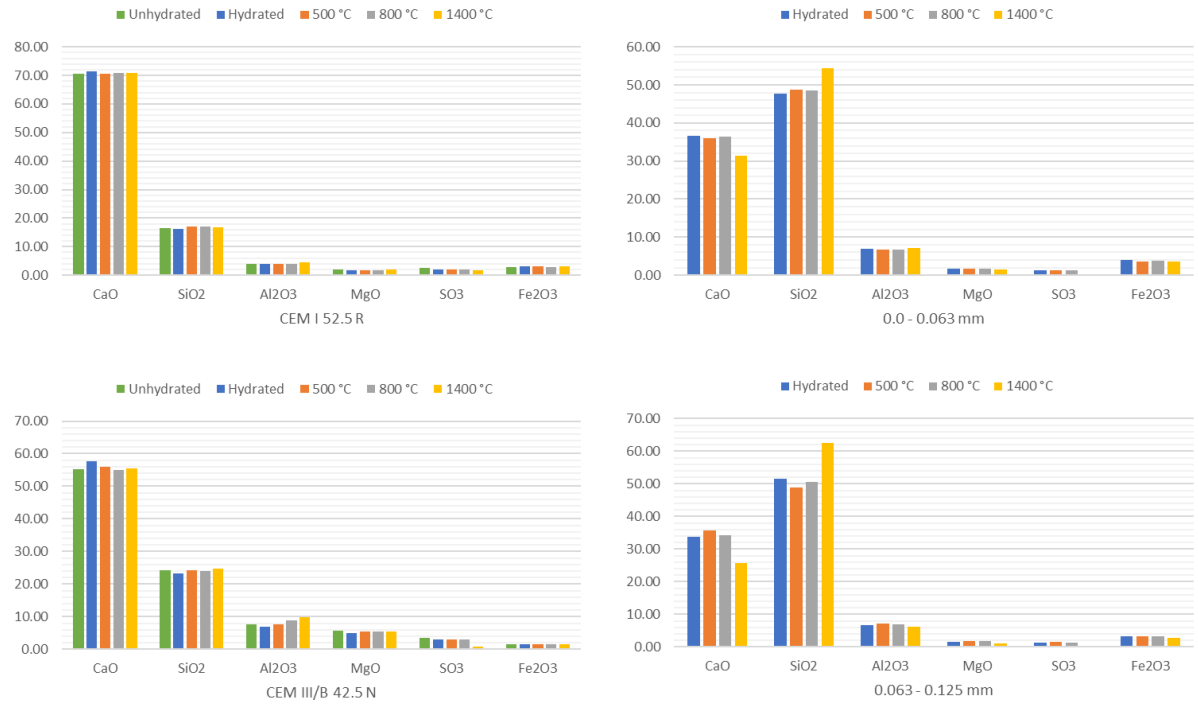

Figure 47: Comparison oxide content under different treatments showing only minor differences in the chemical composition. The SO_3 content decreases as a result of the thermal treatment at 1400 °C.

Bogue (1929) mentions the possibility to calculate the relative amount of the compounds present in cement, when the chemical composition is known. He assumes that the relative amount of the four main components of cement (C_3S, C_2S, C_3A and C_4AF) depends on the reaction of the components C, S, A and F. Furthermore, part of C is assumed to react with $\overline{S}$, which results in the formation of $C\overline{S}$, and the magnesia is assumed to remain as uncombined MgO [18]. When using Bogue's equations it is important to keep in mind that the calculated amounts are approximations of the actual composition. The accuracy of Bogue's model has its limitations and it is known that variations in the equations and deviations in the results occur. Still, Bogue's equations are widely used to gain insight in the relative amount of the compounds present in cement [17]. The Bogue equations can be derived from the Bogue matrix [99]:

$$\begin{bmatrix} CaO \\ SiO_2 \\ Al_2O_3 \\ Fe_2O_3 \\ SO_3 \end{bmatrix} = \begin{bmatrix} 0.7368 & 0.6512 & 0.6226 & 0.4610 & 0.4119 \\ 0.2632 & 0.3488 & 0.0000 & 0.0000 & 0.0000 \\ 0.0000 & 0.0000 & 0.3774 & 0.2100 & 0.0000 \\ 0.0000 & 0.0000 & 0.0000 & 0.3290 & 0.0000 \\ 0.0000 & 0.0000 & 0.0000 & 0.0000 & 0.5881 \end{bmatrix} \begin{bmatrix} C_3S \\ C_2S \\ C_3A \\ C_4AF \\ C\bar{S} \end{bmatrix}$$

By taking the inverse of the matrix the Bogue equations are derived as a set of equations for alite, belite, aluminate and ferrite. When a chemical analysis is done the mineralogical composition can be calculated using the following Bogue equations [99]:

$$\begin{aligned} C_3S &= 4.071(CaO) - 7.600(SiO_2) - 6.718(Al_2O_3) - 1.430(Fe_2O_3) - 2.852(SO_3) \\ C_2S &= 2.867(SiO_2) - 0.7544(C_3S) \\ C_3A &= 2.65(Al_2O_3) - 1.692(Fe_2O_3) \\ C_4AF &= 3.043(Fe_2O_3) \end{aligned} \quad (7.1)$$

The Bogue equations can only be used for Portland cement. For blast furnace cement, complex cement blends and powders the Bogue equations cannot be used. Furthermore, there are no equations equivalent to the Bogue equations for blended cements [26]. The XRF results made clear that the chemical composition of the cementitious Smart Crusher fractions deviate significantly from the hydrated reference samples. Therefore, only the CEM I 52.5 R samples can be calculated, using the Bogue equations. During this calculation the influence of the particle size effect was also taken into account. Table 8 shows the results of the calculation with the Bogue equations of CEM I 52.5 R. Taylor (1997) mentioned that 50 – 70% consists of C_3S, 15 – 30% of C_2S, 5 – 10% of C_3A and 5 – 15% of C_4AF [101]. From table 8 follows that the obtained results for both the untreated as well as the treated samples fall within these ranges. Because the literature mentioned that there are no equations equivalent to the Bogue equations for blended cements, it is not possible to compare the results in table 8 with the cementitious Smart Crusher fractions and the CEM III/B 42.5 N samples.

		C_3S [%]	**C_2S [%]**	**C_3A [%]**	**C_4AF [%]**
CEM I 52.5 R	Unhydrated	65.04	12.40	5.72	9.01
	Dehydrated	64.63	13.51	6.49	9.25

Table 8: Mineral composition of CEM I 52.5 R showing only minor differences in the amount of cement minerals of the unhydrated and dehydrated samples.

7.3 Crystalline Phases

For the upcycling of the cementitious materials different dehydration temperatures are used. The temperatures used, will influence the minerals in the samples. X-ray diffraction (XRD) is used for a mineralogical analysis of the crystalline phases present in the samples and to gain insight in the effect of the different dehydration temperatures on the minerals in the samples. For three target temperatures, namely 500 °C, 800 °C and 1400 °C, the formed minerals were identified. Changes in minerals due to the different upcycling treatments, together with the results of the XRF analysis, will give an indication which dehydration temperature will have the highest upcycling potential. This can be determined based on the presence of hydraulic minerals in the samples. The expected results of this analysis were translated into the following main hypotheses:

1. For higher dehydration temperatures the amount of hydration products will decrease and the amount of hydraulic minerals will increase. For each dehydration temperature the following can be expected:

    a. 500 °C: Ettringite and portlandite will be fully decomposed, while calcium carbonate can still be distinguished.
    b. 800 °C: Calcium carbonate will be fully decomposed and an increase in hydraulic cement minerals can be seen.
    c. 1400 °C: The samples will be fully dehydrated and have the highest amount of hydraulic cement minerals.
2. The 0.0 – 0.063 mm fractions have a larger relative amount of cement than the 0.063 – 0.125 mm fractions. Therefore the cement minerals will be more distinct in the diffraction patterns of the 0.0 – 0.063 mm fractions.
3. The hydrated reference samples have a larger relative amount of cement, which means that the hydraulic cement minerals will be more distinct in the diffraction patterns.

Figure 48 shows an overview of the diffraction patterns of the 0.0 – 0.063 mm fraction after undergoing different thermal treatments, namely no thermal treatment, dehydration at 500 °C, 800 °C and 1400 °C. For the identification of the peaks, the focus was on the main cement phases, hydrated and unhydrated, as well as phases which could be linked to fly ash and blast furnace slag. The untreated sample seems to consists mainly of quartz (SiO_2) and calcite ($CaCO_3$), but the cement hydration products such as ettringite and portlandite ($Ca(OH)_2$) were also detected. The diffraction pattern of the sample treated with a dehydration temperature of 500 °C shows the presence of quartz and calcite. Ettringite and portlandite are not detected, because ettringite dehydrates between 80 – 150 °C and portlandite decomposes between 400 - 550 °C [41]. In the diffraction patterns of the sample dehydrated at a temperature of 800 °C the main cement phases can be detected. The calcite peaks disappeared, because calcite starts decomposing around 700 °C [2] and the formation of alite, belite and the aluminate phase peaks occurs. Especially between 31 – 34° peak formations of these peaks could be distinguished. Additional, a small CaO peak was also detected. Quartz seems to be clearly present, which corresponds well with the results of the XRF analysis. The sample treated with a dehydration temperature of 1400 °C showed a completely different diffraction pattern in which close to no peaks could be identified as peaks linked to cement phases. The diffraction pattern indicates that the 1400 °C treatment resulted in a completely amorphous material.

Figure 49 shows an overview of the diffraction patterns of the CEM I samples after undergoing the same treatments as the 0.0 – 0.063 mm fractions. The hydrated sample seems to be composed mainly of portlandite together with some calcium silicate hydrates. The diffraction pattern of the sample dehydrated using 500 °C seems to contain a small amount of portlandite, although most of the peaks assigned to portlandite could also be linked to belite. Alite, belite and aluminate phases were also detected in the sample, which was not the case for the 0.0 – 0.063 mm fractions. For the sample dehydrated with 800 °C the alite, belite and aluminate phase were also found. Additionally, amounts of brownmillerite (ferrite phase) were also detected. The peaks are more distinct than the peaks in the 500 °C sample. Most of the peaks linked to belite and portlandite in the 500 °C sample are still present in the 800 °C sample and identified as belite in most cases. Therefore, it seems that the portlandite peaks in the 500 °C sample might be mostly allocated to the presence of belite. The sample dehydrated with a target temperature at 1400 °C showed a diffraction pattern, which was mainly composed out of alite and belite peaks. Most of the peaks with a higher peak intensity could be ascribed to both alite and belite. Overlapping diffraction peaks make it difficult, if one or both components are present within the sample. Additionally, the cooling of the samples after heating them to the target temperature also has to be mentioned. During the cement production the cement clinker is cooled down very quickly to around 1300 °C. Fast cooling is done to avoid that alite will revert back to belite, because alite can be metastable [58]. Therefore, it has to be considered that the overlapping peaks

could be only belite peaks formed due to the decomposition of alite as a result of the slow cooling of the sample.

An overview of the diffraction patterns of the CEM III/B samples after undergoing the same treatments as the previously mentioned materials is shown in figure 50. The hydrated sample is composed mainly of hydration products, such as portlandite and ettringite. Portlandite is less distinguishable compared to the CEM I hydrate. This is the result of the reaction of portlandite with the slag in CEM III/B as was explained before (page 61). The diffraction pattern of the sample dehydrated using 500 °C seems to be largely amorphous. Portlandite and ettringite are decomposed and a calcite peak can still be distinguished. At 800 °C calcite is decomposed and mainly peaks linked to alite or belite can be distinguished. The sample dehydrated with a target temperature at 1400 °C showed none of the main cement phases in the diffraction pattern. An explanation for this can be the slow cooling of the material. It is known that gehlenite ($Ca_3Al_2SiO_7$) starts to form around 900 °C and merwinite ($Ca_3Mg(SiO_4)_2$) forms in the temperature range of 880 – 1430 °C. Due to slow cooling of blast furnace cements it is possible for these two components to be present within the material. It was found in literature that a fast cooling process of the material resulted in the observation of brownmillerite and belite [5; 52; 68]. In view of the CEM I sample showing alite and belite after the thermal treatment at 1400 °C, faster cooling of the CEM III/B sample might also result in the appearance of alite and belite peaks. Especially, since literature already provided that brownmillerite and belite were more typical to find after fast cooling.

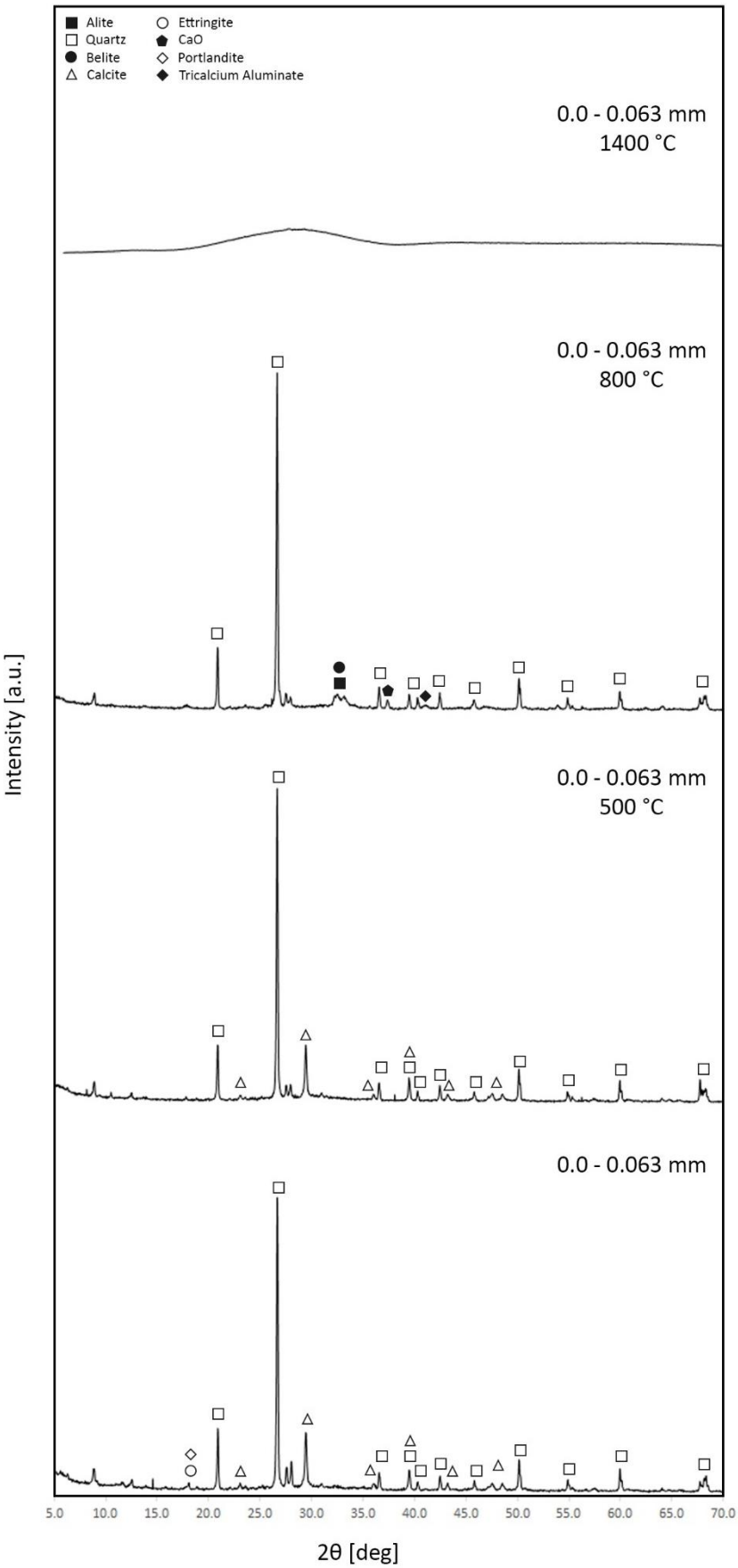

Figure 48: Diffraction pattern of the 0.0 - 0.063 mm cementitious Smart Crusher fraction with and without thermal treatment showing the decomposition of the cement hydration products (500 °C) and calcite (800 °C) and the formation of alite, belite, calcium oxide and tricalcium aluminate (800 °C). The thermal treatment at 1400 °C resulted in an amorphous material.

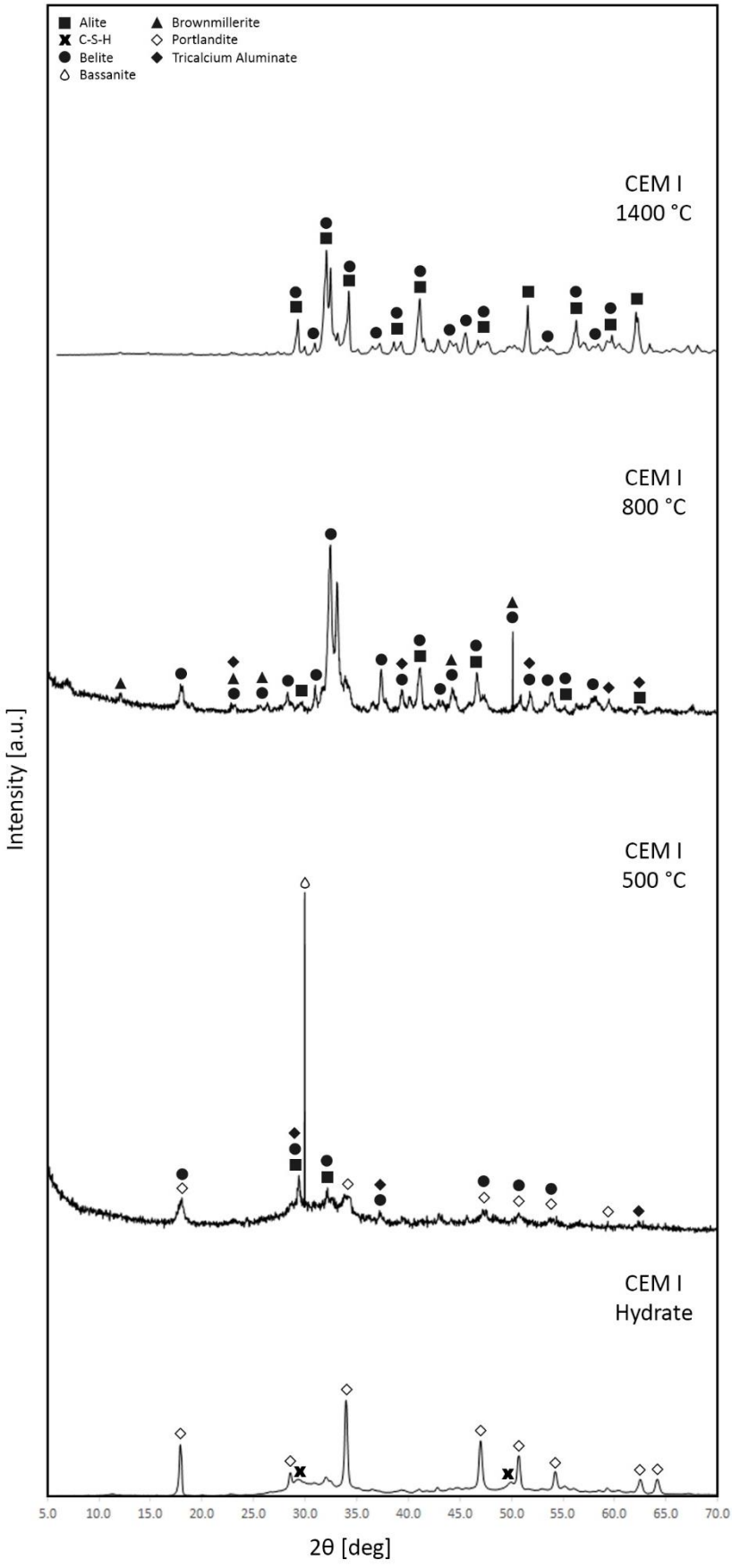

Figure 49: Diffraction pattern of the CEM I 52.5 R samples with and without thermal treatment showing the decomposition of the cement hydration products (500 °C, 800 °C) and the formation of alite and belite (500 °C, 800 °C, 1400 °C), brownmillerite (800 °C) and tricalcium aluminate (500 °C, 800 °C).

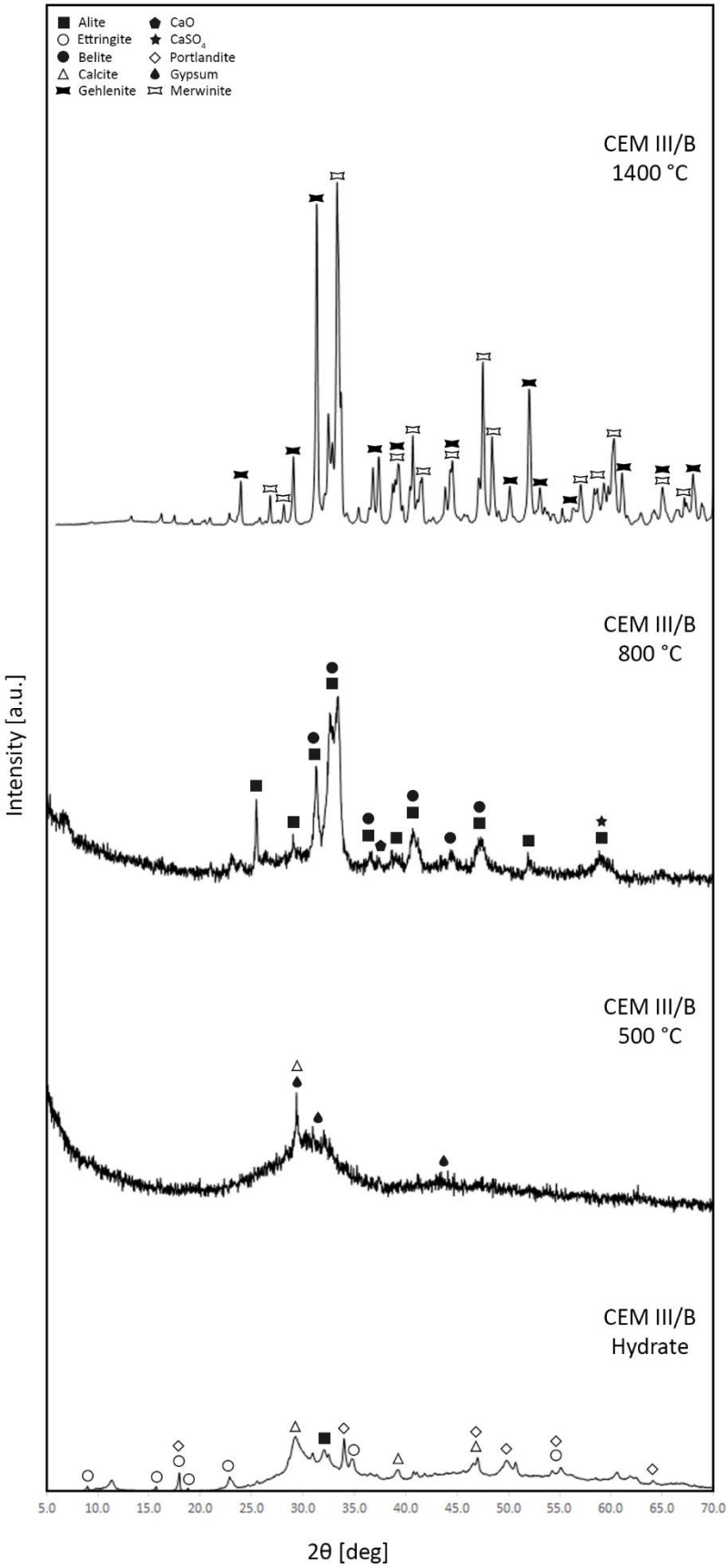

Figure 50: Diffraction pattern of the CEM III/B 42.5 N samples with and without thermal treatment showing the decomposition of the cement hydration products (500 °C) and the formation of alite, belite and calcium oxide (800 °C), gehlenite and merwinite (1400 °C).

From the results of the two previous figures the thermal treatments at 800 °C and 1400 °C seem to be the most interesting with respect to the occurrence of the main cement phases. Both thermal treatments will be analysed further to determine the thermal treatment which will be used for the compression tests. With this in mind the focus was mainly placed on the appearance of alite and belite peaks in the diffraction patterns as these components are important for the compressive strength of the materials.

In figure 51 an overview can be found of the diffraction pattern of the samples which underwent a thermal treatment at 800 °C. In the diffraction pattern of the cementitious Smart Crusher fractions the quartz peaks with a high peak intensity were neglected to compare the peaks corresponding to the cement phases. From the diffraction pattern it follows that the cement minerals are most distinct within the CEM I and CEM III/B samples. The cementitious Smart Crusher fractions show mostly quartz peaks and only a few peaks are identified as cement minerals. For all four samples a comparable peak, which was identified as a belite and/or alite peak, can be found between 30° and 35°. For the reference materials alite and belite peaks can also be found for other 2θ values, whereas for the cementitious Smart Crusher fractions this peak is the most distinct alite/belite peak. Based on the diffraction pattern it can be concluded that the thermal treatment at 800 °C results in the occurrence of the main cement minerals.

The diffraction pattern of the samples, which had a thermal treatment at 1400 °C can be found in figure 52. The cementitious Smart Crusher fractions show a diffraction pattern which is mainly amorphous. Only for the 0.063 – 0.125 mm fraction some peaks could be identified, but these peaks belong to quartz or a polymorphic form of quartz. Quartz can transform into tridymite and cristobalite under the influence of the thermal treatment. Around 870 °C quartz can transform into tridymite and around 1470 °C a transformation of tridymite into cristobalite can occur. It is also possible for quartz to transform directly into cristobalite at temperatures above 1300 °C, although this results in mainly disordered cristobalite [98]. The diffraction pattern of CEM III/B also shows no alite or belite peaks, whereas the diffraction patterns of CEM I shows multiple peaks identified as alite and/or belite. From literature it follows that the formation of gehlenite ($Ca_3Al_2SiO_7$) starts around 900 °C and the formation of merwinite ($Ca_3Mg(SiO_4)_2$) occurs in the temperature range of 880 – 1430 °C. Both phases can be found in blast furnace slags when the material is slowly cooled. After fast cooling brownmillerite and belite were more typical to find [5; 52; 68]. This indicates that the cooling rate of the samples may play an important role in the presence of alite and belite in the samples. Because the diffraction patterns of the CEM III/B sample does not show alite or belite peaks, the diffraction patterns of the unhydrated CEM III/B sample deviates largely from the thermally treated sample. Comparing the unhydrated CEM I sample with the thermally treated CEM I sample it becomes clear that the diffraction pattern show comparable peaks with comparable 2θ values.

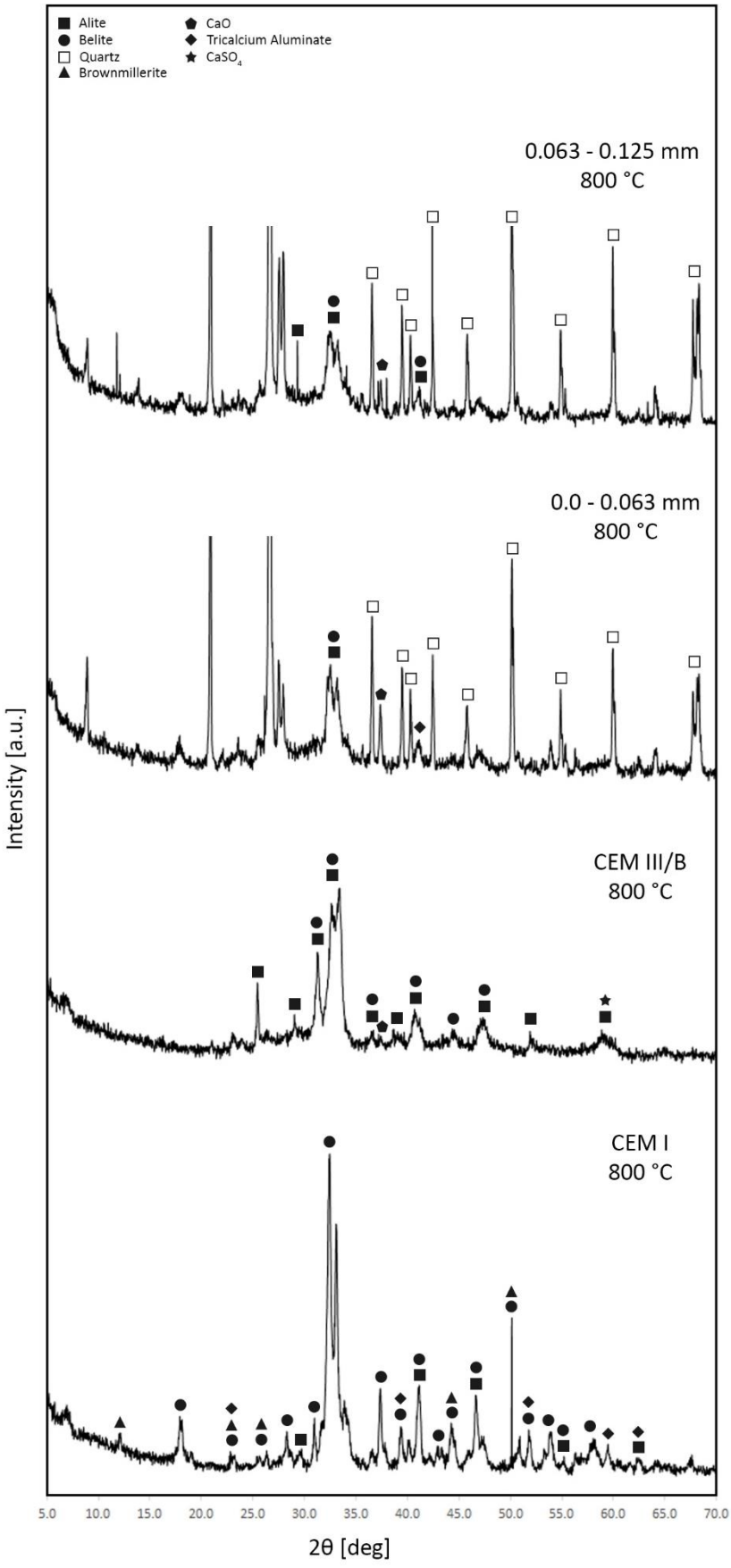

Figure 51: Diffraction pattern of the samples after a thermal treatment at 800 °C showing the formation of alite and belite. The cementitious Smart Crusher fractions are dominated by quartz, while the reference samples (CEM I and CEM III/B) are dominated by alite and belite.

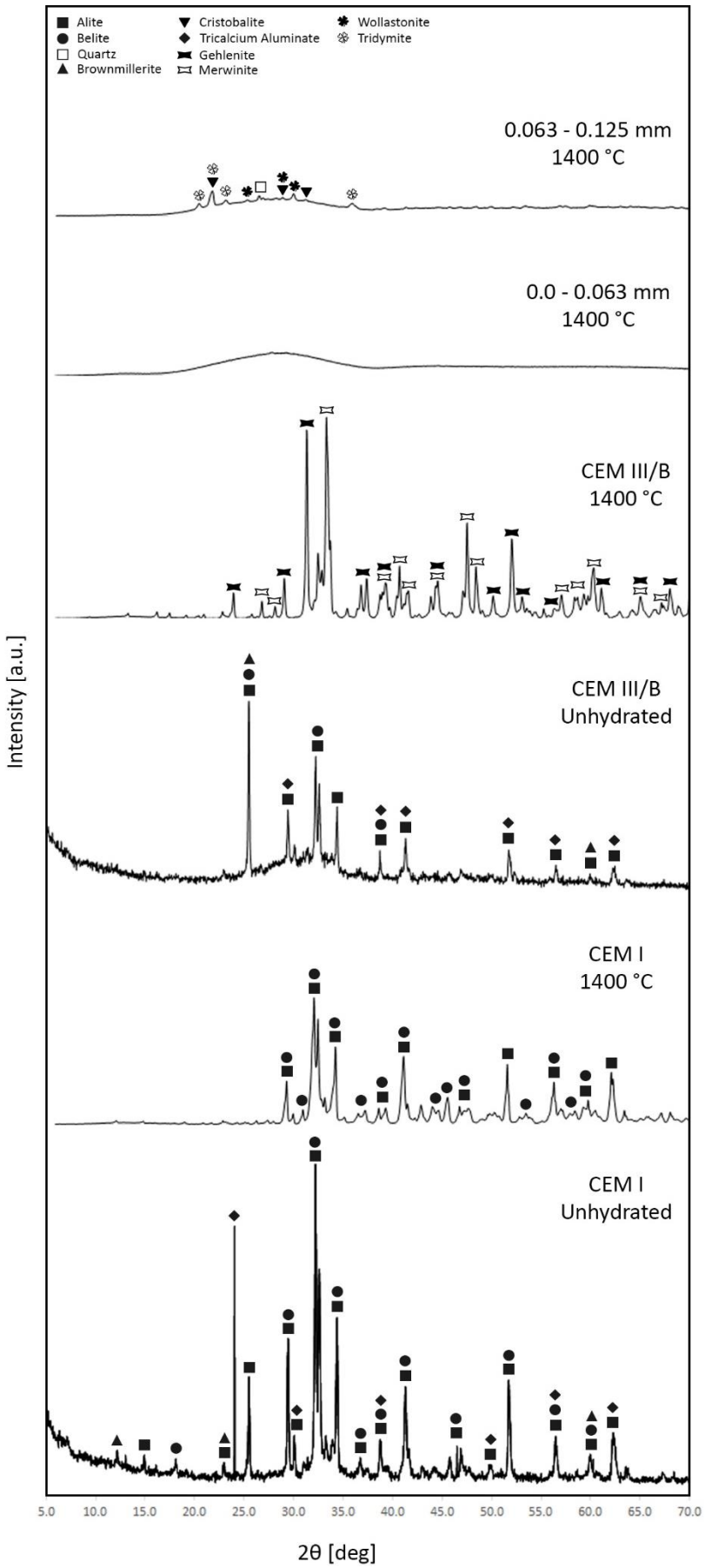

Figure 52: Diffraction pattern of the samples after a thermal treatment at 1400 °C showing amorphous cementitious Smart Crusher fractions, the formation of gehlenite and merwinite in CEM III/B and the formation of alite and belite in CEM I.

8 PERFORMANCE CEMENTITIOUS BINDER

The performance of the cementitious binder is assessed by conducting strength tests of the different cementitious binders. Based on the previous chapters the thermal treatment of 800 °C seemed the most promising and was therefore used for the upcycling of the cementitious binders before conducting a strength test. Mortar prisms were made and the mixture was observed to gain insight in the influence of the different cementitious binder types and the thermal treatment on the consistency. Subsequently, the mortar prisms underwent a strength test after 1 day and 28 days. Two types of strength tests were conducted, namely flexural and compressive strength tests. The results of these tests will give insight in the possibility of obtaining cementitious binder from recycled cement stone with strength comparable to the strength of primary cement.

8.1 Samples

Mortar prisms of the two cementitious Smart Crusher fractions and the two hydrated reference materials were made after thermal treatment at 800 °C. The mortar prisms were made following the mixture design as mentioned in NEN-EN-196-1 [73]. Figure 53 gives insight in the consistency of the different materials after making the mortar mixtures. Just as with the powders in chapter 7, a clear difference can be observed in the colour of the materials. The red colouration of the mortar mixture of the cementitious Smart Crusher fractions as a result of the dehydration or oxidization of the iron from the aggregates present within the cementitious powder [42; 56], can still be observed.

For all the mortar mixtures, the reference mixtures and the mixtures containing upcycled cementitious powders, a water/cement ratio of 0.5 was used as specified in NEN-EN-196-1 [73]. After making the mortar mixtures, a difference in the consistency of the mixtures could be observed. Where the reference mixtures had a consistency as expected, the consistency of the mortar mixtures containing the thermally treated cementitious binders seemed to be rather dry. A reason for this could be an increase in the water demand for the secondary binders to form cement paste. There are multiple factors which could result in an increase of the water demand. Examples of such factors are the grading of the material and an increase in the specific surface area of the dehydrated cementitious materials. An increase in the specific surface area of the material can be related to the evaporation of the free water and the release of chemically bound water from the hydrated materials. Additionally, changes in the morphology and the development of a rougher surface compared with Portland cement occurs due to the thermal treatment [8; 85; 109].

CEM III/B 42.5 N | CEM I 52.5 R | Cementitious Smart Crusher fractions

Figure 53: Mortar mixtures containing thermally treated cementitious binder showing the rather dry consistency of the mixtures.

8.2 Mortar Strength

The mortar prisms of the thermally treated binders are compared with each other and with untreated CEM I 52.5 R and CEM III/B 42.5 N to see if the strength is influenced by the secondary binder and the type of material. Two types of strength tests were carried out, namely a flexural strength test and a compressive strength test after 1 and 28 days. A strength test after 1 day was chosen to gain insight in the reactivity of the material and after 28 days, because after this time interval the result is an important indication for its final strength value. The expected results of the strength tests were translated into the following main hypotheses:

1. The untreated reference materials have higher strength values than the thermally upcycled materials.
2. The thermally upcycled CEM I and CEM III/B have higher strength values than the thermally upcycled 0.0 – 0.063 mm and 0.063 – 0.125 mm fractions.
3. CEM III/B will have a lower strength than CEM I after 1 day due to the presence of slag, but will reach a comparable strength after 28 days.

The 1 day strength of the mortar prisms containing the upcycled binders could not be tested. The mortar mixture was dry, which could be the result of an increase in the water demand of the upcycled binders. Therefore, the upcycled binders could not form a paste that was able to bind the components together. For that reason, only the strength tests of the reference cements after 1 day produced results. The reference samples showed for both the flexural as compressive strength higher strengths for the CEM I samples. CEM III/B is a blast furnace cement and it is known that these cement types have a slow hydration. This explains the lower strength values after 1 day. Slow hydration results in a lower early strength and a higher strength gain after longer time intervals compared to CEM I [12]. This also follows from figure 54. Untreated CEM III/B shows lower early strength compared to untreated CEM I, but its strength increases quicker and this results in a comparable compressive strength after 28 days.

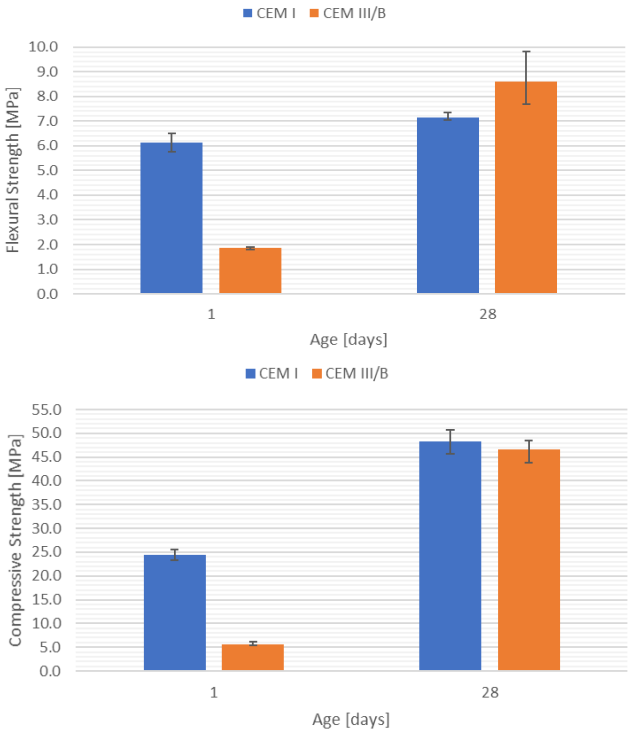

Figure 54: Flexural (top) and compressive (bottom) strength showing the low early strength and the higher strength gain of untreated CEM III/B compared to untreated CEM I.

The strength tests of the thermally treated samples did not produce measurable results. During demoulding of the prisms parts of the prisms crumbled or broke off. The flexural strength test showed no measurable results, which meant a strength value below 0.3 kN. For the compressive strength tests the same could be observed. The samples were crushed almost immediately. During the preparation of the mortar mixtures it was already observed that the mixtures seemed to be dry and did not reach the consistency of the untreated reference mixtures, which can be explained by an increase of the demand of water. This phenomenon can also explain why the thermally treated samples did not produce any measurable results. The problem lies within the compaction of the samples. Improper compaction of mortar mixtures reduces the strength of the prisms, because the prisms will contain voids and it is known that these imperfections have a negative effect on the strength properties [104]. Due to the dryness of the mortar mixtures, the mixtures are harder to compact and will contain more voids. This lower degree of compaction leads to a decrease in the strength properties. Taking into account the increase in water demand and therefore ensuring proper compaction, the strength properties of the mixtures containing thermally treated binder may increase.

Figure 55: Mortar prisms containing thermally treated CEM I before and after testing. The prisms crumbled or parts broke off and no measurable strength results were obtained.

PART III
CONCLUSIONS

9 CONCLUSIONS AND RECOMMENDATIONS

This chapter answers the main research question stated in chapter 1: Does cementitious binder retrieved from recycled cement stone still contain reactivity to obtain a fully functional binder that can replace primary cement in constructions and structural elements? Based on the experimental results the research questions can be answered. First the main conclusions drawn from this research are presented. From the answers of the sub-questions a final conclusion is drawn as the answer of the main research question. Subsequently, this chapter will suggest recommendations for future research.

9.1 Conclusions

The aim of this research was to evaluate the reactivity of the cementitious binder retrieved from recycled cement stone. The cementitious binder used in this research could be divided in two different groups. The first group contained the cementitious binder retrieved from the novel concrete crushing technique the Smart Crusher. The cementitious fractions in this group were separated from the other concrete components by sieving the 0 – 4 mm Smart Crusher material before being studied. The second group contained the reference materials CEM I 52.5 R and CEM III/B 42.5 N. For this second group contact with other concrete components was avoided and no aggregates were added. Both groups underwent equal treatments and the outcome of the experiments were compared.

Because the origin of the cementitious fractions retrieved from the Smart Crusher is unknown the fractions are seen as a Blackbox, therefore the binder types are characterized first. Different characterization methods, such as TGA, DSC, MS, XRF and XRD, were used to gain insight in the characteristics of the Smart Crusher and reference materials. Based on these methods it was found that the cementitious fractions of the Smart Crusher contain a large amount of silica, which indicates the presence of aggregates. Especially the phase transition of α-quartz into β-quartz around 573 °C in the DSC curves and the quartz peaks in the diffraction patterns, both of which were not present in the DSC curves and diffraction patterns of the treated reference materials, confirmed this. For the XRF results the P_2O_5 content also was of interest. Because the origin of the cementitious Smart Crusher fractions is unknown, the characterization might shed some light on which type of cement it could be. The absence of P_2O_5 in the cementitious Smart Crusher fractions provided an indication that there is no or a not measurable amount of fly ash present. Unfortunately, based on the results it was not possible to discriminate between the cement types.

Hydrated cement normally shows transitions in the TGA curves at three temperature ranges, namely 30 – 250 °C, 400 – 550 °C and 700 – 900 °C. The transitions indeed occurred within the mentioned temperature ranges for all the samples, except for the temperature range in which the decomposition of calcium carbonate is expected to takes place. This can be explained by the age and preparation of the hydrated reference samples. A difference between the samples can be found in the water content. The non-evaporable water content is considerably larger for the hydrated reference samples than for the cementitious Smart Crusher fractions. This is an indication that the relative amount of cement is lower for the cementitious Smart Crusher fractions and that, as a result, the reactivity could also be lower. In all samples the presence of portlandite was found, based on the TGA and XRD results. The presence of portlandite is an indication that hydration has occurred in the hydrated reference and Smart Crusher samples, which means that all samples could show a certain reactivity after upcycling. CEM I hydrate has the highest amount of portlandite, followed by CEM III/B hydrate. For CEM III/B

hydrate this is lower because portlandite is used as an activator for slag. The lowest amount of portlandite is found in the cementitious Smart Crusher fractions. Because it is not possible to confirm if the cementitious Smart Crusher fractions contain CEM I or CEM III/B, the low portlandite content could be due to the portlandite being used as an activator. Another possibility is that the cementitious Smart Crusher fractions have a smaller relative amount of cement and a lower reactivity.

For the upcycling of the secondary materials, thermal treatments at three different dehydration temperatures, namely 500 °C, 800 °C and 1400 °C, were used. After the thermal treatments a first distinction could be made between the samples. The red colouration, after treatment at 500 °C and 800 °C, and melting of the material, after a treatment at 1400 °C, of the cementitious Smart Crusher fractions were of interest. This confirmed the presence of aggregates such as quartz in the material. To determine the most promising thermal treatment, the focus was on the temperature at which the four major cement phases, especially alite and belite, were formed. Furthermore, the presence of alite and belite in the material can be used as an indication that the material has a certain reactivity after the thermal treatment. Before the thermal treatment, the hydrated samples, reference and cementitious Smart Crusher fractions, contained mainly hydration products. These hydration products are almost fully decomposed after the thermal treatment of 500 °C. Additionally, it could be seen that CEM I was the only material where some alite and belite could be identified after the 500 °C treatment. After the treatment of 800 °C all the hydration products and the calcite were fully decomposed. All the samples showed peaks in the diffraction patterns which could be linked to alite and belite, though the number and height of these peaks varied for the different materials. Furthermore, the cementitious Smart Crusher fractions contained large quartz peaks for both the hydrated and treated samples. The treatment at 1400 °C showed only an alite and belite content for the CEM I samples. The cementitious Smart Crusher fractions became mainly amorphous and CEM III/B showed different compounds other than alite or belite. Based on these results, it is concluded that the best approach for the upcycling of the hydrated materials is the thermal treatment at 800 °C, because this treatment showed an alite and belite content for all samples.

The functional quality of the different binder types is estimated by flexural and compressive strength tests. From the results it follows that CEM III/B has a lower early strength than CEM I, but after 28 days a higher gain of strength results in comparable strengths. The strength development of the thermally treated binders could not be determined. A higher water demand resulted in a lower workability and compaction, which resulted in unmeasurable strength values. These samples have a low functional quality, which cannot be used in structures. It is likely that application of the right admixtures, an adjusted w/c ratio or a combination of the two would have led to a better workability. After such an adjustment, it is to be expected that also compaction and mechanical properties will show improvement. Additionally, taking into account the amount of quartz, less sand should be added to the mortar mixtures of the recycled cement to compensate for the amount of quartz already present and to use the proper proportion cement-sand-water. Therefore, the estimation of the amount of quartz (sand) might be very important.

To conclude, the thermal treatment of 800 °C showed the presence of alite and belite in all the samples. This is an indication that a certain reactivity can be expected in the secondary binders after this thermal treatment. If the reactivity is adequate, is not certain. The thermally treated samples did not result in prisms with measurable strength properties, because the higher water demand resulted in improper compaction. Therefore, more research is required to assess the reactivity of the secondary binders.

9.2 Recommendations

The previous paragraph presents the final conclusions of this research. A first indication is given about the reactivity of the cementitious binder retrieved from recycled cement stone and its possibility of being used as a fully functional binder that can replace primary cement in constructions and structural elements. Some interesting results were found, sparking the interest for further research. Based on the outcome of this research and with regards to further development of secondary cement recommendations will be given for future research.

Compensating the silica amount

The outcome of the experimental research showed that the cementitious fractions of the Smart Crusher contained a considerably larger amount of silica than that of the reference materials. Additionally, a phase transition of α-quartz into β-quartz was observed as well as the presence of quartz peaks in the diffraction patterns. This indicates that aggregates such as sand particles are present within the material. Because the amount of silica due to the presence of sand particles is considerable, compensating for the silica content by reducing the amount of sand added in the mortar mixture might have a positive effect on the material properties. Therefore, the amount of sand particles should be quantified and a method for this quantification has to be determined.

More dehydration temperatures

During this research three dehydration temperatures were investigated. The temperature of 800 °C showed the largest potential and was used for the strength tests. The strength development of upcycled material using other dehydration temperatures might also be of interest. For the reference CEM I the 1400 °C treatment showed in the diffraction pattern alite and belite peaks and might therefore be of interest. Besides the dehydration temperatures between 800 °C and 1400 °C, which are used in this research, other dehydration temperatures in this temperature interval can be of interest. Especially since the melting point of the cementitious Smart Crusher fractions seems to be lowered due to the presence of sand particles, resulting in a melt. CEM III/B seems to form gehlenite and merwinite during the 1400 °C treatment instead of alite and belite, which are formed during the 1400 °C of the CEM I material. Other dehydration temperatures might show an increase in the formation of alite and belite if melting of the material can be prevented and the formation of gehlenite and merwinite for CEM III/B is taken into account. Additionally, decomposition of calcium carbonate occurs in the temperature range of 700 – 900 °C, which indicates that a temperature above 800 °C can be of interest.

Cooling regime

Cooling procedures of the samples after thermal treatment might be reviewed. During the production of cement the clinker is cooled down very quickly to around 1300 °C to avoid that alite will revert back to belite. During heating of the hydrated samples bonds are broken and new bonds are formed. The cooling rates can influence the phases present in the samples and slow cooling can result in the transformation of for example alite to other phases. Therefore, the influence of different cooling rates might be important to investigated.

Heating regime

Investigation on the time a sample is conditioned at a certain target temperature might be studied. Insight in the influence of the time that samples are kept at the target temperature can have a positive effect on the environmental impact of the thermal treatment. Not only the length of the isothermal period can have a positive effect on the phases in the samples, e.g. that no hydration products remain

in the sample. A shorter time period, might be enough to decompose the hydration products and can positively influence the environmental impact.

Separating hydrated and non-hydrated cement fractions
Insight in the separation of hydrated and non-hydrated cement fractions is needed. Part of the cement in concrete structures is assumed to be non-hydrated and should still be primarily fully functional cement. The non-hydrated part needs no thermal treatment, but can still be affected by the concrete composition. Investigation might make clear if this part can directly be used or that improvement is necessary. Additionally, the separation efficiency of the hydrated cement fractions, non-hydrated cement fractions and other concrete components are important to establish.

Other treatments
Besides thermal treatment for the upcycling of hydrated secondary binders, other treatments can be of interest to obtain a secondary binder, which can fully replace primary cement. Treatments such as grinding of the material or adding admixtures can positively influence the material properties of the secondary binders. This research indicated that the upcycled cementitious binders seem to have an increased water demand. Investigating the water demand of the upcycled materials to form a paste is needed as well as the reason for the increased water demand and possible treatments to take the increased water demand into account. Additionally, the Blaine value might be of interest to gain insight in the fineness of the upcycled material. Not only the fineness of the material influences the water demand, but other factors, such as changing morphology and roughness of the particles, can change the material in such a way that the water demand increases. Therefore, research into factors influencing the water demand as a result of upcycling of the material is needed. This can also give more insight into the influence of the thermal treatment on the cementitious particles.

Other cement types
Besides CEM I and CEM III/B, other cement types can also occur in practice. Although CEM I and CEM III/B are by far the most used cement types, at least in the Netherlands, there is still the possibility that other cement types are present. This research showed that CEM I and CEM III/B react differently on the upcycling treatments. Therefore, looking into other cement types can be of interest to make cement fully circular. Circular cement does not only include CEM I and CEM III/B, but all cement types used in practice.

Separation of cementitious binder and sand
This research showed that the separation of sand and the cementitious binder is not complete. Therefore, research to find a method to increase the separation might be of great interest.

Influence of sand on the chemical composition
During this research a red colouration of the cementitious powders containing sand particles was observed at elevated temperatures. Additionally, when a certain temperature was reached the samples containing the cementitious Smart Crusher fractions melted. The melting point was decreased due to the presence of quartz in combination with the cement components. Therefore, more research is needed to investigate the influence of sand on the chemical composition of a cementitious binder. This might show that, besides change of colour and lowering of the melting point, the sand has influence on chemical changes in the cementitious material during upcycling treatments.

Recycling of the 0.125 – 4.0 mm fraction

During this research the cementitious Smart Crusher fractions were separated from the retrieved material (0 – 4 mm). To fully recycle concrete, the remaining 0.125 – 4.0 mm fraction is also of interest. This research showed that the cementitious Smart Crusher fractions still contained sand and that a complete separation of the cementitious binder and sand did not occur. Therefore, the question is whether cementitious material remains in the 0.125 – 4.0 mm fraction or is fully separated from the cementitious material. Research has to be done to gain insight into the direct usage of the 0.125 – 4.0 mm fraction in concrete. Additionally, possible problems which may occur as a result of the presence of cementitious material in that fraction have to be taken into account. When cementitious material does remain in the 0.125 – 4.0 mm fraction, the water demand might be influenced. Therefore, research into the water demand of this fraction is also of interest.

Life Cycle Assessment (LCA)

Life Cycle Assessment (LCA) of the environmental footprint of cement by comparing the use of secondary materials with primary materials. For the secondary materials the upcycling treatments and the use of traditional crushers versus the Smart Crusher have to be taken into account. This will help to gain insight in how much the environmental footprint will change when using secondary cementitious materials instead of primary.

Application potential

Evaluation of the application potential of cementitious binder from recycled cement stone will help to pinpoint possible bottlenecks. Different barriers can be of influence on the implementation of the secondary binder by for example environmental, economic, cultural and technological reasons. The current building and product regulations and standards can result in possible bottlenecks. To make recycling of cement more attractive some options will be mentioned: taxes on the mining of raw materials and on CO_2 emission, adding circular cement as a “new” binder type in the codes, grants for the use of high-grade cement recycling. High-grade recycling in this case means the use of secondary cement to replace primary cement. To increase the application potential of the secondary cementitious binder changes on different levels have to be made.

REFERENCES

[1] A&A Custom Crushing. (2014). CRUSHED AND RECYCLED CONCRETE AGGREGATE 5. In.

[2] Alarcon-Ruiz, L., Platret, G., Massieu, E., & Ehrlacher, A. (2005). The use of thermal analysis in assessing the effect of temperature on a cement paste. *Cement and Concrete Research, 35*(3), 609-613.

[3] Alonso, C., & Fernandez, L. (2004). Dehydration and rehydration processes of cement paste exposed to high temperature environments. *Journal of materials science, 39*(9), 3015-3024.

[4] ASTM, C. (1999). 989, Standard specification for ground granulated blast furnace slag for use in concrete and mortars. *Annual Book of ASTM Standards, 4*.

[5] Aydın, S. (2008). Development of a high-temperature-resistant mortar by using slag and pumice. *Fire safety journal, 43*(8), 610-617.

[6] B:ton. (2018). Smartcrusher in race voor Circular Award. In.

[7] Bakker, M., & Hu, M. (2015). Closed-loop Economy: Case of Concrete in the Netherlands. *Delft University of Technology, Delft, Netherlands*.

[8] Baldusco, R., Nobre, T. R. S., Angulo, S. C., Quarcioni, V. A., & Cincotto, M. A. (2019). Dehydration and Rehydration of Blast Furnace Slag Cement. *Journal of Materials in Civil Engineering, 31*(8), 04019132.

[9] Barbier, J., & Hyde, B. G. (1985). The structures of the polymorphs of dicalcium silicate, Ca2SiO4. *Acta Crystallographica Section B: Structural Science, 41*(6), 383-390.

[10] Barcelo, L., Kline, J., Walenta, G., & Gartner, E. (2014). Cement and carbon emissions. *Materials and Structures, 47*(6), 1055-1065.

[11] Barnes, P., & Bensted, J. (2002). *Structure and performance of cements*: CRC Press.

[12] Bellmann, F., & Stark, J. (2009). Activation of blast furnace slag by a new method. *Cement and Concrete Research, 39*(8), 644-650.

[13] Benarchid, M. Y., Diouri, A., Boukhari, A., Aride, J., & Elkhadiri, I. (2005). Hydration of iron–phosphorus doped dicalcium silicate phase. *Materials Chemistry and Physics, 94*(2-3), 190-194.

[14] Benhelal, E., Zahedi, G., Shamsaei, E., & Bahadori, A. (2013). Global strategies and potentials to curb CO2 emissions in cement industry. *Journal of cleaner production, 51*, 142-161.

[15] Betoniek. (2008). Binnen de lijnen. *Betoniek 14/15*.

[16] Betoniek. (2011). Oud beton wordt jong beton. *Betoniek 15/19*.

[17] Bezerra, U. T., Martinelli, A. E., Melo, D. M. A., Melo, M. A. F., & Lima, F. M. (2011). A correlation between Bogue's equations and Taylor's procedure for the evaluation of crystalline phases in special class Portland oilwell cement clinker. *Cerâmica, 57*(341), 122-128.

[18] Bogue, R. H. (1929). Calculation of the compounds in Portland cement. *Industrial & Engineering Chemistry Analytical Edition, 1*(4), 192-197.

[19] Bouw en Uitvoering. (2018). SmartCrusher finalist Circular Award 2018.

[20] Bullard, R. A. (2015). *Effect of Cooling Rates on Mineralization in Portland Cement Clinker.*

[21] C2CA. (n.d.). The recycling process. Retrieved from http://www.c2ca.eu/activities/the-recycling-process/

[22] Carr, N. N. (2019). Biomass Derived Binder: Development of the scientific basis for methodologies that enable the production of renewable sustainable cement based on ashes derived from the conversion of biomass residues as determined by qualitative mineralogical analysis.

[23] Carrasco, M. F., Menéndez, G., Bonavetti, V., & Irassar, E. F. (2005). Strength optimization of “tailor-made cement” with limestone filler and blast furnace slag. *Cement and Concrete Research, 35*(7), 1324-1331.

[24] Cement&BetonCentrum. (n.d.). Cementmarkt. Retrieved from http://www.cementenbeton.nl/marktinformatie/cementmarkt

[25] Chan, C. J., Kriven, W. M., & Young, J. F. (1992). Physical stabilization of the β → γ transformation in dicalcium silicate. *Journal of the American Ceramic Society, 75*(6), 1621-1627.
[26] De Schutter, G., Yuan, Y., Liu, X., & Jiang, W. (2015). Degree of hydration-based creep modeling of concrete with blended binders: from concept to real applications. *Journal of Sustainable Cement-Based Materials, 4*(1), 1-14.
[27] de Vries, W., Rem, P., & Berkhout, P. (2009). *ADR: a new method for dry classification.* Paper presented at the Proceedings of the ISWA international conference.
[28] Dijksma, S. A. M., & Kamp, H. G. J. (2016). *Nederland circulair in 2050*.
[29] Dunstetter, F., De Noirfontaine, M.-N., & Courtial, M. (2006). Polymorphism of tricalcium silicate, the major compound of Portland cement clinker: 1. Structural data: review and unified analysis. *Cement and Concrete Research, 36*(1), 39-53.
[30] ENCI. (n.d.). Producten verpakt cement. Retrieved from https://www.enci.nl/nl/producten-verpakt-cement
[31] ENCI, & CBR Cementbedrijven. (2015). Blast Furnace Cement.
[32] Favier, A., De Wolf, C., Scrivener, K., & Habert, G. (2018). *A sustainable future for the European Cement and Concrete Industry: Technology assessment for full decarbonisation of the industry by 2050*. Retrieved from
[33] Florea, M. V. A. (2014). Secondary materials applied in cement-based products: treatment, modelling and environmental interaction.
[34] Florea, M. V. A., Ning, Z., & Brouwers, H. J. H. (2014). Activation of liberated concrete fines and their application in mortars. *Construction and Building Materials, 50*, 1-12.
[35] Garcia-Lodeiro, I., Palomo, A., & Fernández-Jiménez, A. (2015). Crucial insights on the mix design of alkali-activated cement-based binders. In *Handbook of alkali-activated cements, mortars and concretes* (pp. 49-73): Elsevier.
[36] Gastaldi, D., Canonico, F., Capelli, L., Buzzi, L., Boccaleri, E., & Irico, S. (2015). An investigation on the recycling of hydrated cement from concrete demolition waste. *Cement and Concrete Composites, 61*, 29-35.
[37] Ghosh, S. N. (1983). *Advances in cement technology: Critical Reviews and Case Studies on Manufacturing, Quality Control, Optimization and Use*. Oxford: Pergamon.
[38] Ghosh, S. N. (1991). *Cement and concrete science and technology. Pt. 1*. New Delhi: ABI Books Private Ltd.
[39] Gobbo, L., Sant'Agostino, L. l., & Garcez, L. (2004). C3A polymorphs related to industrial clinker alkalies content. *Cement and Concrete Research, 34*(4), 657-664.
[40] Gruyaert, E., Robeyst, N., & De Belie, N. (2010). Study of the hydration of Portland cement blended with blast-furnace slag by calorimetry and thermogravimetry. *Journal of thermal analysis and calorimetry, 102*(3), 941-951.
[41] Hager, I. (2013). Behaviour of cement concrete at high temperature. *Bulletin of the Polish Academy of Sciences: Technical Sciences, 61*(1), 145-154.
[42] Hager, I. (2014). Colour change in heated concrete. *Fire Technology, 50*(4), 945-958.
[43] Hansen, T. (1992). RILEM Report 6—Recycling of Demolished Concrete and Masonry. *E&FN Spon, Bodmin, UK*.
[44] Hansen, T. C. (1992). *Recycling of demolished concrete and masonry*: CRC Press.
[45] Hewlett, P. (2004). *Lea's Chemistry of Cement and Concrete*. In. Retrieved from http://public.ebookcentral.proquest.com/choice/publicfullrecord.aspx?p=404673
https://ebookcentral.proquest.com/lib/columbia/detail.action?docID=404673
[46] International Energy Agency, & World Business Council for Sustainable Development. (2018). Technology Roadmap Low-Carbon Transition in the Cement Industry.
[47] Jadhav, R., & Debnath, N. C. (2011). Computation of X-ray powder diffractograms of cement components and its application to phase analysis and hydration performance of OPC cement. *Bulletin of Materials Science, 34*(5), 1137-1150.

[48] Kakhia, T. I. (2012). Encyclopedia Of Cement, Concrete, Construction, & Building Materials.
[49] Kalyoncu, R. S. (1998). Minerals yearbook: Slag—iron and steel. *Report, US Geological Survey, Reston, US*.
[50] Kourounis, S., Tsivilis, S., Tsakiridis, P. E., Papadimitriou, G. D., & Tsibouki, Z. (2007). Properties and hydration of blended cements with steelmaking slag. *Cement and Concrete Research, 37*(6), 815-822.
[51] Krikhaar, H. M. M., Soen, H. H. M., de Vries, P., & Deliën, V. (2005). *Betonpocket 2006*: ENCI Media.
[52] Kriskova, L., Pontikes, Y., Cizer, Ö., Malfliet, A., Dijkmans, J., Sels, B., . . . Blanpain, B. (2014). Hydraulic behavior of mechanically and chemically activated synthetic merwinite. *Journal of the American Ceramic Society, 97*(12), 3973-3981.
[53] Kristmann, M. (1977). Portland cement clinker: Mineralogical and chemical investigations: Part I Microscopy, X-ray fluorescence and X-ray diffraction. *Cement and Concrete Research, 7*(6), 649-658.
[54] Kwon, E., Ahn, J., Cho, B., & Park, D. (2015). A study on development of recycled cement made from waste cementitious powder. *Construction and Building Materials, 83*, 174-180.
[55] Lee, F. C., Banda, H. M., & Glasser, F. P. (1982). Substitution of Na, Fe and Si in tricalcium aluminate and the polymorphism of solid solutions. *Cement and Concrete Research, 12*(2), 237-246.
[56] Lee, J., Choi, K., & Hong, K. (2010). *The effect of high temperature on color and residual compressive strength of concrete.* Paper presented at the Proc., 7th Int. Conf. on Fracture Mechanics of Concrete and Concrete Structures. High Performance, Fiber Reinforced Concrete, Special Loadings and Structural Applications.
[57] Li, C., Sun, H., & Li, L. (2010). A review: The comparison between alkali-activated slag (Si+ Ca) and metakaolin (Si+ Al) cements. *Cement and Concrete Research, 40*(9), 1341-1349.
[58] Li, X., Shen, X., Tang, M., & Li, X. (2014). Stability of tricalcium silicate and other primary phases in Portland cement clinker. *Industrial & Engineering Chemistry Research, 53*(5), 1954-1964.
[59] Luangcharoenrat, C., Intrachooto, S., Peansupap, V., & Sutthinarakorn, W. (2019). Factors influencing construction waste generation in building construction: Thailand's perspective. *Sustainability, 11*(13), 3638.
[60] Ludwig, H.-M., & Zhang, W. (2015). Research review of cement clinker chemistry. *Cement and Concrete Research, 78*, 24-37.
[61] Marchon, D., & Flatt, R. J. (2016). Mechanisms of cement hydration. In *Science and technology of concrete admixtures* (pp. 129-145): Elsevier.
[62] Marsh, B. K., & Day, R. L. (1988). Pozzolanic and cementitious reactions of fly ash in blended cement pastes. *Cement and Concrete Research, 18*(2), 301-310.
[63] Mehta, P. K., & Monteiro, P. J. M. (2006). *Concrete: Microstructure, Properties, and Materials* (Third Edition ed.): McGraw-Hill Publishing.
[64] Mihara, N., Kuchar, D., Kojima, Y., & Matsuda, H. (2007). Reductive decomposition of waste gypsum with SiO 2, Al 2 O 3, and Fe 2 O 3 additives. *Journal of Material Cycles and Waste Management, 9*(1), 21-26.
[65] Mindess, S., Young, F., & Darwin, D. (2003). Concrete 2nd Edition.
[66] Mohamed, B. M., & Sharp, J. H. (2002). Kinetics and mechanism of formation of tricalcium aluminate, Ca3Al2O6. *Thermochimica acta, 388*(1-2), 105-114.
[67] Mondal, P., & Jeffery, J. W. (1975). The crystal structure of tricalcium aluminate, Ca3Al2O6. *Acta Crystallographica Section B: Structural Crystallography and Crystal Chemistry, 31*(3), 689-697.
[68] Neto, J. B. F., Faria, J. O., Fredericci, C., Chotoli, F. F., Silva, A. N., Ferraro, B. B., . . . Lotto, A. A. (2016). Modification of molten steelmaking slag for cement application. *Journal of Sustainable Metallurgy, 2*(1), 13-27.
[69] Nettleship, I., Slavick, K. G., Kim, Y. J., & Kriven, W. M. (1992). Phase transformations in dicalcium silicate: I, fabrication and phase stability of fine-grained β phase. *Journal of the American Ceramic Society, 75*(9), 2400-2406.

[70] Neville, A. M., & Brooks, J. J. (1987). *Concrete technology*: Longman Scientific & Technical England.
[71] Nielsen, A. R., Larsen, M. B., Glarborg, P., & Dam-Johansen, K. (2011). High-temperature release of SO2 from calcined cement raw materials. *Energy & fuels, 25*(7), 2917-2926.
[72] Normalisatie-instituut, N. (2011). NEN-EN 197-1 Cement. Part 1: Composition, specifications and conformity criteria for common cements. In: CEN Brussels, Belgium.
[73] Normalisatie-instituut, N. (2016). NEN-EN 196-1 Methods of testing cement - Part 1: Determination of strength. In: CEN Brussels, Belgium.
[74] Normalisatie-instituut, N. (2016). NEN-EN 206+A1 (en). Concrete - Specification, performance, production and conformity. In: CEN Brussels, Belgium.
[75] Palys, T. S., & Atchison, C. (2014). *Research decisions: Quantitative, qualitative, and mixed method approaches*: Nelson Education.
[76] Pane, I., & Hansen, W. (2005). Investigation of blended cement hydration by isothermal calorimetry and thermal analysis. *Cement and Concrete Research, 35*(6), 1155-1164.
[77] Pardo, N., Moya, J. A., & Mercier, A. (2011). Prospective on the energy efficiency and CO2 emissions in the EU cement industry. *Energy, 36*(5), 3244-3254.
[78] Peray, K. E. (1986). *The Rotary Cement Kiln* (2nd ed.): Edward Arnold.
[79] Pimienta, P., McNamee, R. J., & Mindeguia, J.-C. (2018). *Physical Properties and Behaviour of High-Performance Concrete at High Temperature*: Springer.
[80] Purohit, R., & Venugopalan, P. (2009). Polymorphism: an overview. *Resonance, 14*(9), 882-893.
[81] Rejmak, P., Dolado, J. S., Aranda, M. A., & Ayuela, A. (2019). First-Principles Calculations on Polymorphs of Dicalcium Silicate-Belite, a Main Component of Portland Cement. *The Journal of Physical Chemistry C*.
[82] Rennison, C. M., & Hart, T. C. (2018). *Research methods in criminal justice and criminology*: SAGE Publications.
[83] Rijksoverheid Nederland. (1997). Besluit stortplaatsen en stortverboden afvalstoffen. Retrieved from https://wetten.overheid.nl/BWBR0009094/2013-07-01
[84] RJ Smith Construction. (2016). rj-smith-concrete-recycling-3. In.
[85] Rueda, J., & Alaejos, P. (2019). Quantitative Effect on Water Demand of Absorption and Fine Particles Content of Recycled Concrete Sands. *Journal of Materials in Civil Engineering, 31*(5), 04019038.
[86] Rutte Groep (Writer). (2019). How does the SmartLiberator work? [Video file]. In.
[87] Schenk, K. J. (2011). The Netherlands Patent No. WO 2011/142663 A1.
[88] Scrivener, K. L., John, V. M., & Gartner, E. M. (2017). Eco-efficient cements: Potential economically viable solutions for a low-CO2 cement-based materials industry.
[89] Sereda, P., & Litvan, G. (1980). *Durability of building materials and components*.
[90] Shi, C., Krivenko, P. V., & Roy, D. (2006). *Alkali-Activated Cements and Concretes*: Taylor & Francis
[91] Shui, Z., Xuan, D., Chen, W., Yu, R., & Zhang, R. (2009). Cementitious characteristics of hydrated cement paste subjected to various dehydration temperatures. *Construction and Building Materials, 23*(1), 531-537.
[92] Singh, J., Singh, H., & Singh, R. (2015). Portland slag cement using ground granulated blast furnace slag (GGBFS)—a review. *Int. J. Res. Eng. Appl. Sci, 5*(11), 47-53.
[93] SmartCrusher (Writer). (2015). SmartCrusher - Concrete Recycling - a Circulair Production Chain for concrete - c2c [Video file]. In.
[94] Smith, D. K., Majumdar, A., & Ordway, F. (1965). The crystal structure of γ-dicalcium silicate. *Acta Crystallographica, 18*(4), 787-795.
[95] Smith, F. (1999). *Industrial applications of X-ray diffraction*: CRC press.
[96] Staněk, T., & Sulovský, P. (2002). The influence of the alite polymorphism on the strength of the Portland cement. *Cement and Concrete Research, 32*(7), 1169-1175.

[97] Stephan, D., & Wistuba, S. (2006). Crystal structure refinement and hydration behaviour of 3CaO· SiO2 solid solutions with MgO, Al2O3 and Fe2O3. *Journal of the European Ceramic Society, 26*(1-2), 141-148.
[98] Stevens, S. J., Hand, R. J., & Sharp, J. H. (1997). Polymorphism of silica. *Journal of materials science, 32*(11), 2929-2935.
[99] Stutzman, P., Heckert, A., Tebbe, A., & Leigh, S. (2014). Uncertainty in Bogue-calculated phase composition of hydraulic cements. *Cement and Concrete Research, 61*, 40-48.
[100] Szabó, L., Hidalgo, I., Ciscar, J. C., & Soria, A. (2006). CO2 emission trading within the European Union and Annex B countries: the cement industry case. *Energy policy, 34*(1), 72-87.
[101] Taylor, H. F. W. (1997). *Cement chemistry*: Thomas Telford.
[102] The European Parliament, & The Council of the European Union. (2008). Directive 2008/98/EC on waste and repealing certain Directives.
[103] The European Parliament, & The Council of the European Union. (2018). Directive (EU) 2018/850 amending Directive 1999/31/EC on the landfill of waste.
[104] TUNCAN, M., ARIÖZ, Ö., RAMYAR, K., & KARASU, B. EFFECT OF COMPACTION ON ASSESSED CONCRETE STRENGTH SIKIŞTIRMANIN TAHMİN EDİLEN BETON DAYANIMI ÜZERİNDEKİ ETKİSİ.
[105] Van Oss, H. G., & Padovani, A. C. (2002). Cement Manufacture and the Environment: Part I: Chemistry and Technology. *Journal of Industrial Ecology, 6*(1), 89-105.
[106] Varma, S. P., & Wall, C. D. (1981). A monoclinic tricalcium aluminate (C3A) phase in a commercial Portland cement clinker. *Cement and Concrete Research, 11*(4), 567-574.
[107] Villagrán-Zaccardi, Y. A., Egüez-Alava, H., De Buysser, K., Gruyaert, E., & De Belie, N. (2017). Calibrated quantitative thermogravimetric analysis for the determination of portlandite and calcite content in hydrated cementitious systems. *Materials and Structures, 50*(3), 179.
[108] VROM. (2001). Bouw- en sloopafval.
[109] Wang, J., Mu, M., & Liu, Y. (2018). Recycled cement. *Construction and Building Materials, 190*, 1124-1132.
[110] Wang, P., Trettin, R., & Rudert, V. (2005). Effect of fineness and particle size distribution of granulated blast-furnace slag on the hydraulic reactivity in cement systems. *Advances in cement research, 17*(4), 161-167.
[111] Wesselsky, A., & Jensen, O. M. (2009). Synthesis of pure Portland cement phases. *Cement and Concrete Research, 39*(11), 973-980.
[112] Wichitpunya, E., & Alamy Stock Photo. (2017). cement texture background / rugged floor concrete with cement mixer for construction glue tiled on ground background. In.
[113] Wills, B. A., & Napier-Munn, T. J. (2005). *Wills' mineral processing technology: an introduction to the practical aspects of ore treatment and mineral recovery* (7th ed.): Butterworth-Heinemann.
[114] Zhao, M. (2012). *Quantitative control of C2S crystal transformation.* Paper presented at the Applied Mechanics and Materials.

APPENDICES

Appendix A. Particle Size Distribution

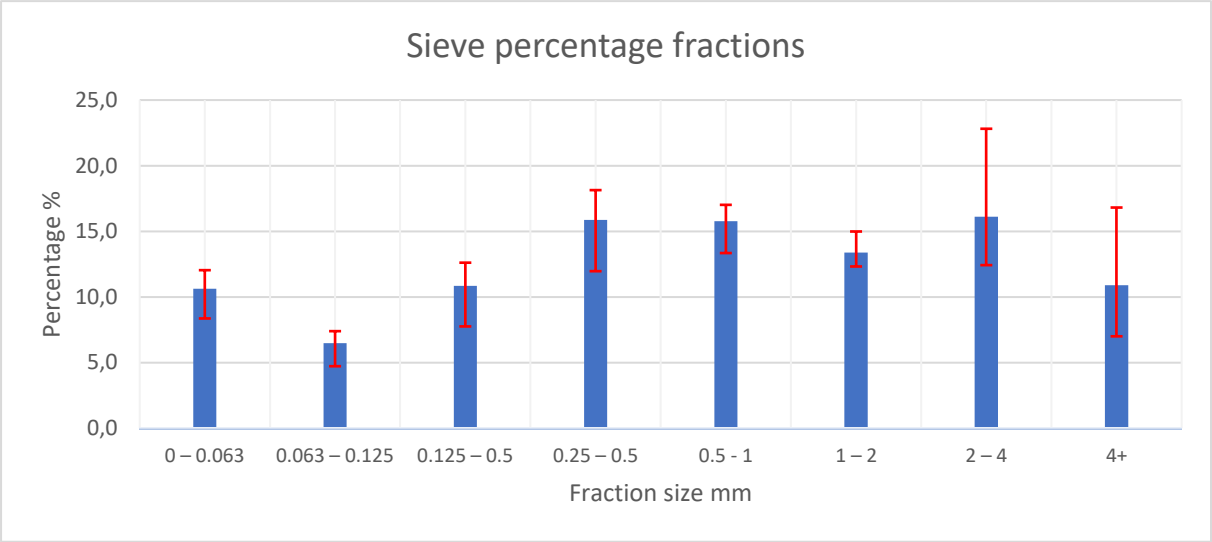

A. 1: Percentages of sieved fractions including their deviations present in the 0 – 4 mm Smart Crusher fraction.

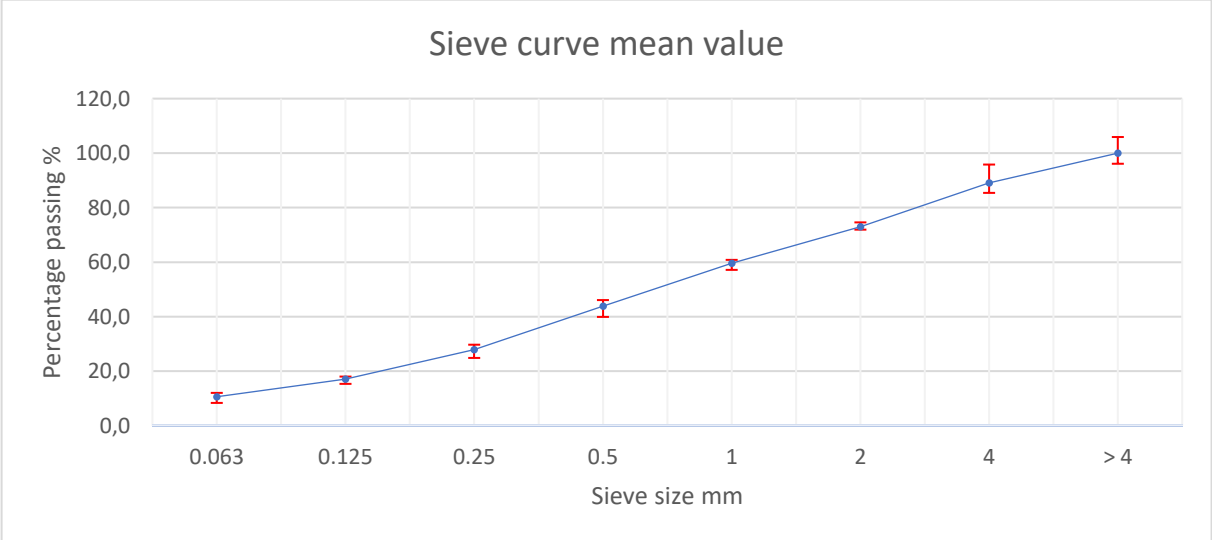

A. 2: Sieve curve of the mean values of the sieved fractions including their deviations present in the 0 – 4 mm Smart Crusher fraction.

Appendix B. TG results

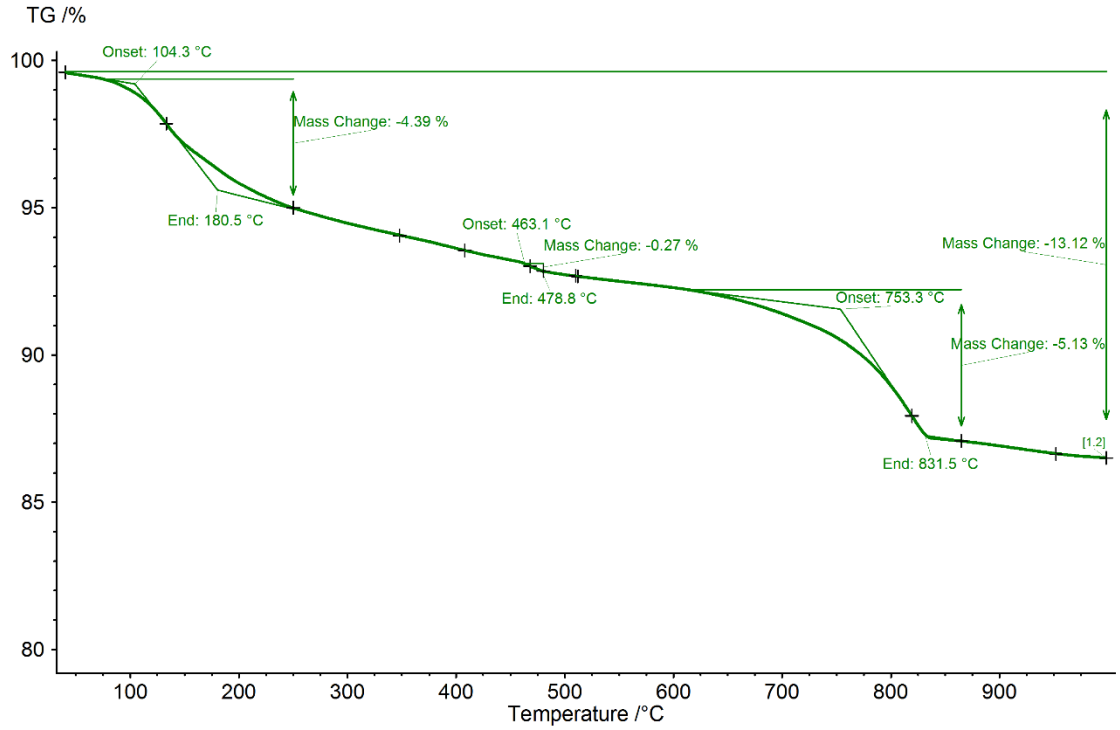

B. 1: TG curve of sample 1 (0.063 – 0.125 mm) showing abrupt mass loss in three temperature ranges and their characteristic values.

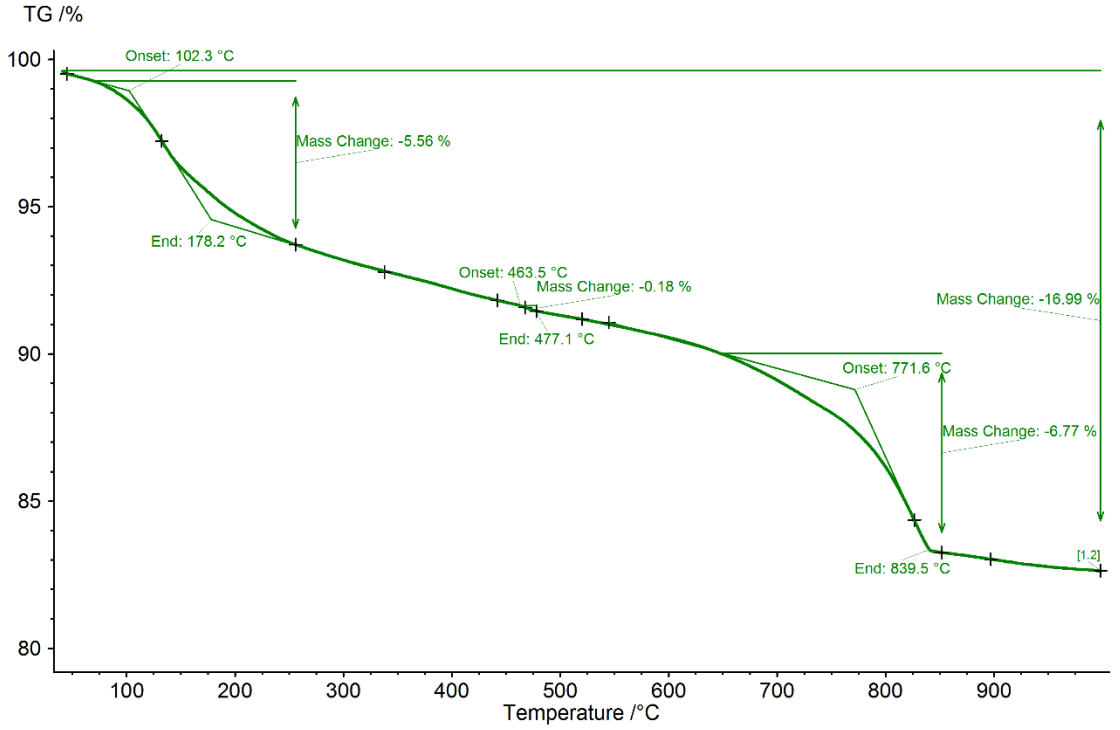

B. 2: TG curve of sample 2 (0.000 - 0.063 mm) showing abrupt mass loss in three temperature ranges and their characteristic values.

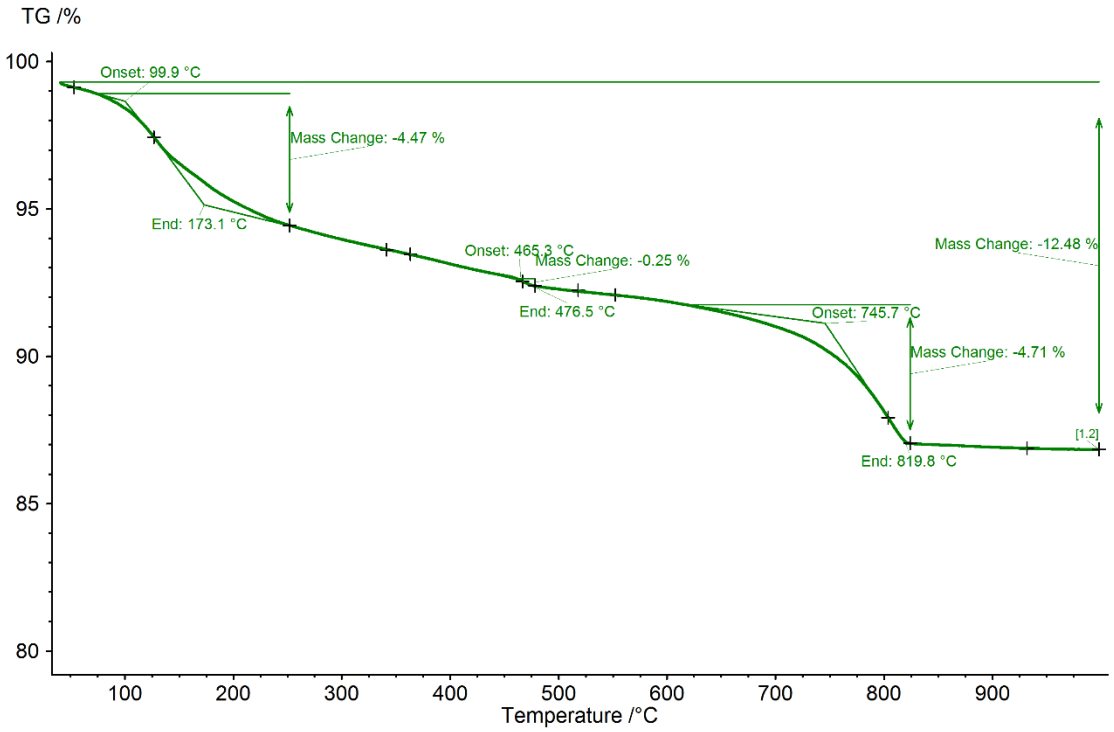

B. 3: TG curve of sample 3 (0.063 - 0.125 mm) showing abrupt mass loss in three temperature ranges and their characteristic values.

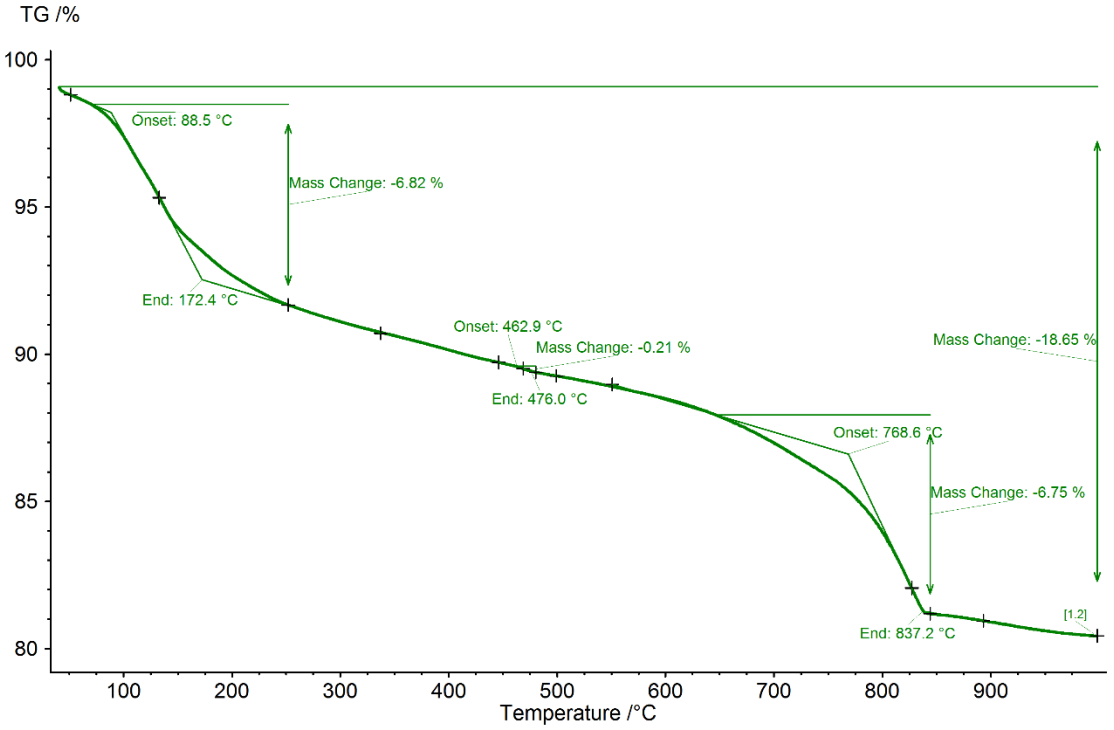

B. 4: TG curve of sample 4 (0.000 - 0.063 mm) showing abrupt mass loss in three temperature ranges and their characteristic values.

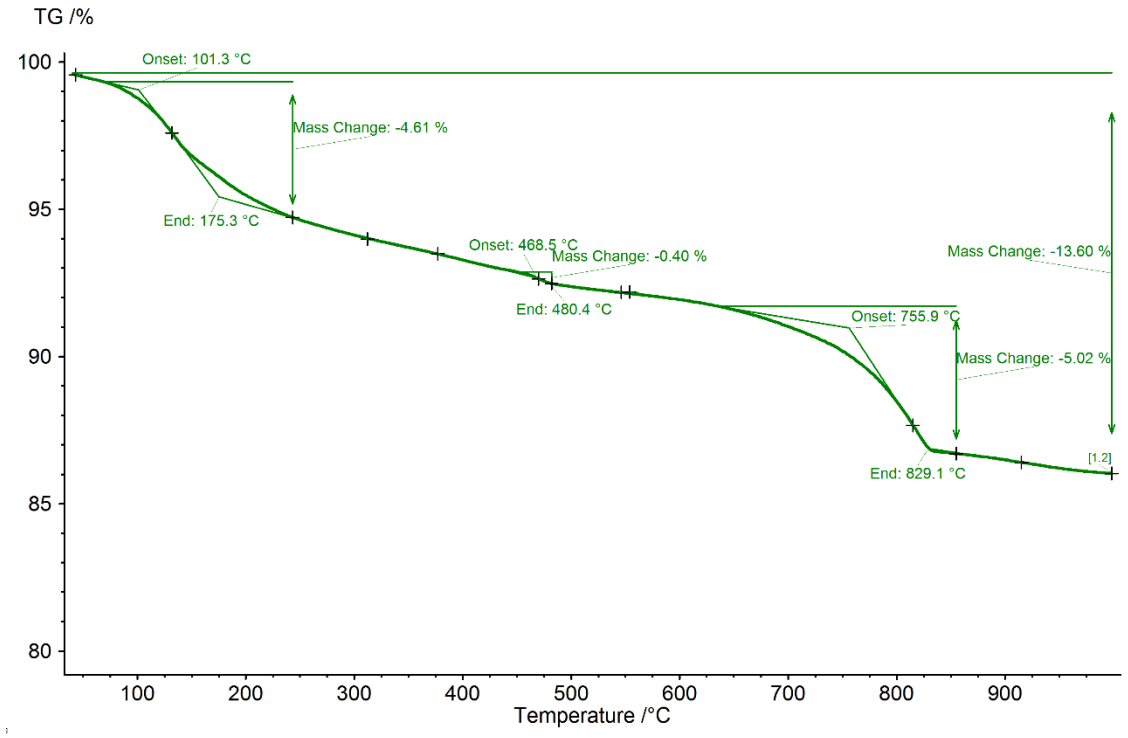

B. 5: TG curve of sample 5 (0.063 - 0.125 mm) showing abrupt mass loss in three temperature ranges and their characteristic values.

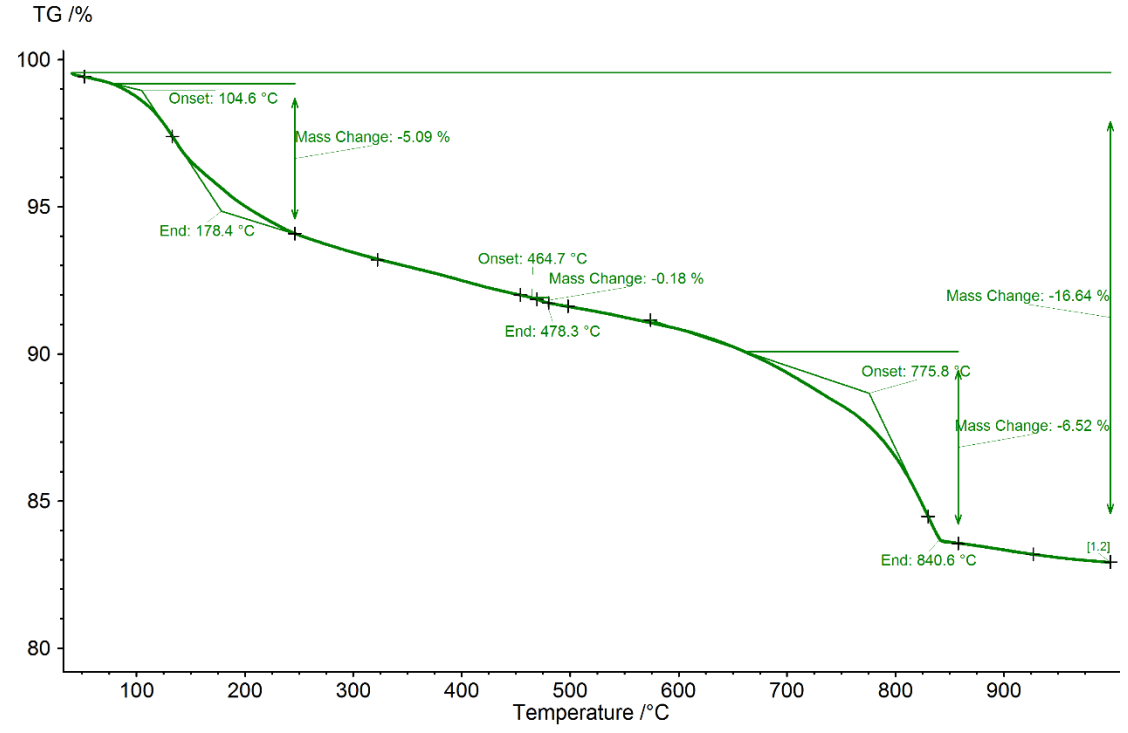

B. 6: TG curve of sample 6 (0.000 - 0.063 mm) showing abrupt mass loss in three temperature ranges and their characteristic values.

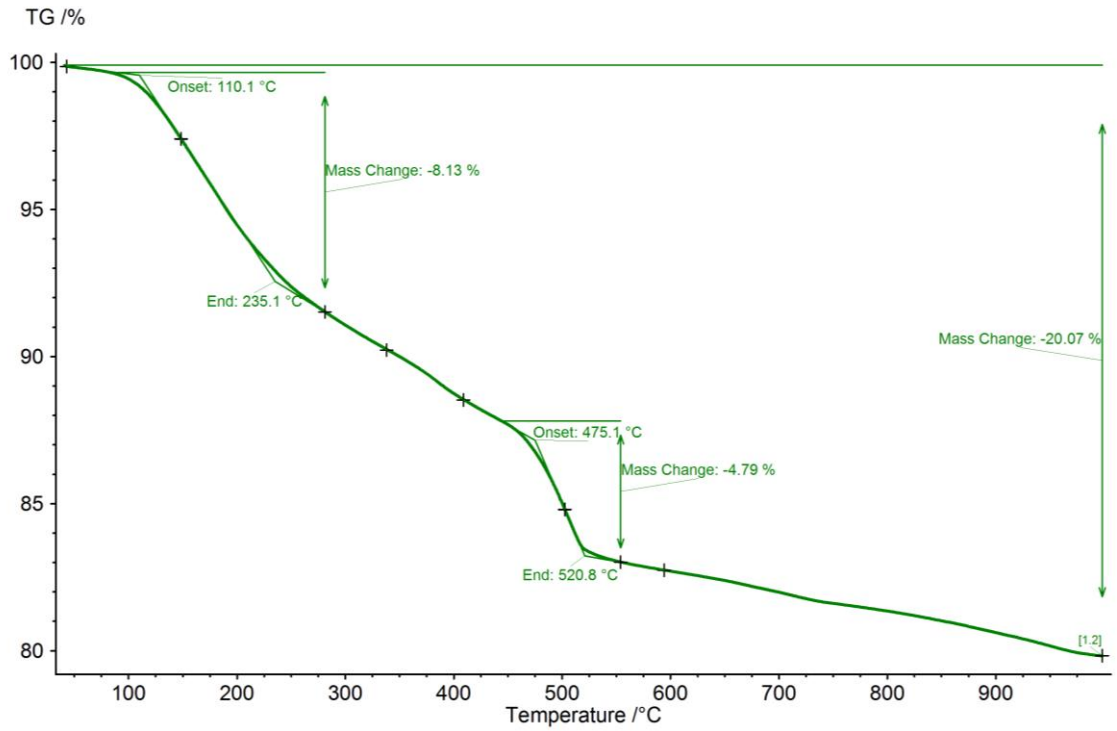

B. 7: TG curve of CEM I hydrate showing abrupt mass loss in two temperature ranges and their characteristic values.

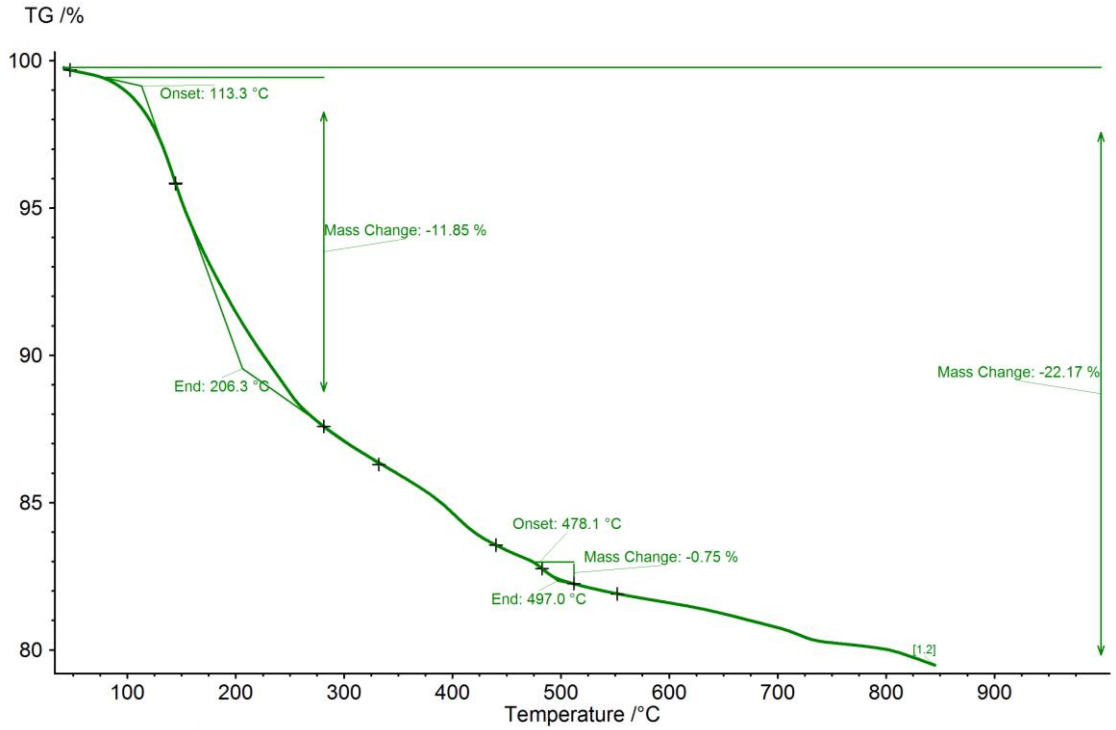

B. 8: TG curve of CEM III/B hydrate showing abrupt mass loss in two temperature ranges and their characteristic values.

Appendix C. DTG results

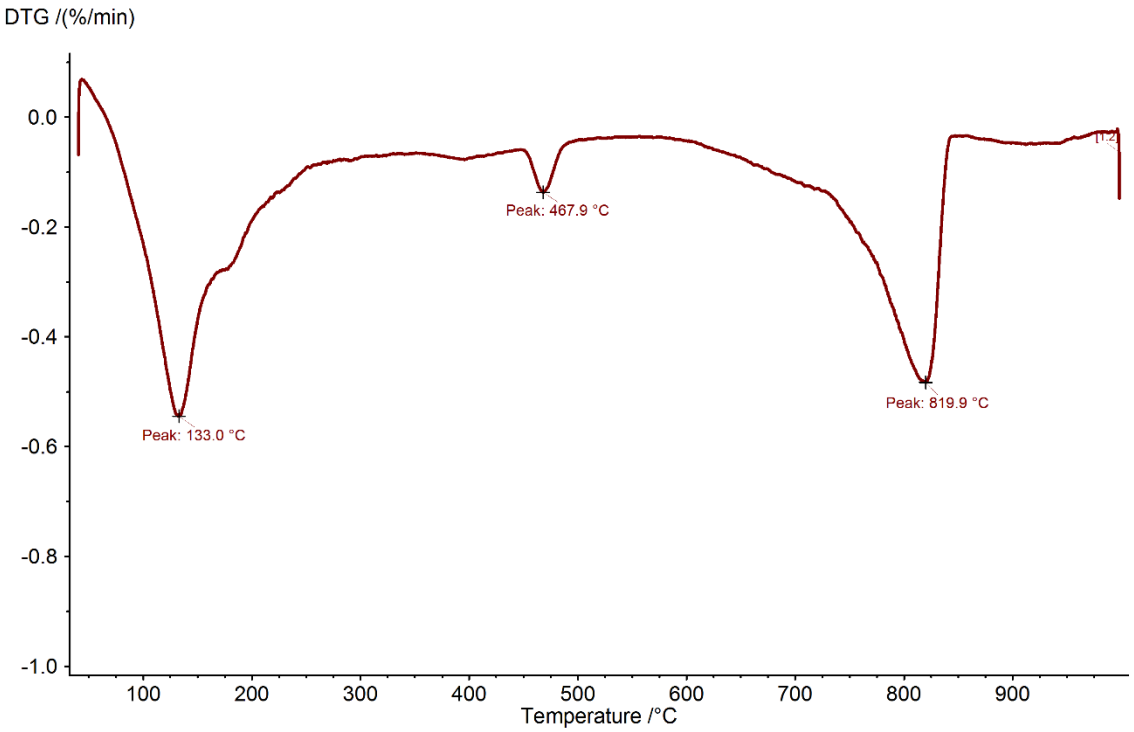

C. 1: DTG curve of sample 1 (0.063 – 0.125 mm) showing peaks in three temperature ranges and their peak temperature.

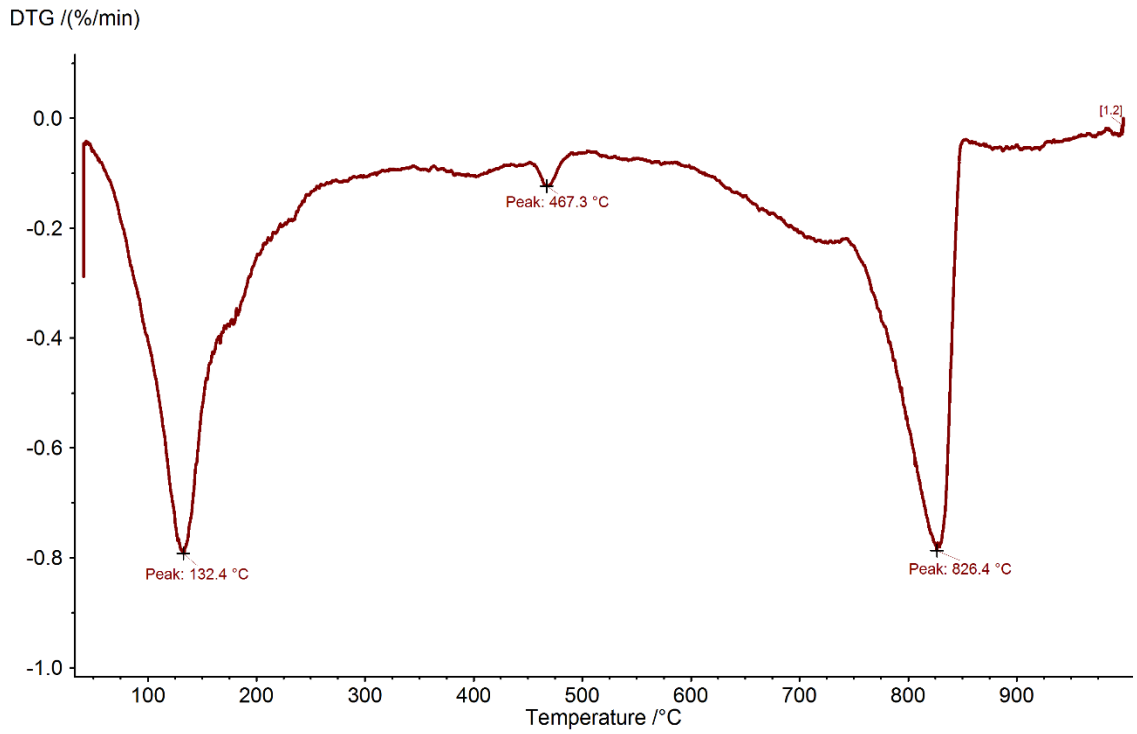

C. 2: DTG curve of sample 2 (0.000 - 0.063 mm) showing peaks in three temperature ranges and their peak temperature.

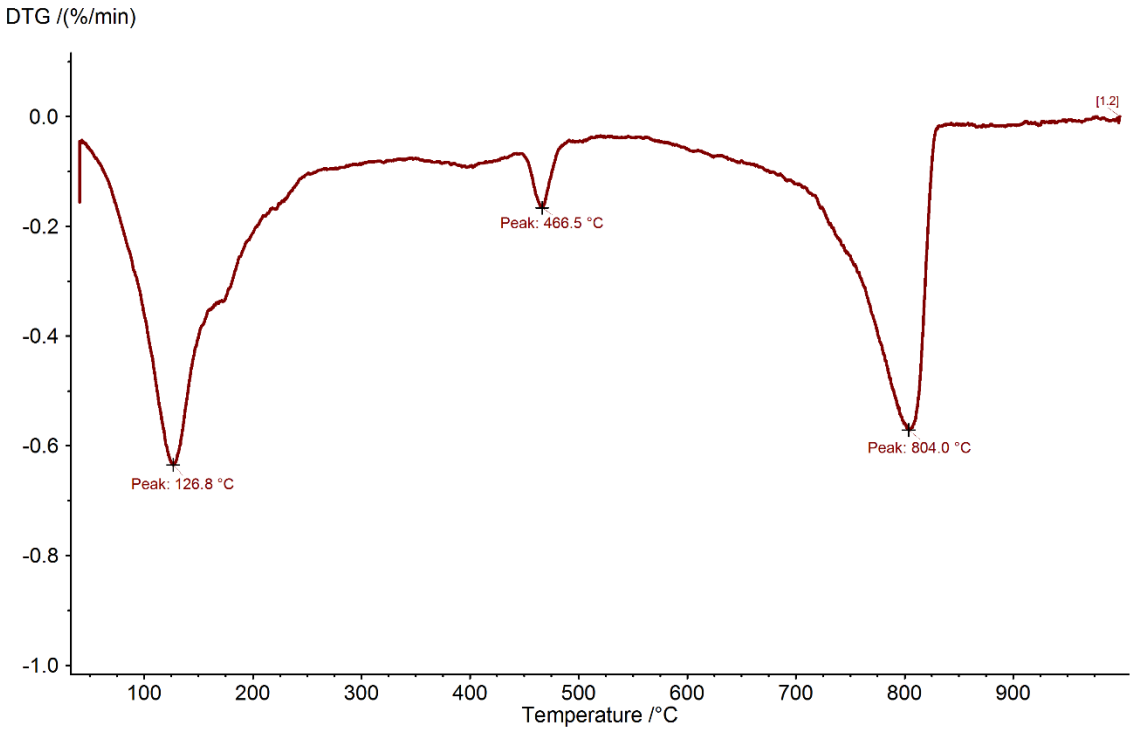

C. 3: DTG curve of sample 3 (0.063 - 0.125 mm) showing peaks in three temperature ranges and their peak temperature.

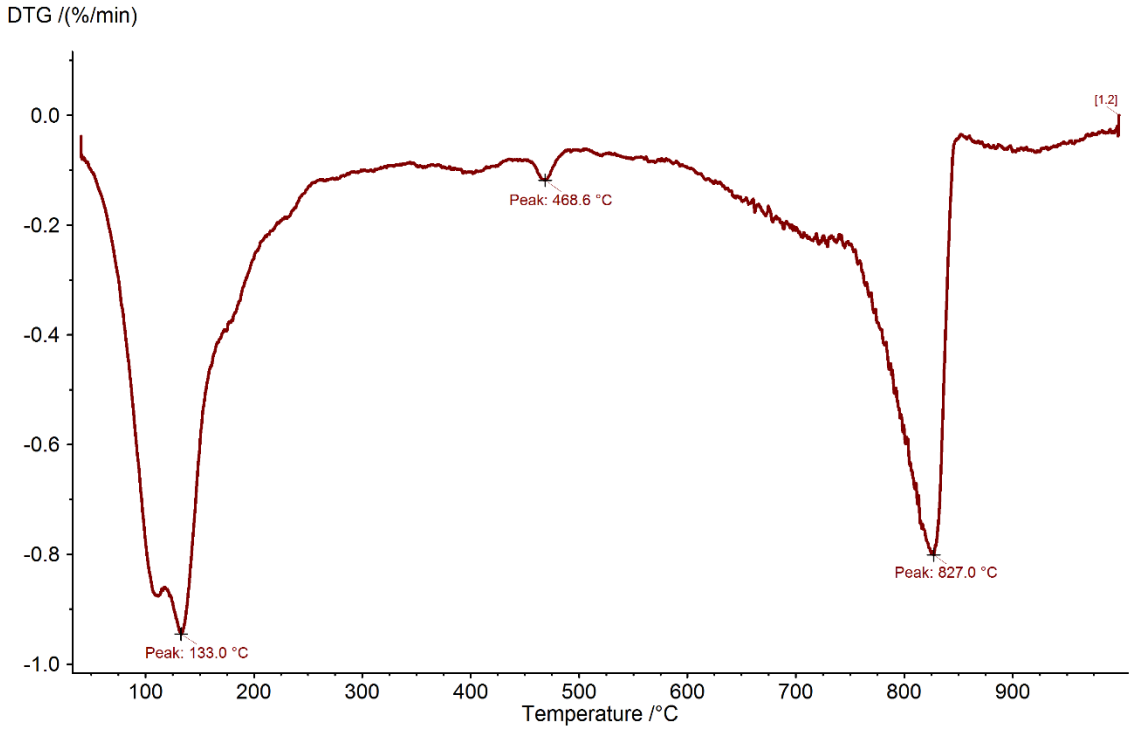

C. 4: DTG curve of sample 4 (0.000 - 0.063 mm) showing peaks in three temperature ranges and their peak temperature.

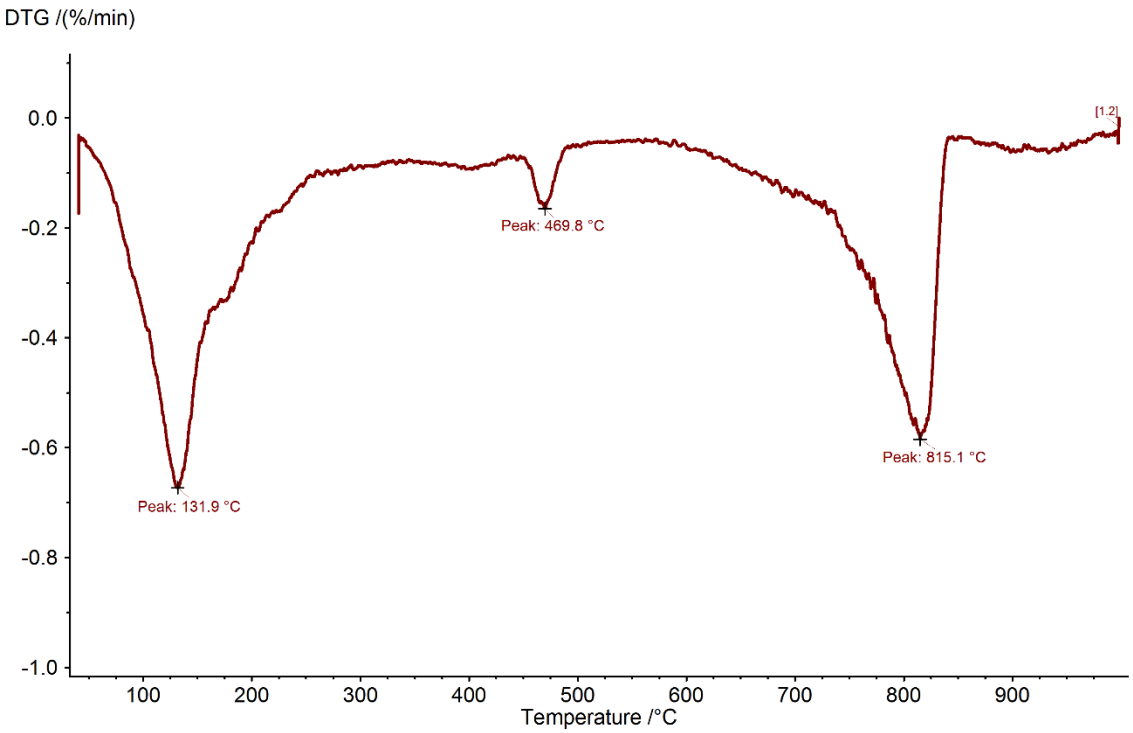

C. 5: DTG of sample 5 (0.063 - 0.125 mm) showing peaks in three temperature ranges and their peak temperature.

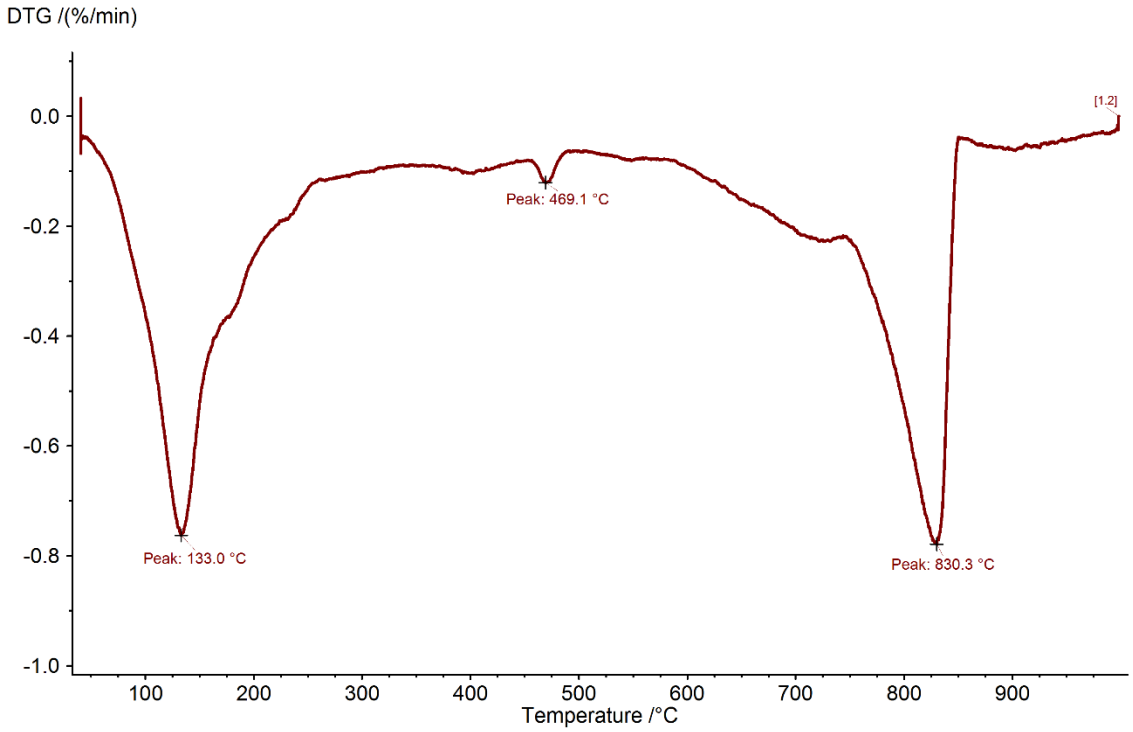

C. 6: DTG of sample 6 (0.000 - 0.063 mm) showing peaks in three temperature ranges and their peak temperature.

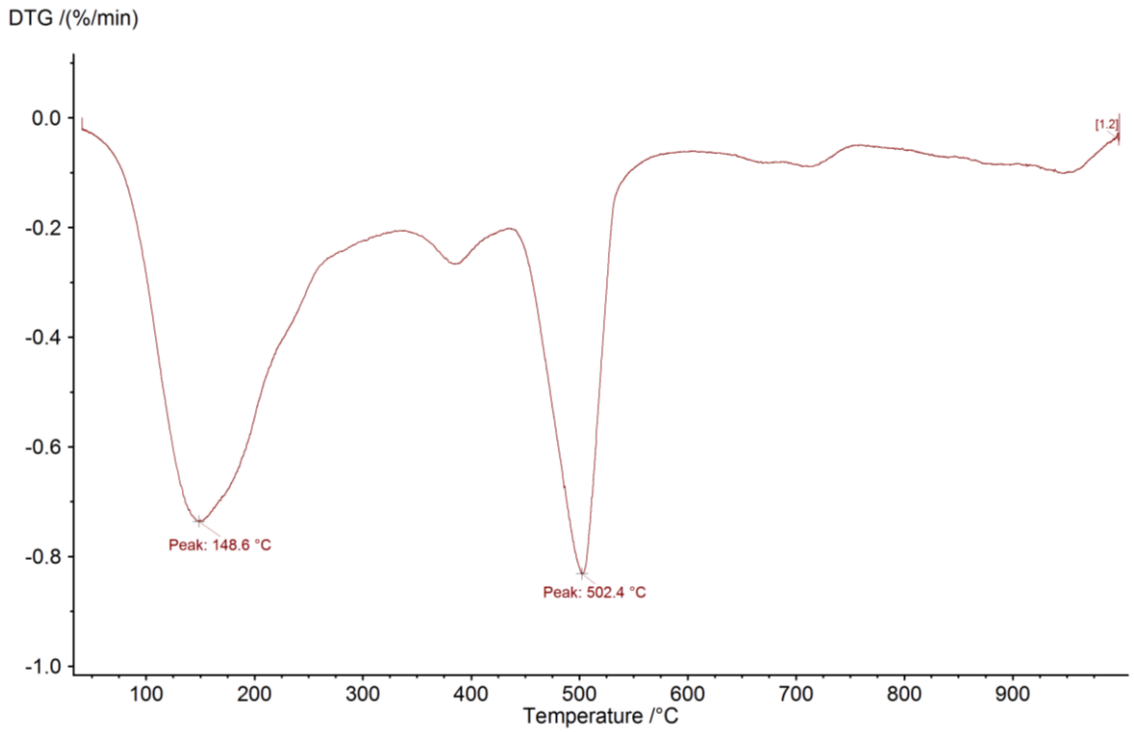

C. 8: DTG curve of CEM I hydrate showing peaks in two temperature ranges and their peak temperature.

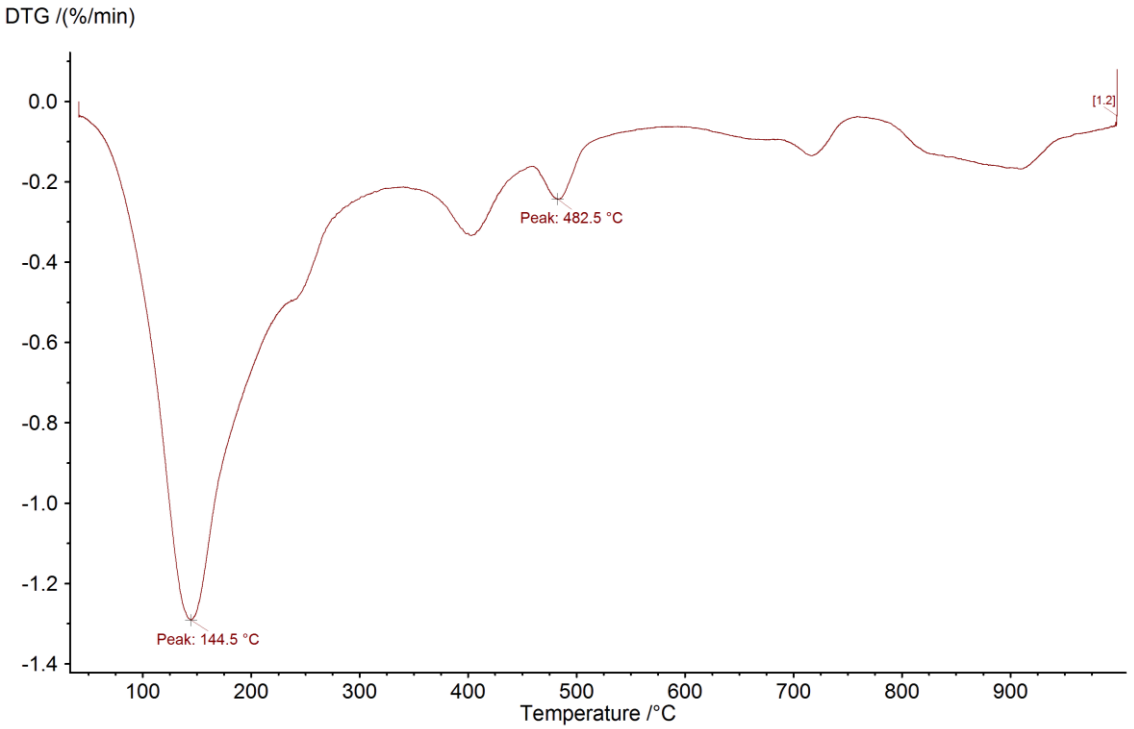

C. 7: DTG curve of CEM III/B hydrate showing peaks in two temperature ranges and their peak temperature.

Appendix D. DSC results

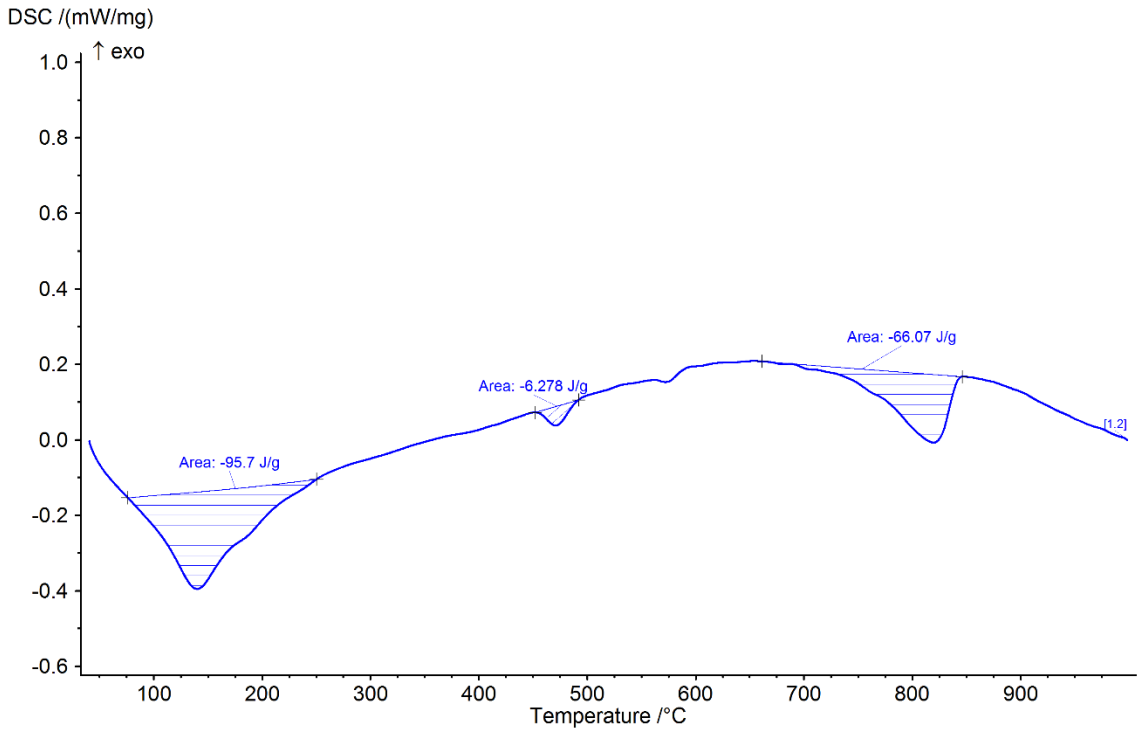

D. 1: DSC curve of sample 1 (0.063 – 0.125 mm) showing endothermic peaks in three temperature ranges and their area. Around 570 °C another endothermic peak caused by the phase transition of α-quartz to ß-quartz can be distinguished.

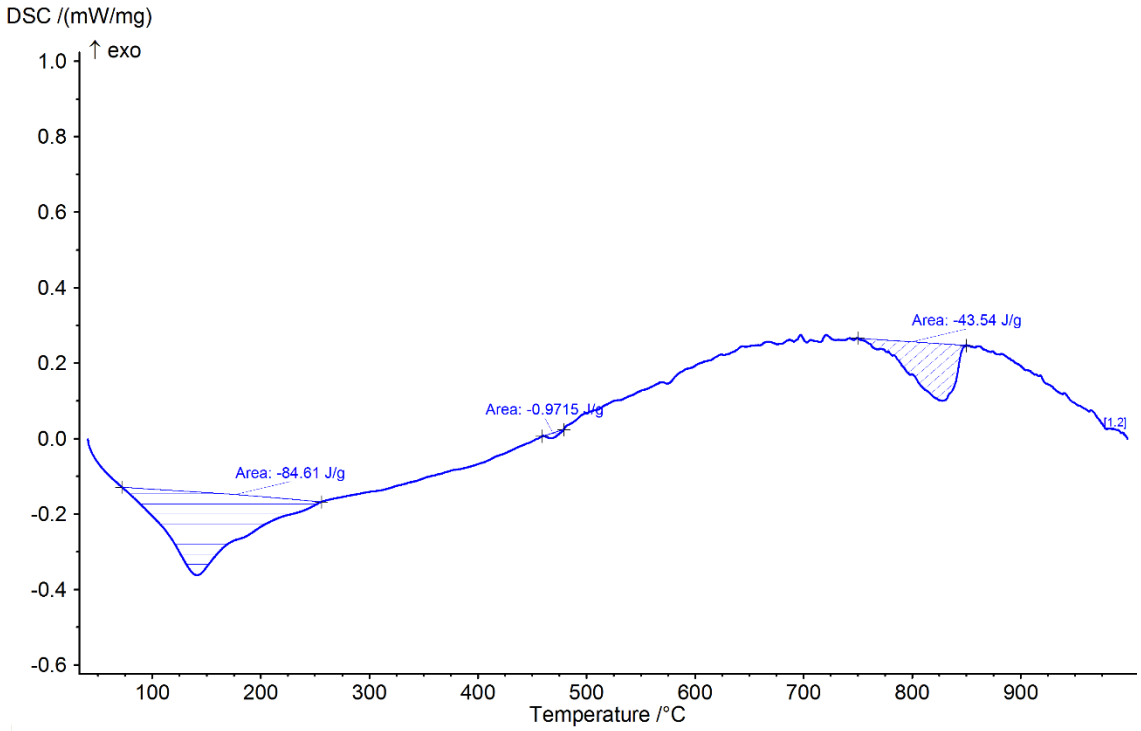

D. 2: DSC curve of sample 2 (0.000 - 0.063 mm) showing endothermic peaks in three temperature ranges and their area. Around 570 °C another endothermic peak caused by the phase transition of α-quartz to ß-quartz can be distinguished.

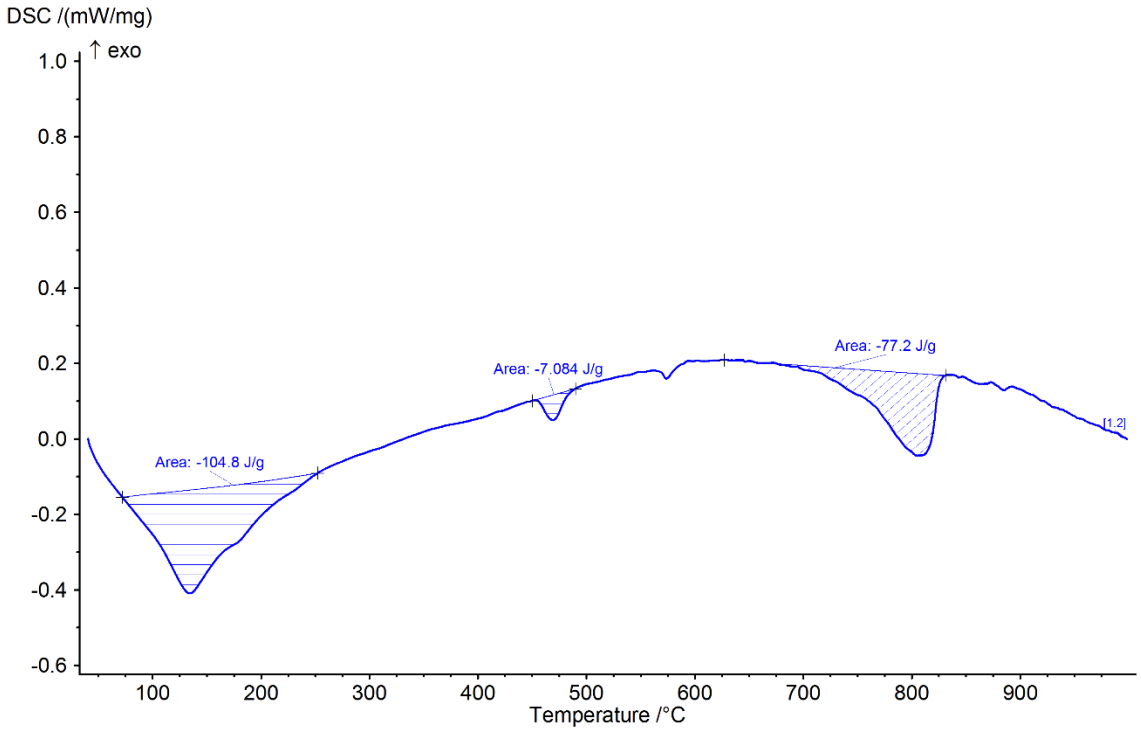

D. 3: DSC curve of sample 3 (0.063 - 0.125 mm) showing endothermic peaks in three temperature ranges and their area. Around 570 °C another endothermic peak caused by the phase transition of α-quartz to ß-quartz can be distinguished.

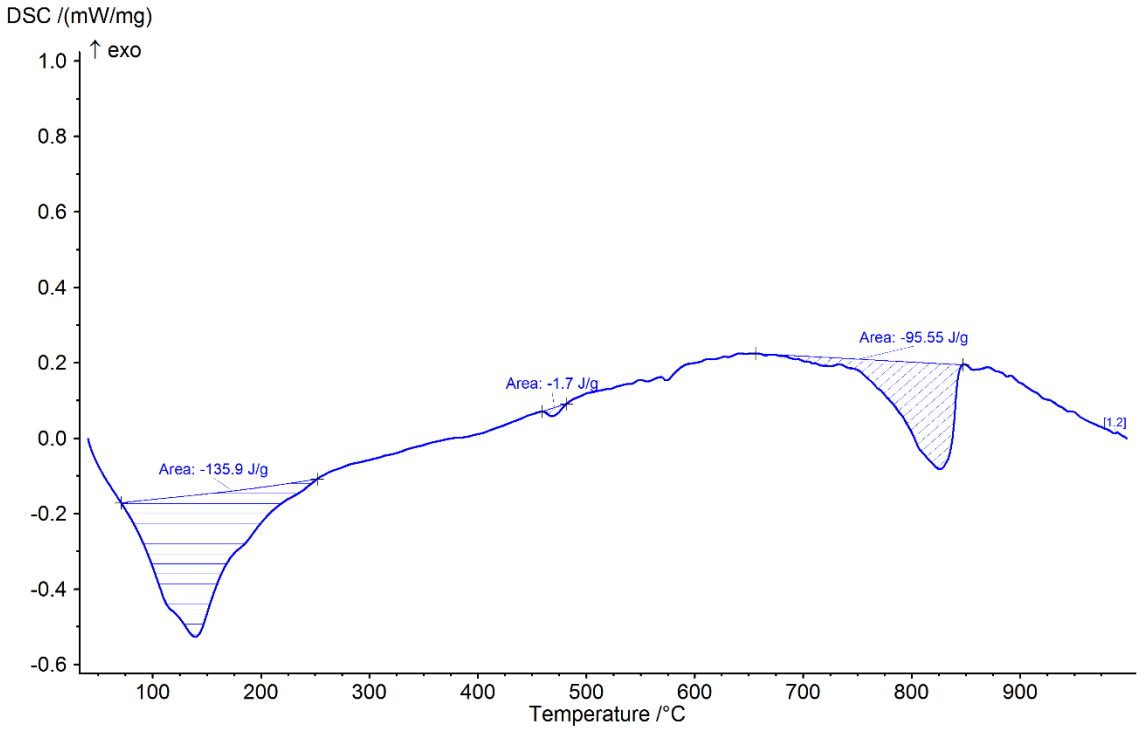

D. 4: DSC curve of sample 4 (0.000 - 0.063 mm) showing endothermic peaks in three temperature ranges and their area. Around 570 °C another endothermic peak caused by the phase transition of α-quartz to ß-quartz can be distinguished.

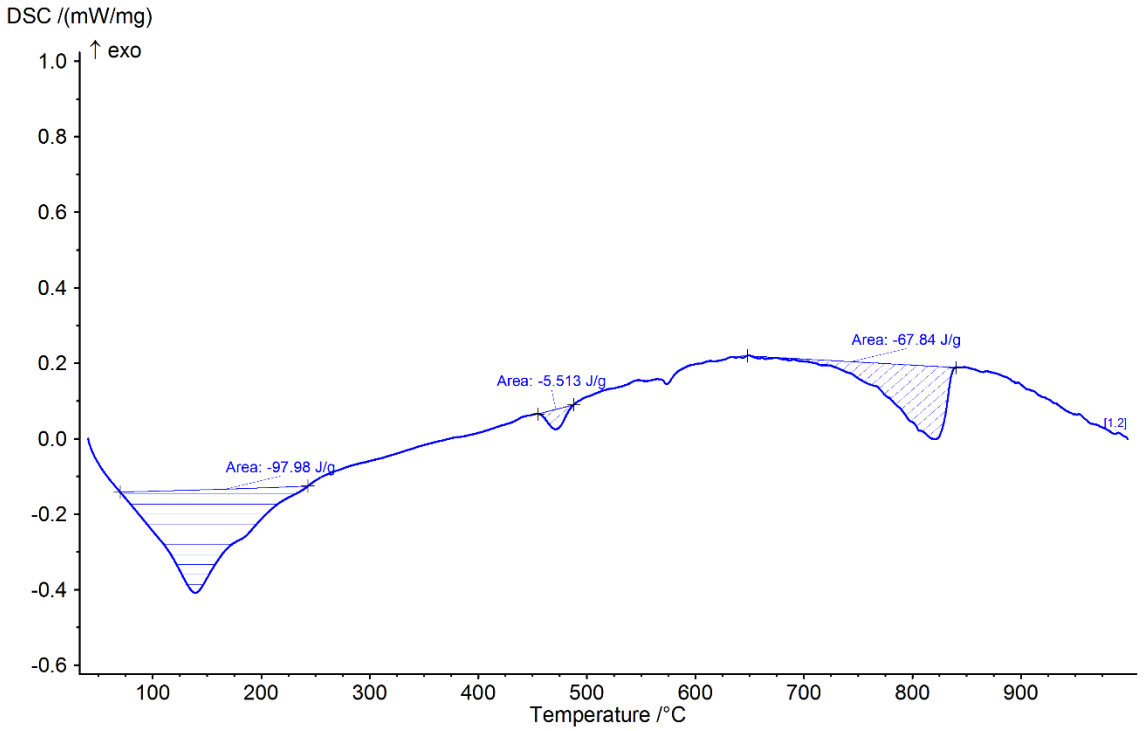

D. 5: DSC curve of sample 5 (0.063 - 0.125 mm) showing endothermic peaks in three temperature ranges and their area. Around 570 °C another endothermic peak caused by the phase transition of α-quartz to β-quartz can be distinguished.

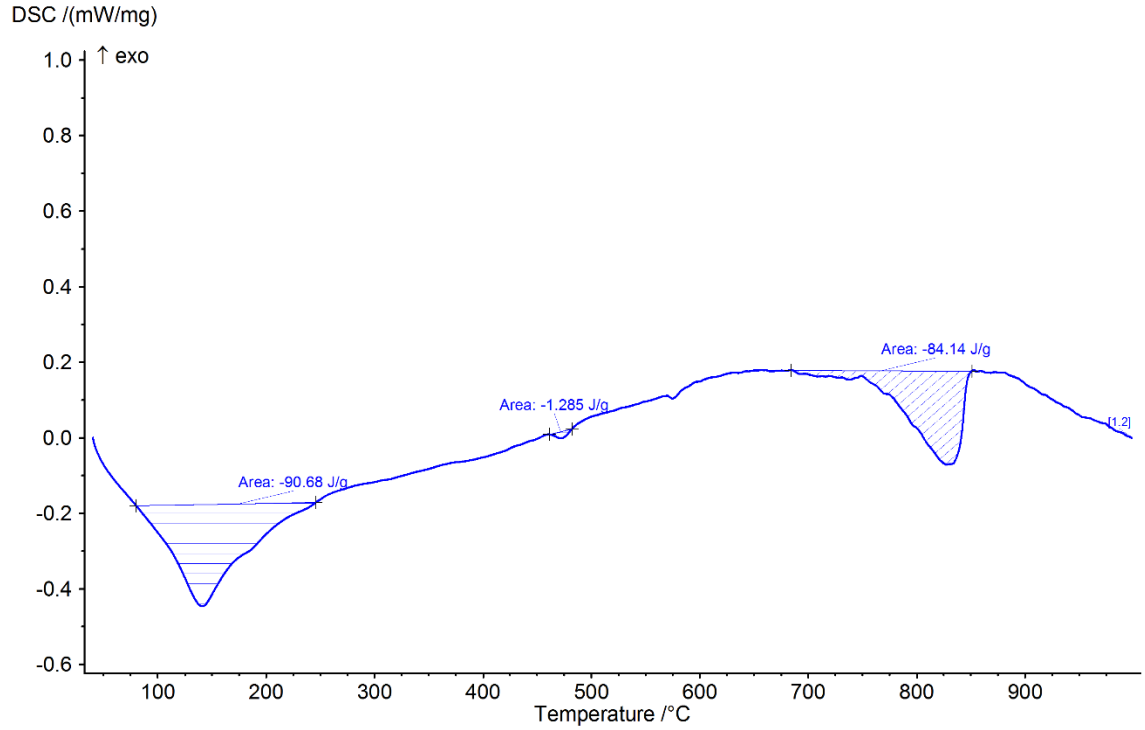

D. 6: DSC curve of sample 6 (0.000 - 0.063 mm) showing endothermic peaks in three temperature ranges and their area. Around 570 °C another endothermic peak caused by the phase transition of α-quartz to β-quartz can be distinguished.

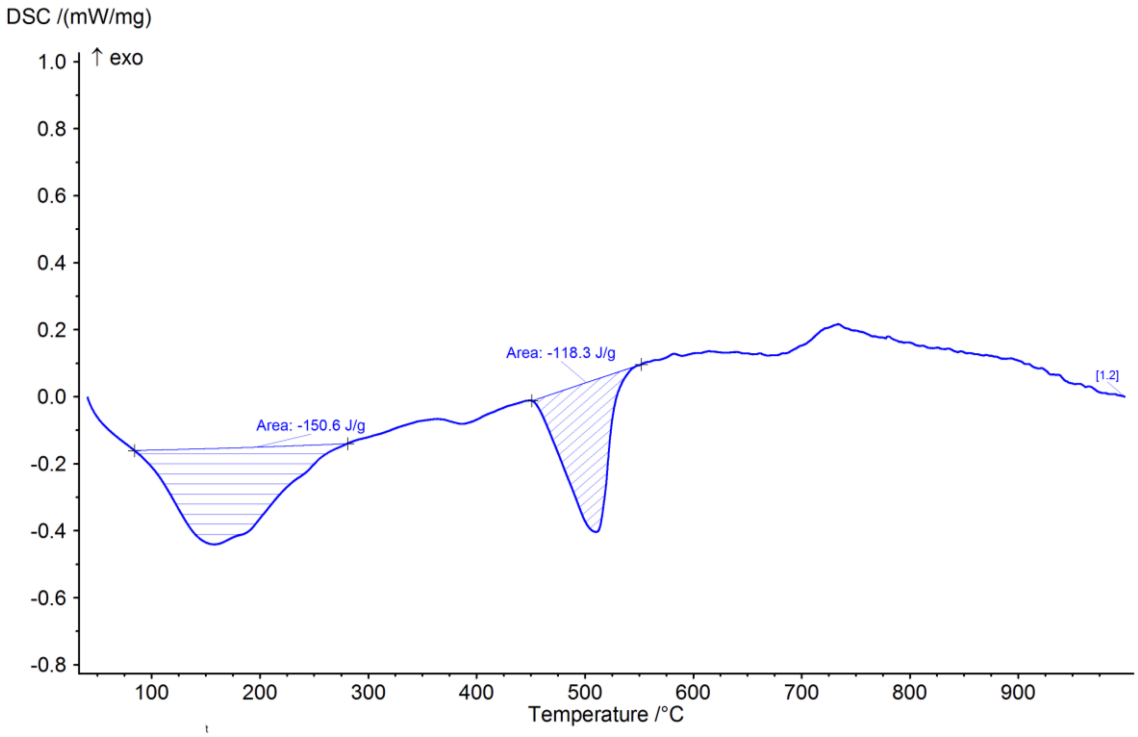

D. 8: DSC curve of CEM I hydrate showing endothermic peaks in two temperature ranges and their area.

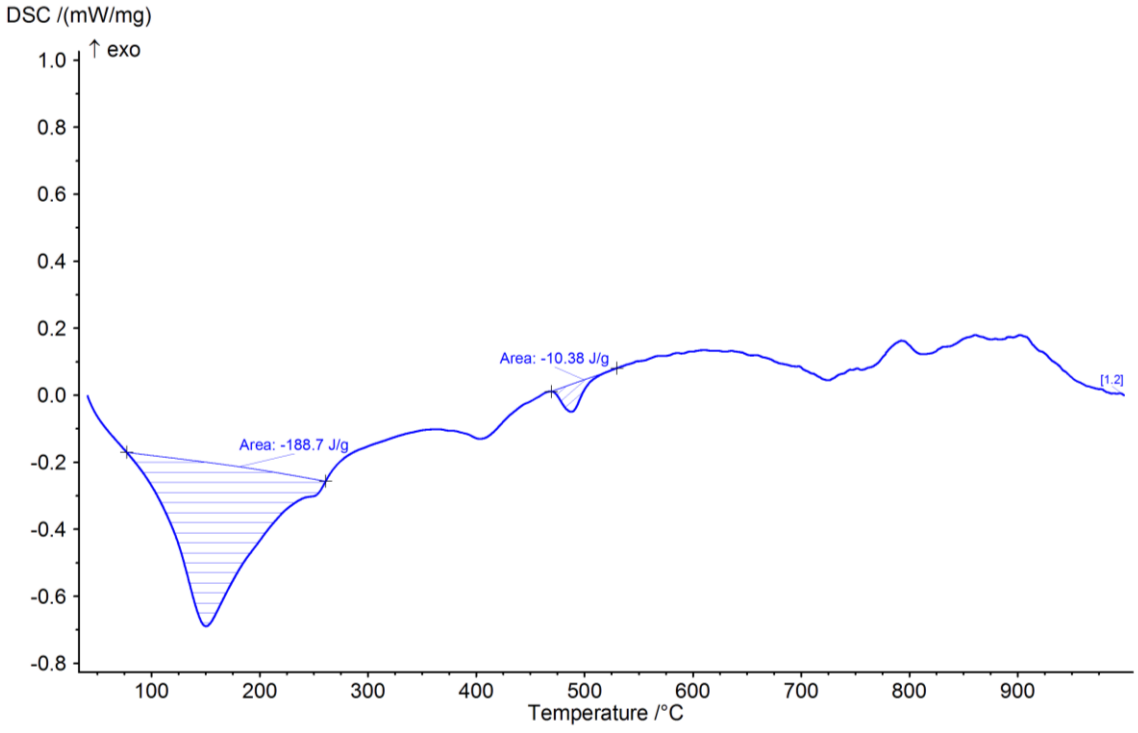

D. 7: DSC curve of CEM III/B hydrate showing endothermic peaks in two temperature ranges and their area.

Appendix E. MS results

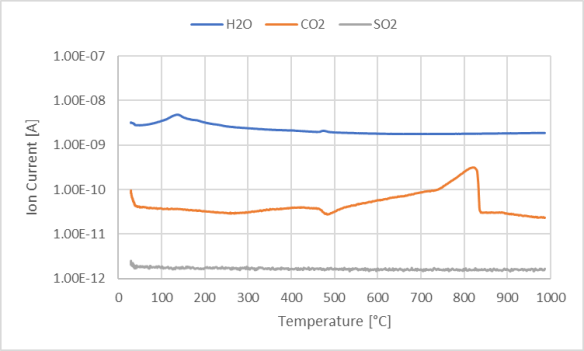

E. 2: MS of the 0.0 - 0.063 mm fraction showing the temperatures at which H_2O, CO_2 and SO_2 are released.

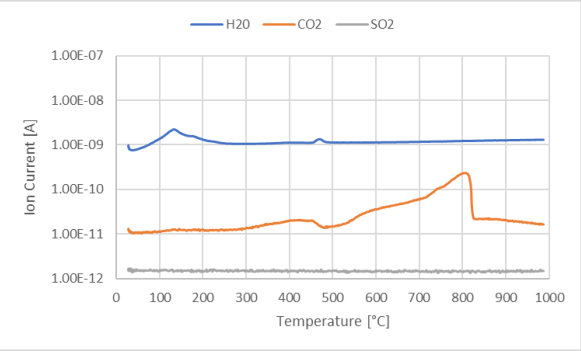

E. 1: MS of the 0.063 - 0.125 mm fraction showing the temperatures at which H_2O, CO_2 and SO_2 are released.

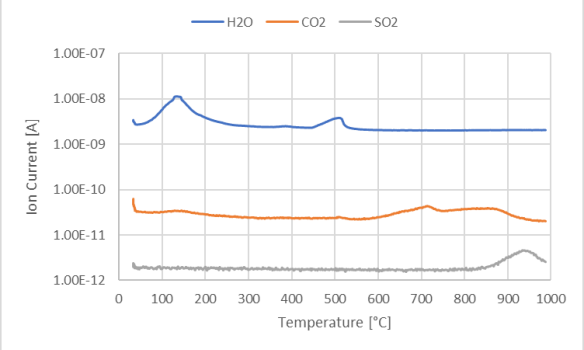

E. 4: MS of the CEM I hydrate showing the temperatures at which H_2O, CO_2 and SO_2 are released.

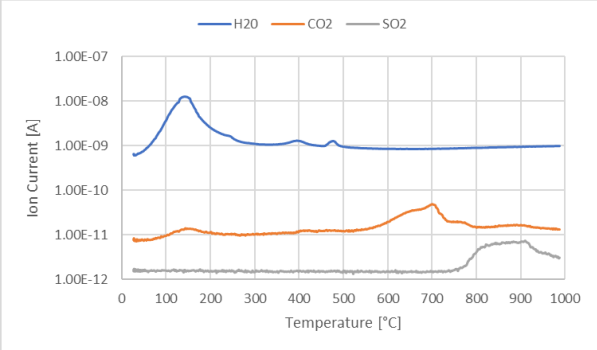

E. 3: MS of the CEM III/B hydrate showing the temperatures at which H_2O, CO_2 and SO_2 are released.

Appendix F. XRF results

Sample type		CaO	SiO_2	Al_2O_3	MgO	SO_3	Fe_2O_3	TiO_2	K_2O	MnO	SrO	Cl	ZnO	Cr_2O_3	P_2O_5	Other
0.0 - 0.063	Hydrated	36.65	47.63	6.94	1.67	1.32	3.91	0.46	0.95	0.13	0.10	0.03	0.04	0.02	0.00	0.15
	500 °C	35.94	48.85	6.71	1.70	1.32	3.67	0.43	0.92	0.12	0.10	0.04	0.04	0.01	0.00	0.15
	800 °C	36.35	48.51	6.62	1.68	1.35	3.71	0.40	0.90	0.12	0.10	0.03	0.04	0.02	0.00	0.17
	1400 °C	31.44	54.42	7.10	1.39	0.24	3.66	0.42	0.91	0.12	0.09	0.00	0.04	0.02	0.00	0.15
0.063 - 0.125	Hydrated	33.74	51.46	6.72	1.66	1.30	3.31	0.40	0.97	0.12	0.08	0.05	0.04	0.01	0.00	0.14
	500 °C	35.72	48.82	7.10	1.85	1.47	3.26	0.41	0.94	0.11	0.08	0.05	0.04	0.01	0.00	0.14
	800 °C	34.35	50.62	6.96	1.72	1.40	3.18	0.36	0.96	0.11	0.08	0.05	0.03	0.01	0.00	0.17
	1400 °C	25.71	62.52	6.20	1.11	0.12	2.83	0.33	0.85	0.10	0.06	0.01	0.03	0.02	0.00	0.11
CEM I 52.5 R	Unhydrated	70.47	16.44	4.05	1.98	2.49	2.96	0.34	0.63	0.06	0.17	0.06	0.06	0.00	0.15	0.14
	Hydrated	71.54	16.25	3.84	1.63	2.02	3.18	0.36	0.58	0.06	0.18	0.05	0.07	0.01	0.13	0.10
	500 °C	70.56	17.07	4.03	1.74	2.10	2.99	0.33	0.58	0.06	0.17	0.07	0.06	0.01	0.12	0.11
	800 °C	70.95	16.97	4.00	1.71	1.97	2.94	0.32	0.53	0.06	0.17	0.06	0.06	0.01	0.14	0.11
	1400 °C	70.92	16.72	4.39	1.91	1.69	3.04	0.34	0.40	0.06	0.17	0.00	0.06	0.01	0.16	0.13
CEM III/B 42.5 N	Unhydrated	55.28	24.27	7.60	5.83	3.46	1.50	0.92	0.53	0.23	0.11	0.07	0.02	0.00	0.00	0.18
	Hydrated	57.80	23.28	7.00	5.08	3.06	1.67	0.96	0.52	0.24	0.12	0.06	0.03	0.00	0.00	0.18
	500 °C	56.00	24.23	7.67	5.42	3.11	1.56	0.90	0.52	0.23	0.11	0.06	0.02	0.00	0.00	0.17
	800 °C	55.01	23.92	8.98	5.57	3.09	1.54	0.86	0.49	0.21	0.11	0.04	0.02	0.00	0.00	0.16
	1400 °C	55.49	24.82	9.92	5.52	0.90	1.58	0.85	0.41	0.21	0.11	0.00	0.02	0.01	0.00	0.16
CEM I 42.5 N	Unhydrated	69.63	16.03	4.46	2.09	2.15	4.13	0.46	0.55	0.09	0.14	0.04	0.09	0.01	0.00	0.13
Fly Ash	Untreated	6.32	54.48	23.77	1.10	0.86	9.20	1.23	1.88	0.05	0.21	0.00	0.03	0.03	0.47	0.37
Blast Furnace Slag	Untreated	44.80	30.25	12.62	8.24	1.33	0.56	1.13	0.51	0.31	0.07	0.00	0.00	0.00	0.00	0.18

F. 1: Results of the analysed samples. The cementitious Smart Crusher fractions show a higher SiO_2 content and lower CaO content than the hydrated reference samples. The thermal treatments result in only minor differences in the chemical composition. The SO_3 content decreases as a result of the thermal treatment of 1400 °C.

Oxide	Composition % mass fraction Bead number						
	1	2	3	4	5	6	7
SiO_2	24,0	19,5	20,4	22,3	18,0	18,7	21,4
Al_2O_3	7,2	8,1	2,6	5,4	4,5	6,3	3,6
Fe_2O_3	1,5	6,1	6,8	4,2	5,3	2,3	3,4
CaO	61,2	62,4	63,3	64,5	66,0	67,3	68,8
MgO	1,1	1,7	4,0	2,6	2,2	3,2	0,5
K_2O	1,0	0,4	0,2	0,8	0,6	1,2	0,0
SO_3	4,0	1,8	2,7	0,2	3,4	1,0	2,3
Total	100,0	100,0	100,0	100,0	100,0	100,0	100,0

F. 2: Composition of CEM I cements [73]

	Units	Average Values	Requirements	
			Min.	Max.
CaO	%	44	-	-
SiO_2	%	28	-	-
Al_2O_3	%	11	-	-
Fe_2O_3	%	1	-	-
Sulfate SO_3	%	2,8	-	4,0

F. 3: Composition of CEM III/B [31]

Appendix G. XRD results

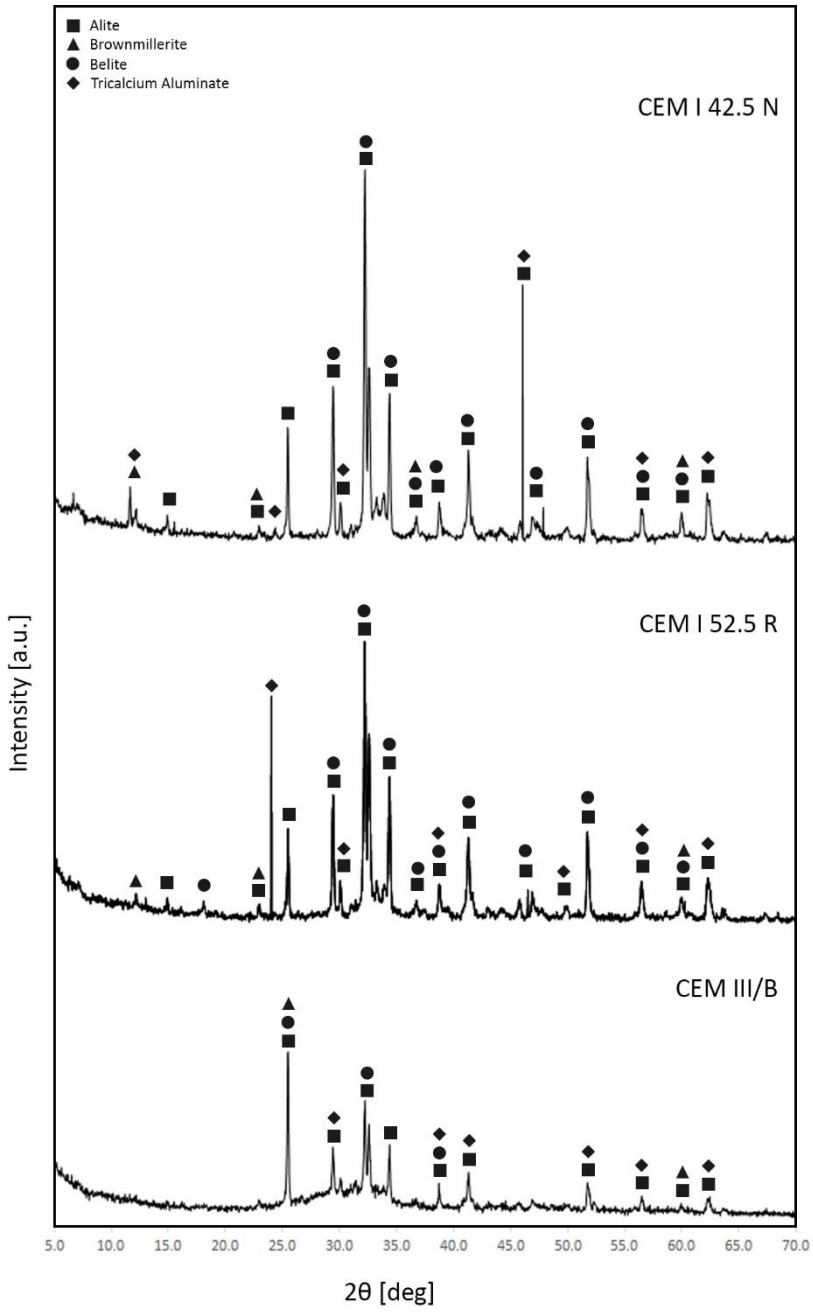

G. 1: Diffraction pattern of the unhydrated CEM III/B 42.5 N, CEM I 52.5 R and CEM I 42.5 N showing the presence of the cement minerals alite, belite, brownmillerite and tricalcium aluminate.

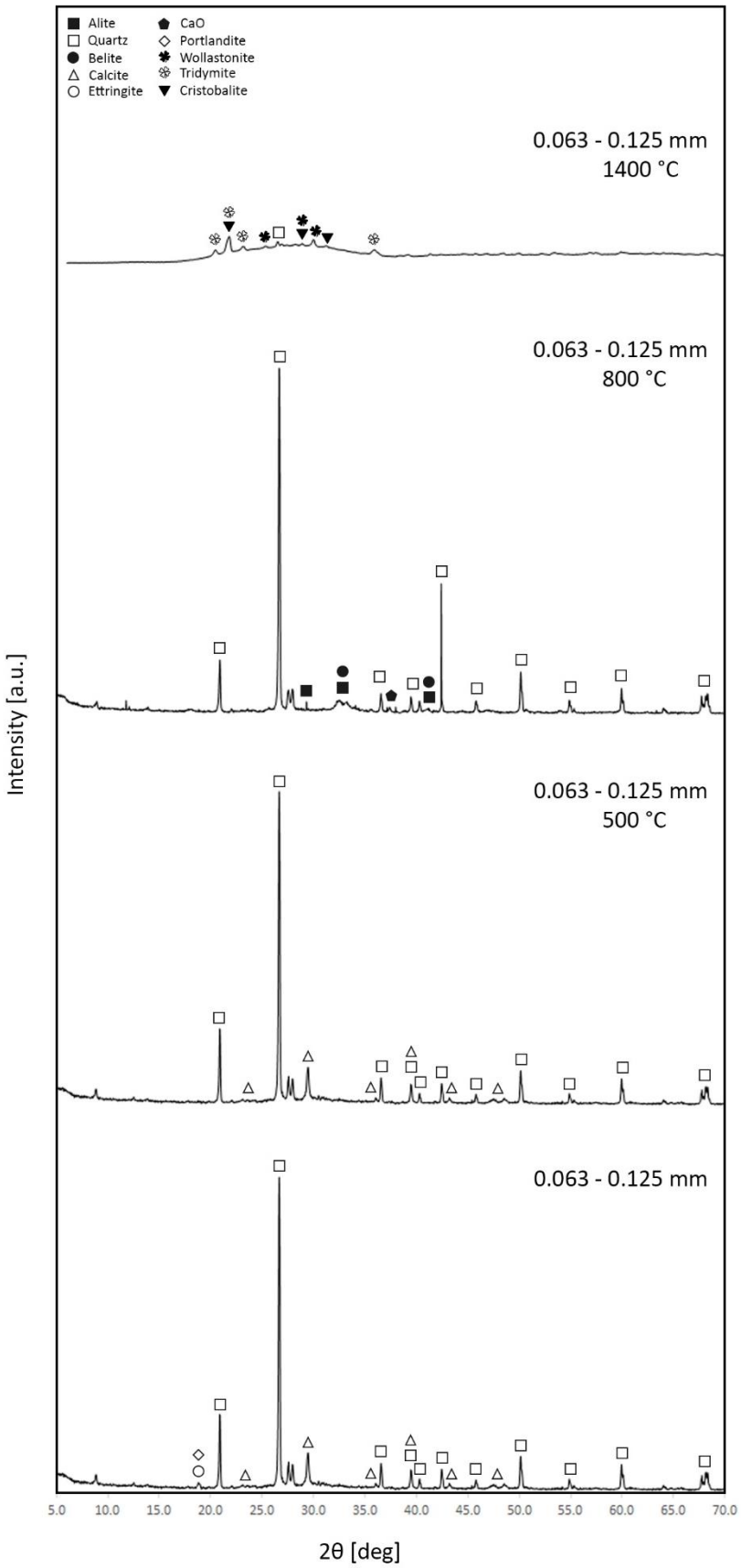

G. 2: Diffraction pattern of the 0.063 - 0.125 mm fraction with and without thermal treatment showing the decomposition of the cement hydration products (500 °C) and calcite (800 °C) and the formation of alite, belite and calcium oxide (800 °C). The thermal treatment of 1400 °C resulted in an amorphous material.

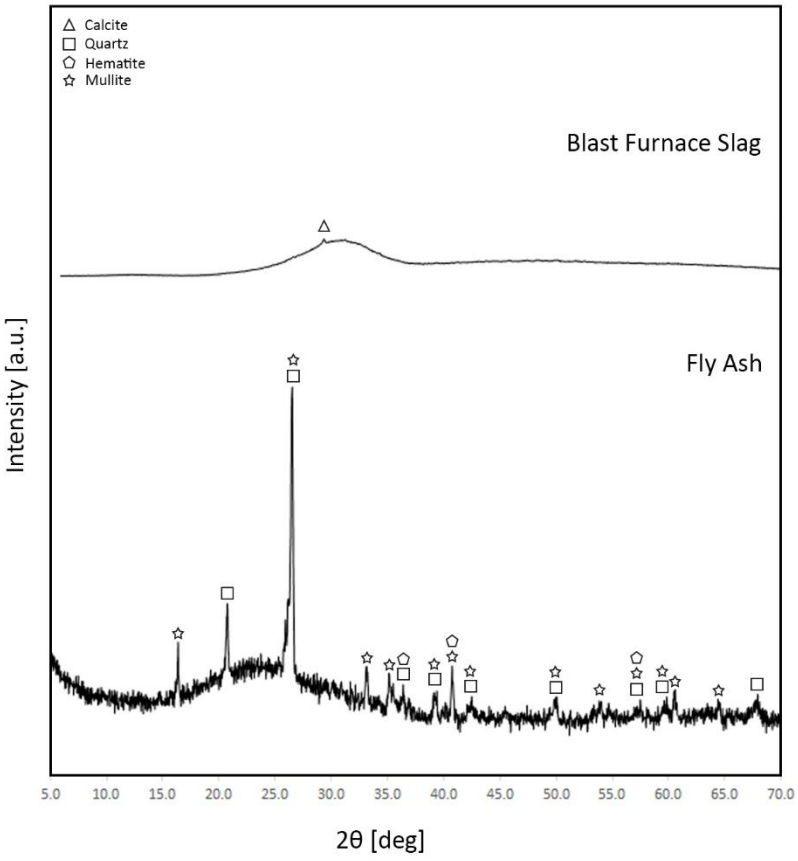

G. 3: Diffraction pattern of fly ash and blast furnace slag showing the presence of mullite, hematite and quartz in fly ash and quartz in blast furnace slag.

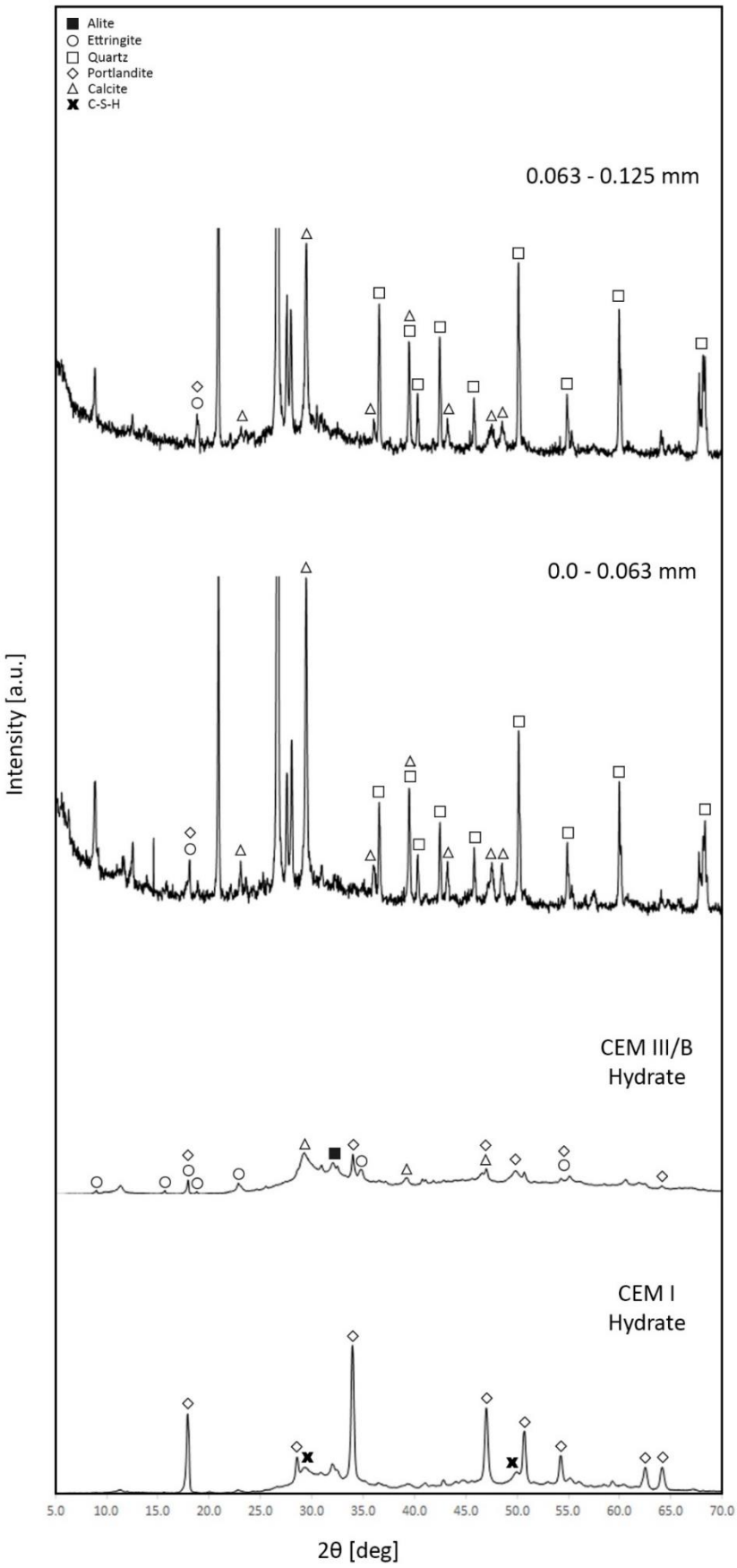

G. 4: Diffraction pattern of the hydrated samples. The cementitious Smart Crusher fractions show mainly distinct quartz and calcite peaks and the hydrated reference samples show mainly peaks associated with portlandite, ettringite and C-S-H.

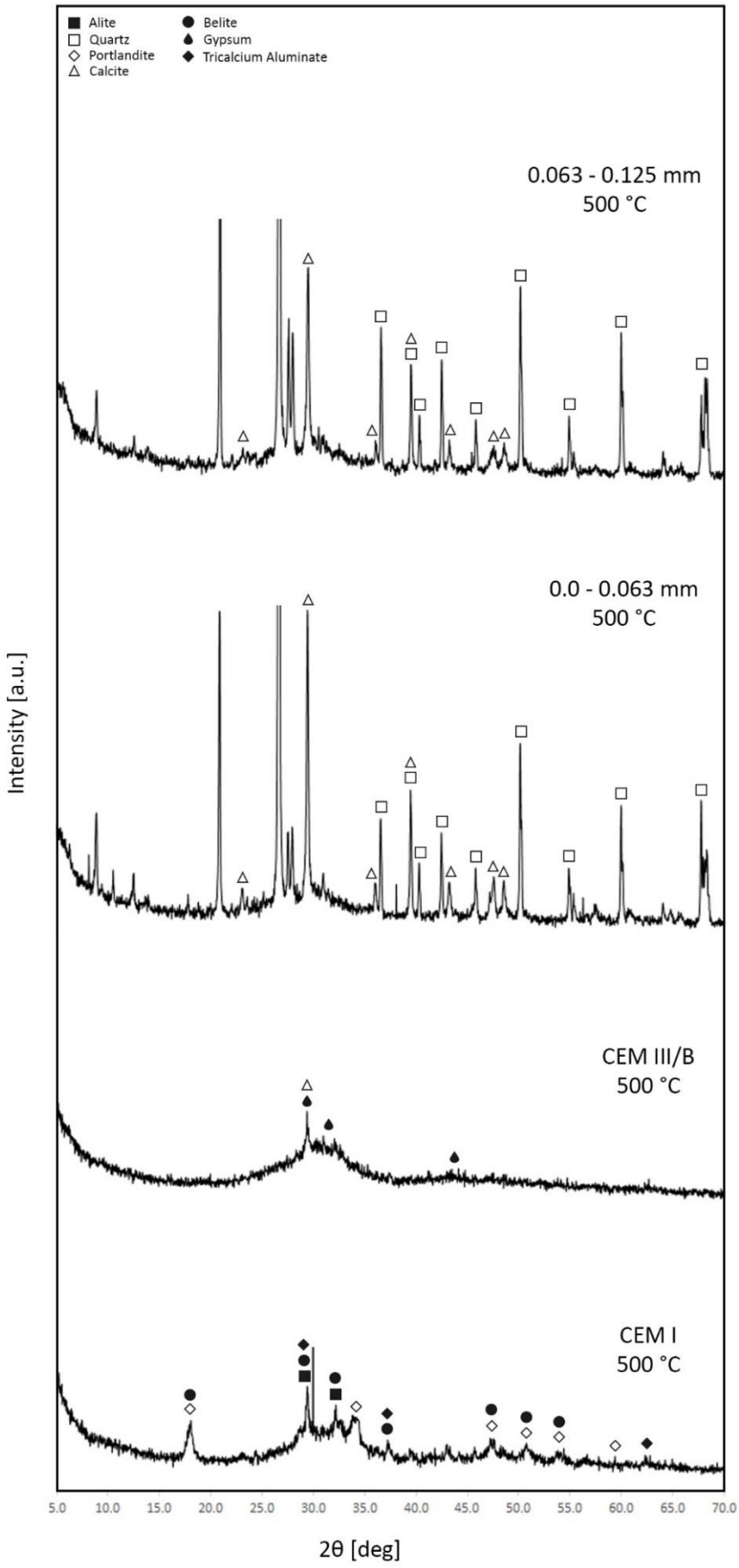

G. 5: Diffraction pattern of the samples after a thermal treatment of 500 °C. The cementitious Smart Crusher fractions are dominated by quartz and calcite. The formation of alite and belite can only be observed for the CEM I sample.